SAINT-PETERSBURG UNIVERSITY

Lezova Irina Evgenievna

Heat capacity and magnetocaloric properties of series of rare-earth garnets, aluminates and pentaphosphates

Scientific specialty
1.3.8. Condensed matter physics

Dissertation for the degree of
Candidate of Physical and Mathematical Sciences

Translation from Russian

Research advisor:
Doctor of Physical and Mathematical science, professor
Charnaya Elena Vladimirovna

Saint Petersburg — 2024

Table of contents

Pages.

Pages.

Introduction

The creation of lasers was a significant step in the development of fundamental and applied science. The prospect of their use has focused the attention of researchers on the problems related to the development and creation of new materials that can be used to create new lasers that meet the specified characteristics. Solid-state lasers with high output power in both continuous and require the active medium material to have high spectral-luminescent characteristics, as well as high strength and thermal conductivity.

It is known that perovskites, pentaphosphates, aluminates [**1**; **2**], borates [**3**; **4**], garnets [**5**; **6**] and simple oxides [**7**; **8**] of rare-earth elements (*REE*) have good scintillation properties, high temperature resistance, high hardness and high refractive index value. For example, due to these properties *REE* aluminates are used in optical instrumentation and semiconductor technology [**9**]. Of great interest is the use of rare-earth elements to obtain compounds with the structure of garnet or perovskite, which are the basis for obtaining high-strength ceramics and piezomaterials, luminophores and semiconductors, active material in optical quantum generators [**10**].

Among many different types of materials, one can also emphasize glass media, which have a number of advantages over crystals [**11**].The first is the relative simplicity of obtaining glasses with specified optical characteristics and the possibility of manufacturing active elements of different shapes and sizes on their basis. The second is the possibility of obtaining materials with improved optical properties by adding various rare-earth ions to the glass composition [**12**].

An important feature of all the materials considered above, both crystalline and glass, is the manifestation of the magnetocaloric effect (*MCE*). After application and subsequent switching off of an external magnetic field acting on the sample, the sample is cooled. This effect was the basis for the development of a magnetic cooling system.

Initially, *MCE* was mainly used to reach temperatures below 1 K. Later, materials in which *MCE* is observed near room temperature were discovered, which led to an active investigation of magnetic cooling as an alternative to conventional liquefied gas cooling. The results showed that magnetic cooling

has several advantages over its conventional implementation especially at room temperature. Its high energy efficiency should also be mentioned [**13**].

The cooling process can be viewed as a process of entropy reduction. Since the entropy (or degree of disorder) of a system at constant volume or constant pressure decreases with decreasing temperature, cooling in a medium can be observed in any process that reduces the entropy of the medium. For example, liquefaction of gases is achieved through isothermal entropy reduction by reducing the volume V_1 at temperature T_1 to a smaller volume V_2. In this process, heat is released by contact with a cold reservoir. This is followed by adiabatic or isoentropic expansion, which leads to cooling of the gas to a temperature below T_1 [**14**].

In the process of magnetic cooling, a system of disordered magnetic dipoles associated with a particular ion in a particular medium forms a system similar to the one described above. When a magnetic field is applied, the dipoles are oriented along the field, which leads to a decrease in the entropy of the system. The process can involve either electron dipoles (electron cooling due to electron spins) or nuclear dipoles (nuclear cooling due to nuclear spins) depending on the desired final temperature. For temperatures above a few millikelvin, electron cooling is used, while for temperatures below a millikelvin, nuclear cooling is used. If the applied field is subsequently switched off, dipole disorder will occur, leading to cooling of the medium in contact with the refrigerator [**13**].

The first models of electron cooling were proposed by Debye [**15**] in 1926 and by Jiok [**16**] in 1927. The first experimental setup was demonstrated by De Haas, Wiersma and Kramers [**17**], Jiok and McDougall [**16**] in 1933, and Curti and Simon [**18**] in 1934 [**19**; **20**]. In 1933, the first magnetic refrigerator was realized. Gadolinium salt $Gd_2(SO_4)_3 \cdot 8H_2O$ was chosen as the working substance, which allowed D. McDougall and W. Jiok to go down to a temperature of 0.25 K [**16**].

The nuclear cooling system was first realized only in 1956, when Curti and colleagues were able to realize cooling from 12 millikelvin to 20 microkelvin by demagnetizing nuclear spins [**18**].

Returning to the problem of searching for an active laser medium material with specified optical and thermal characteristics, it should be noted that the most promising in this field are compounds with *REE* addition, in particular, garnets and pentaphosphates.

Dynamic electric fields can excite transitions between energy levels. This effect underlies the creation of laser environments in a wide range of energies [**21**]. In

addition, the strong magnetocaloric effect in crystalline materials and glasses that contain impurities of paramagnetic ions allows their use in magnetic refrigerators [**22**; **23**].

The analysis of literature has shown that at present the thermodynamic properties and behavior of aluminates, garnets and pentaphosphates in the low-temperature region under the application of external magnetic fields are insufficiently studied. The study of the magnetocaloric effect will make it possible to expand the areas of practical application of these materials.

Aims of this dissertation work is to investigate the influence of the type of rare earth ions and the degree of doping on the heat capacity of garnet, aluminate and pentaphosphate single crystals and pentaphosphate glasses in external magnetic fields. In the present work, a series of yttrium-disprosium aluminum garnets $Y_{3-x}Dy_xAl_5O_{12}$ $(0 \leqslant x \leqslant 3)$, crystals and glasses of pentaphosphates with the general formula AP_5O_{14}, where $A = Nd$, Gd, Sm, Ce, and a series of aluminates with the general formula $Y_{1-x}Er_xAlO_3$ $(x = 0; 0.7; 0.1; 0.15; 0.2; 0.45)$, and a crystal of gallium-gadolinium garnet $Gd_3Ga_5O_{12}$, doped with erbium $(GGG{:}Er)$, in comparison with unalloyed garnet (GGG).

Objectives and **purposes**:

1. To carry out measurements and comparative analysis of heat capacity values in crystals of gallium-gadolinium garnet (GGG), gallium-gadolinium garnet doped with erbium $(GGG{:}Er)$, a series of garnets $Y_{3-x}Dy_xAl_5O_{12}$ $(0 \leqslant x \leqslant 3)$, a series of pentaphosphates AP_5O_{14}, where $A = Nd$, Gd, Sm, Ce, and a series of aluminate crystals $Y_{1-x}Er_xAlO_3$ $(x = 0; 0.07; 0.1; 0.15; 0.2; 0.45)$ in a zero magnetic field. Process the obtained data and interpret the experimental temperature dependences of heat capacity in the framework of the existing theoretical models.
2. To investigate the effect of magnetic field on the heat capacity of gallium-gadolinium garnet (GGG), gallium-gadolinium garnet doped with erbium $(GGG : Er)$, garnet series $Y_{3-x}Dy_xAl_5O_{12}$ $(0 \leqslant x \leqslant 3)$, pentaphosphate series AP_5O_{14}, where $A = Nd$, Gd, Sm, Ce, and aluminate series $Y_{1-x}Er_xAlO_3$ $(x = 0;\ 0.07;\ 0.1;\ 0.15;\ 0.2;\ 0.45)$. To reveal the peculiarities of magnetic field influence on heat capacity.
3. Calculate the magnetic entropy of erbium-doped gallium-gadolinium garnet $(GGG{:}Er)$ crystal compared to pure garnet (GGG), garnet series $Y_{3-x}Dy_xAl_5O_{12}$ $(0 \leqslant x \leqslant 3)$, single crystals and glasses of

AP_5O_{14}, где $A = Nd$, Gd, Sm, Ce, Yb, and a series of $Y_{1-x}Er_xAlO_3$ aluminates ($x = 0; 0.07; 0.1; 0.15; 0.2; 0.45$).

4. To evaluate the possibility of using the studied garnets, pentaphosphates and aluminates in magnetic refrigerators.
5. Determine the value of the g - factor for a series of garnets $Y_{3-x}Dy_xAl_5O_{12}$ ($0 \leqslant x \leqslant 3$), single crystals and glasses of AP_5O_{14}, where $A = Nd$, Gd, Sm, Ce, Yb, and aluminate series $Y_{1-x}Er_xAlO_3$ (x = 0; 0.07; 0.1; 0.15; 0.2; 0.45) from the experimental data obtained for the magnitude of heat capacity in a magnetic field.

To solve the set tasks it is necessary to carry out the following experiments using a relaxation calorimeter of the *PPMS-9+Evercool II Quantum Design* system in wide:

1. Measurement of temperature dependences of heat capacity of gallium-gadolinium garnet (GGG), gallium-gadolinium garnet doped with erbium (GGG:Er), garnet series $Y_{3-x}Dy_xAl_5O_{12}$ ($0 \leqslant x \leqslant 3$).
2. 2. Measurement of temperature dependences of heat capacity in single crystals and glasses of AP_5O_{14} pentaphosphates, where $A = Nd$, Gd, Sm, Ce, Yb.
3. 3. Measurement of temperature dependences of heat capacity of aluminate series $Y_{1-x}Er_xAlO_3$ (x = 0; 0.07; 0.1; 0.15; 0.2; 0.45).

Scientific and practical significance. On the basis of the experimental data obtained and their processing within the framework of modern theories it is possible to draw conclusions about the peculiarities of heat capacity and structure of garnets doped with rare-earth metals, single crystals and glasses of pentaphosphates, as well as crystals of aluminates. Special attention in the presented work was paid to the analysis of the low-temperature region of the heat capacity dependence for the considered crystals. The studies were carried out in a wide range of applied magnetic fields, which allowed us to draw conclusions about its influence on the heat capacity of the studied crystals.

The data obtained in this work can be used in the development of various devices and elements for a wide field of applied physics and engineering, in which the studied materials are used. The results obtained on the influence of the composition and type of paramagnetic ions on the heat capacity open up the possibility of designing systems with predictable properties.

Research conducted as part of the work has shown that garnets, pentaphosphates and aluminates can be used in the construction of adiabatic magnetic refrigerators. This contributes to a broader set of materials for use in magnetic refrigerators.

Academic novelty:

1. The heat capacity features of single crystals of gallium-gadolinium garnet doped with erbium ($GGG{:}Er$), and a series of $Y_{3-x}Dy_xAl_5O_{12}$ ($0 \leqslant x \leqslant 3$) garnets in the temperature range of $1.9 - 220$ K and the range of $1.9 - 80$ K, respectively, have been studied in detail for the first time.
2. Experimental studies of the heat capacity of mixed aluminate single crystals with the general formula $Y_{1-x}Er_xAlO_3$ ($x = 0$; 0.07; 0.1; 0.15; 0.2; 0.45) in the temperature range of $1.9 - 100$ K.
3. Experimental temperature dependences of heat capacity in single crystals and glasses of AP_5O_{14} pentaphosphates, where $A = Nd$, Gd, Sm, Ce, Yb, in the temperature range of $1.9 - 100$ K.
4. It is shown that the obtained temperature dependencies of heat capacity in a zero magnetic field for all investigated materials are described in the framework of Debye and Einstein theories and the multilevel Schottky model.
5. The influence of magnetic field on the value of heat capacity for all considered samples was investigated for the first time.
6. The presented results demonstrated the potential of magnetocalorimetry to study the substitution order in crystalline solutions.
7. Entropy and magnetic contribution to entropy were calculated from the obtained data. The presence of magnetocaloric effect was demonstrated, and the possibility of using the studied materials with paramagnetic ions in magnetic refrigerators was shown. It is shown that the maximum magnetocaloric effect is observed in mixed garnets with dysprosium.
8. The value of the g - factor for the garnet series $Y_{3-x}Dy_xAl_5O_{12}$ ($0 \leqslant x \leqslant 3$), in single crystals and glasses of AP_5O_{14} pentaphosphates, where $A = Nd$, Gd, Sm, Ce, Yb, and for the aluminate series $Y_{1-x}Er_xAlO_3$ ($x = 0.07; 0.1; 0.15; 0.2; 0.45$) was determined from the experimental data obtained for the heat capacity in a magnetic field.

Credibility The obtained results are ensured by the use of modern instrumentation in the studies carried out and the consistency of these results with those already available in the scientific literature.

Conferences participation. The main results of the work were reported and discussed at two conferences - International Scientific Conference of Students, Postgraduates and Young Scientists «Lomonosov-2020», 10-27 November 2020, Moscow State University, Moscow, Russia; Twenty-sixth All-Russian Scientific Conference of Physics Students and Young Scientists (VNKSF-26), 10 - 14 March 2022 Republic of Bashkortostan, Ufa, Russia.

Author contribution. The main part of the work was completed by the author herself. It includes direct obtaining of experimental data, development of measurement techniques and interpretation of the results obtained.

The results obtained in this thesis have been published in scientific articles and conference proceedings. Preparation for publication of the results of the experiments was carried out jointly with co-authors. The goals, objectives, methods, and conclusions discussed in the dissertation were interpreted jointly with the supervisor, E.V. Charnaya, who provided general supervision of the work and problem setting. Co-authors of the publications A.S. Bugaev, E.N. Khazanov and A.V. Taranov participated in the interpretation and analysis of the obtained data for heat capacity. Co-authors E.N. Khazanov, A.V. Taranov, and E.I. Salamatov studied phonon kinetics using the thermal pulse method.

The work was performed on the equipment of the resource centre «Centre for Diagnostics of Functional Materials for Medicine, Pharmacology and Nanoelectronics» of the Research Park of SPbU.

Publications. The main results of the dissertation are presented in 4 printed papers in journals included in the *Scopus* and *Web of Science* system:

1. Lezova, I.E. Heat Capacity of Erbium-Doped Gallium-Gadolinium Garnet / I.E. Lezova, E.V. Shevchenko, E.V. Charnaya, E.N. Khazanov, A.V. Taranov // Physics of the Solid State. – 2018. – Vol.60. – №10. – P. 1948-1952.
2. Lezova, I.E. Calorimetry of $Dy_xY_{3-x}Al_5O_{12}$ garnet solid solutions in magnetic field / I.E. Lezova, E.V. Charnaya, E.V. Shevchenko, E.N. Khazanov, A.V. Taranov // Journal of Applied Physics. – 2020. – Vol.128. – №22. – P. 225101.

3. Lezova, I.E. Low-Temperature Heat Capacity and Phonon Kinetics in Some Rare-Earth Pentaphosphate Single Crystals and Glasses / I.E. Lezova, E.I. Salamatov, A.V. Taranov, E.N. Khazanov, E.V. Charnaya, E. V. Shevchenko // Journal of Experimental and Theoretical Physics. – 2019. – Vol.129. – №5. – P. 849-854.
4. Lezova, I.E. Kinetic Characteristics of Phonons and the Structural Heterogeneities of the Monoaluminate $Y_{1-x}Er_xAl_O3$ Solid Solutions / I.E. Lezova, O.V. Karban', A.V. Taranov, E.N. Khazanov, E.V. Charnaya // Journal of Experimental and Theoretical Physics. – 2020. – Vol.130. – №1. – P. 76-81.

Structure of the dissertation. The dissertation consists of an introduction, five chapters, the main results of the dissertation, a list of the author's publications on the topic of the dissertation and a list of cited literature.

In the first chapter, the theoretical models of heat capacity of solids Debye and Einstein, as well as the Schottky anomaly, which will be needed to describe the heat capacity of the substances investigated in the framework of this work, are considered. Part of the chapter is devoted to the concept of magnetic entropy, which is necessary for the evaluation of the magnetocaloric effect. The methodology of measuring the value of heat capacity is considered. At the end of the first chapter, a review of scientific works devoted to the study of thermal and magnetic properties of pentaphosphates, aluminates and garnets containing rare-earth elements is presented.

The second chapter is devoted to the study of heat capacity of garnets (GGG) and GGG with Erbium impurity (GGG: Er). The first part of the chapter presents the experimentally obtained temperature dependences of the heat capacity in a zero magnetic field. They are described in the framework of Debye, Einstein, and Schottky models. In the second part of the chapter the temperature dependences of heat capacity in magnetic fields up to 9 T are presented and described. The third part is devoted to calculations of the magnetic contribution to entropy.

The third chapter is devoted to the study of heat capacity of mixed garnet single crystals with the general formula $Dy_xY_{3-x}Al_5O_{12}$ (x = 0; 0.15; 0.50; 1.00; 1, 50, 2.25; 3.00). The first part presents the results of measurements carried out in the absence of a magnetic field applied to the samples. In the second part of the chapter the obtained temperature dependences of heat capacity in magnetic fields up to 9 T are given and described. Similarly to the results of Chapter 2, the calculation

of various contributions to the heat capacity was performed. The construction of dependences of heat capacity in magnetic fields allowed us to calculate the g - factor for dysprosium ions in garnets. The third part of the chapter is devoted to calculations of the magnetic contribution to entropy. At the end of the chapter, the nature of heat capacity anomalies in the magnetic field related to the structure peculiarities of mixed garnets is discussed.

Chapter 4 presents the results of heat capacity measurements in single crystals and glasses of a number of rare-earth pentaphosphates (NdP_5O_{14}, GdP_5O_{14}, YbP_5O_{14}, SmP_5O_{14}, CeP_5O_{14}). The features of low-temperature heat capacity in single crystals and glasses of rare-earth pentaphosphates have been considered. The measurements were carried out in the absence of a magnetic field applied to the samples and in fields up to 9 T. On the basis of the experimental data obtained, the value of the g - factor, as well as the values of entropy and magnetic entropy in single crystals and glasses of a number of rare-earth pentaphosphates were calculated.

Chapter 5 presents the results of heat capacity measurements in single crystals of aluminates with the general formula $Y_{1-x}Er_xAlO_3$ (x = 0; 0.07; 0.1; 0.15; 0.2; 0.45). The measurements were carried out in the temperature range from 1.9 to 80 K in the absence of a magnetic field applied to the samples and in fields up to 6 T. Based on the experimental data obtained, the value of g - factor for aluminates with erbium and the values of entropy and magnetic entropy in single crystals of aluminates were calculated

The Conclusion lists the main results of this work. At the end there is a list of the main publications on the subject of the thesis and a list of the cited literature.

Main scientific results:

1. Measurements of heat capacity values of crystalline materials and pentaphosphate glasses in a wide temperature range under the application of constant magnetic fields have been carried out, these data are presented in the works: [**87**] (pp.1948 – 1952), [**97**] (pp. 225101-1 – 225101-8), [**111**] (pp. 849 – 854), [**118**] (pp. 76 – 81).
2. The temperature dependence of the heat capacity of pure and erbium-doped gallium-gadolinium garnet crystals in the range from 1.9 to 40 K can be approximated by the sum of the contributions of Schottky anomalies associated with the presence of gadolinium and erbium ions, as well as the Debye and Einstein contributions. The splitting values of the gadolinium basic spin multiplet have values of the order of magnitude higher than their

theoretical estimates. The introduction of erbium ions into the garnet lattice leads to an increase in the magnetocaloric effect (see [**87**] pp.1948 – 1952).

3. For $Dy_xY_{3-x}Al_5O_{12}$ crystals with x from 0 to 3 at zero external magnetic field in the temperature range from 1.9 to 40 K, the heat capacity value can be described by the sum of the Debye contribution and the Schottky anomaly contribution. In the series of mixed dysprosium-yttrium garnets, the maximum magnetocaloric effect is observed for the $Dy_{2.25}Y_{0.75}Al_5O_{12}$ sample. The study of $Dy_1Y_2Al_5O_{12}$ garnet under the application of different magnetic fields showed that heat capacity measurements can be used to obtain information about clustering in solid solutions (see [**97**] pp. 225101).
4. It is shown that the heat capacity of GdP_5O_{14} pentaphosphate glass in the low temperature region is significantly higher than that of a single crystal of the corresponding composition, which is explained by the contribution to the heat capacity of two-level systems (see [**111**] pp. 849 – 854).
5. It is shown that the heat capacity of aluminates $Y_{1-x}Er_xAlO_3$ at x from 0 to 0.45 in the temperature range from 1.9 to 7 K is determined by Schottky anomalies and Debye contributions (see [**118**] pp. 76 – 81).

The main provisions of the dissertation:

1. Values of heat capacity of the investigated crystalline materials and pentaphosphate glasses measured in the temperature range from 1.9 to 220 K and in magnetic fields up to 9 T.
2. The temperature dependence of the heat capacity of pure and erbium-doped GGG crystals in the range from 1.9 to 40 K can be approximated by the sum of the contributions of Schottky anomalies associated with the presence of gadolinium and erbium ions, as well as the Debye and Einstein contributions. The splitting values of the main spin multiplet of gadolinium are an order of magnitude higher than their theoretical estimates.
3. For solid crystalline solutions $Dy_xY_{3-x}Al_5O_{12}$ and $Y_{1-x}Er_xAlO_3$, as well as pentaphosphate crystals, the value of heat capacity at zero external magnetic field in the temperature range from 1.9 to 40 K can be described by the sum of the phonon contribution and the contribution of Schottky anomalies. To calculate the contribution of Schottky anomalies, it is additionally necessary to take into account the splitting of the main Kramers doublet by magnetic fields created by neighboring ions.

4. Studies of $Dy_1Y_2Al_5O_{12}$ garnet under the application of different magnetic fields have shown that heat capacity measurements can be used to obtain information on clustering in solid solutions.
5. The heat capacity of GdP_5O_{14} pentaphosphate glass in the low temperature region significantly exceeds the heat capacity of a single crystal of the corresponding composition due to the contribution to the heat capacity of two-level systems.
6. The calculated values of magnetic entropy show the possibility of using the investigated materials in magnetic refrigerators.

Chapter 1. Literature Review

This chapter provides a brief review of the thesis topic. In the first part of the chapter, Debye and Einstein theoretical models of heat capacity of solids as well as and Schottky anomaly are considered, which will be used further to describe the heat capacity of the samples investigated in this work. The second part is devoted to the concept of magnetic entropy, which is necessary for the estimation of the magnetocaloric effect. The third part is devoted to the technique of measuring the heat capacity of the samples. The fourth and fifth parts are a review of scientific works devoted to the study of thermal and magnetic properties of pentaphosphates, garnets and aluminates containing rare-earth elements.

1.1 Heat Capacities of Solids

Heat capacity $C(T)$ is a measurable physical quantity defined as the amount of heat ΔQ that must be supplied to a system for its temperature to increase by one degree. It is believed that the concept of heat capacity was first introduced by Joseph Black in 1760 [**24**].

Thus, if the amount of heat imparted to the system is δQ and the temperature rise is dT, the specific heat capacity can be expressed as follows:

$$C_{x,y,...} = \lim_{dT \to 0} \left(\frac{\delta Q}{dT} \right)_{x,y,...} \tag{1.1}$$

where $x, y, ...,$ are quantities such as pressure, volume, magnetic field, etc., which remain constant during the measurement. In most cases, specific heat capacity depends on the temperature of the system and the way it is heated.

There are two basic heat capacities, C_v and C_p. The first refers to processes occurring at constant volume and the refers to processes at constant pressure. These heat capacities are written as:

$$C_p = \left(\frac{\partial Q}{\partial T} \right)_p \tag{1.2}$$

$$C_v = \left(\frac{\partial Q}{\partial T}\right)_v \tag{1.3}$$

Using thermodynamic relations, the following expression can be derived:

$$C_p - C_v = T\left(\frac{\partial P}{\partial T}\right)_v \left(\frac{\partial V}{\partial T}\right)_p \tag{1.4}$$

For solids it is convenient to consider this difference as a function of thermal expansion coefficient α_T and isothermal contraction coefficient χ

$$C_p - C_v = \frac{9\alpha_T^2}{\chi} VT \tag{1.5}$$

For most solids, the difference in heat capacity is small, about 5% (at room temperature), and it decreases rapidly with decreasing temperature.

The heat capacity of a body is proportional to the amount of substance contained in it. The amount of substance can be determined by mass or number of moles, therefore the concepts of specific heat capacity C_v and C_p (heat capacity of a unit of body mass) and molar heat capacity C_v and C_p (heat capacity of one mole of substance) are distinguished.

The units of C_v and C_p are J/kg·K, for C_v and C_p they are J/Mol · K.

Heat capacity is determined by various internal processes of the system, therefore, when analyzing the heat capacity of solids it is necessary to take into account contributions of different nature. The following contributions are distinguished: lattice, magnetic, electronic.

In the very first approximation, we can imagine that each atom of the crystal lattice is a three-dimensional harmonic oscillator whose average energy is kT. Then the average energy of each atom will be $3kT$, where k is Boltzmann's constant, T is temperature. For one mole of a substance, the average internal energy will be determined as follows:

$$U = 3N_A kT = 3RT \tag{1.6}$$

where N_A is Avogadro's constant, R is the universal gas constant. Thus, for the molar heat capacity we obtain:

$$C = \partial U/\partial T = 3R \tag{1.7}$$

Dulong and Petit obtained this relation empirically for solids at temperatures close to room temperature. Numerous studies have shown that at high temperatures

and at temperatures very much lower than room temperature this law is not fulfilled [**25**].

In accordance with experimental data, the heat capacity tends to zero when approaching absolute zero. To describe this behavior of heat capacity at low temperatures, Einstein proposed a theory in which a solid body was considered as N independent oscillators oscillating with the same frequency ν [**26**]. Applying the Planck distribution to find the average energy of a linear oscillator, Einstein obtained a formula for the heat capacity of a system with $3N$ degrees of freedom.

$$C_V = 3R\frac{\left(\frac{\theta_E}{T}\right)^2 e^{\frac{\theta_E}{T}}}{\left(e^{\frac{\theta_E}{T}}-1\right)^2} \tag{1.8}$$

where θ_E is the Einstein characteristic temperature, equal to $h\nu/k$.

Thus, at $T \gg \theta_E$ the dependence of heat capacity in Einstein's model tends to the Dulong and Petit law. At $T \ll \theta_E$, the model predicts heat capacity behavior of the form $C \sim e^{-\frac{\theta_E}{T}}$. However, experiments showed that at low temperatures the heat capacity is proportional to the cube of temperature $C \sim T^3$, which did not fit Einstein's model.

To find the low-temperature dependence of the heat capacity, Debye [**15**] and Born and Karman [**27**] independently considered the problem on the heat capacity of interacting N oscillators with $3N$ degrees of freedom.

Debye assumed that the system of atoms is a continuous isotropic medium (elastic continuum). For such a system of coupled oscillators, the internal energy due to oscillations of ions due to thermal motion is determined by the density function of phonon states (phonon spectrum) $g(\nu) = \frac{\partial n}{\partial \nu}$, which in the Debye approximation is a quadratic function of the frequency ν. For the molar heat capacity at constant volume, Debye derived the following expression:

$$C_D = 9R\left(\frac{T}{\theta}\right)^3 \int_0^{x_D} \frac{x^4 e^x}{(e^x-1)^2} dx \tag{1.9}$$

where R – is the gas constant, θ – is the Debye temperature. Thus, at low temperatures the heat capacity varies proportionally to the third degree of temperature, and at high temperatures the heat capacity at constant volume approaches the values of Dulong and Petit.

Thus, the lattice contribution to the heat capacity can be described by a combination of Debye and Einstein contributions, in which acoustic modes will be well described by the Debye model and optical oscillations by the Einstein model [**28**; **29**; **30**]. The Einstein model can also describe some local oscillations. However, even such a general model uniting Debye and Einstein theories was insufficient to describe the behavior of the heat capacity of some compounds.

At low temperatures, an increase in heat capacity can be observed due to an anomaly called the Schottky anomaly [**31**]. This deviation arises due to the splitting of energy levels of rare-earth ions in the crystal field into energy sublevels [**32**]. When the temperature changes, the population of the levels changes, which in turn affects the character of the heat capacity.

For numerical description, the statistical sum of the system of energy levels is found taking into account the degree of degeneracy [**33**]. For this purpose, we first consider a system of two levels with energies ε_1 and ε_2, where ε_1 is the zero-point energy of the ground level. The difference of energy levels (in kelvins) is defined as

$$\Delta_1 = (\varepsilon_2 - \varepsilon_1)/k \tag{1.10}$$

The statistical sum taking into account degeneracy is written in the following form:

$$Z = g_0 + g_1 e^{-\frac{\Delta_1}{T}} \tag{1.11}$$

where g_0 – degeneracy of level ε_1, g_1 – degeneracy of level ε_2. Then according to the expression for the total internal energy, the energy of the two-level system is equal to

$$U = (kT)^2 \frac{\partial \ln Z}{\partial T} \tag{1.12}$$

As a result, after differentiation and multiplication by Avogadro's constant of expression 1.12, the expression for the Schottky molar heat capacity in the case of a two-level system is obtained:

$$C_S = R \left(\frac{\Delta}{T}\right)^2 \frac{g_0/g_1 \cdot e^{-\frac{\Delta_1}{T}}}{\left(1 + g_0/g_1 \cdot e^{-\frac{\Delta_1}{T}}\right)^2} \tag{1.13}$$

The temperature dependence of the Schottky anomaly is an asymmetric peak, with the ratio of degeneracy degrees of levels playing a major role 1.1).

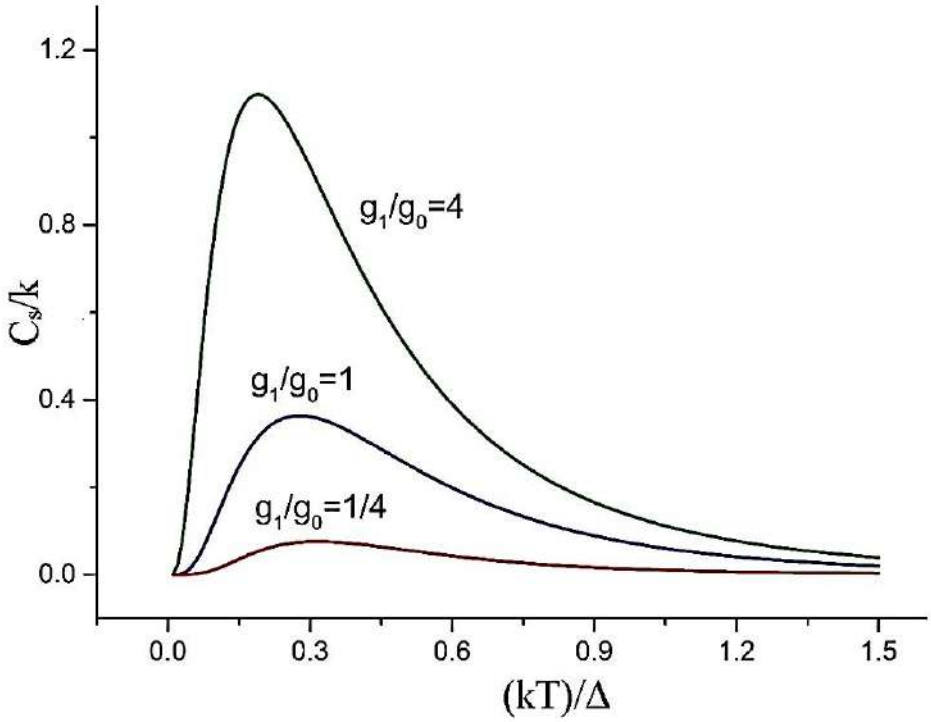

Figure 1.1 — Illustration of the Schottky anomaly of a two-level system with energy difference Δ at different ratios of degeneracy degrees

Thus, for a simple two-level system at $T \ll \Delta$ the molar heat capacity has an exponential character:

$$C_S \sim R \left(\frac{\Delta}{T}\right)^2 e^{\frac{-\Delta_1}{T}} \tag{1.14}$$

For high temperatures $T \gg \Delta$, the dependence $C_S \sim T^{-2}$ is obtained. Let us consider the Schottky heat capacity for a multilevel system. If we consider a system of n-energy levels with energies ε_1 , ε_2, $\ldots \varepsilon_n$, where ε_1 is the energy of the main level. The difference of energies ε_2 , ε_3, $\ldots \varepsilon_n$ with respect to the ground level ε_1 in the general form is written as:

$$\Delta_i = (\varepsilon_{i+1} - \varepsilon_1)/k \tag{1.15}$$

where i = 0,1,2..$(n-1)$. Let g_i be the degeneracy degree of $\varepsilon_{(i+1)}$ level. The statistical sum for such a system will be equal to:

$$Z = \sum_{i=1}^{n-1} g_i e^{-\frac{\Delta_i}{T}} \tag{1.16}$$

Then the molar heat capacity is:

$$C_S = R\frac{\partial}{\partial T}\left(T^2\frac{\partial \ln Z}{\partial T}\right) \tag{1.17}$$

After all transformations the following expression for the Schottky heat capacity in the case of a multilevel system is obtained:

$$C_S = \frac{nR}{T^2}\left[\frac{\sum_{i=1}^{n-1}\Delta_i^2 g_i e^{-\frac{\Delta_i}{T}}}{g_0+\sum_{i=1}^{n-1} g_i e^{-\frac{\Delta_i}{T}}} - \left(\frac{\sum_{i=1}^{n-1}\Delta_i g_i e^{-\frac{\Delta_i}{T}}}{g_0+\sum_{i=1}^{n-1} g_i e^{-\frac{\Delta_i}{T}}}\right)^2\right] \tag{1.18}$$

As is known, the Zeeman effect is observed when a magnetic field is applied to the system of energy levels. There is a removal of degeneracy for degenerate levels and displacement of nondegenerate levels, which in turn leads to a shift of the maximum of the Schottky contribution with increasing temperature, the maximum itself becomes less pronounced. The displacement of the Schottky anomaly under magnetic influence leads to the dependence of heat capacity on the applied magnetic field. Thus, for nonconducting crystals with paramagnetic ion impurities at low temperatures, the Schottky contribution dominates over the lattice contribution, which can lead to a strong magnetocaloric effect (MCE) [**34**; **35**].

1.2 Magnetic entropy

The magnetocaloric effect (MCE) is the release or absorption of heat by a substance, which manifests itself as an increase or decrease in temperature with changes in the external magnetic field under adiabatic conditions [**36**].

The changes in magnetic entropy and MCE can be determined by analyzing the temperature dependences of heat capacity for different magnetic fields [**14**]. The total entropy of a substance in a magnetic field $S(T,H)$ can be calculated as follows:

$$S(t,H) = \int_0^t \frac{C(t,H)}{t}dT + s_0 \tag{1.19}$$

where S_0 is the entropy at $t = 0\ K$ and $C_0(t)$ is the heat capacity at the current temperature t [**40**].

In [**37**] the authors proposed the following equation to calculate entropy from experimental heat capacity data:

$$S(T,H) = \frac{1}{2}\Big\{C(T_1,H) + \sum_{i=1}^{n-1}\left(\frac{C(T_i,H)}{T_i} + \frac{C(T_{i+1},H)}{T_{i+1}}\right)(T_{i-1} - T_i)\Big\} \qquad (1.20)$$

where n is the total number of measured heat capacity points in the temperature range $T_1 - T$, $C(T_i,H)$ is the heat capacity of the sample at temperature T_i in magnetic field H, $C(T_1,H)$ is the contribution to entropy at temperatures below T_1, obtained from the temperature dependences of the total entropy in zero and finite magnetic fields $S(0,T)$ and $S(H,T)$, respectively.

From experimental data for heat capacity in magnetic fields and in zero field, the magnetic contribution to entropy can be calculated as follows:

$$\Delta S = S(T) - S(T_0) = \int_{T_0}^{T}\left(\frac{C(t)}{t}\right)dt \qquad (1.21)$$

If we assume that, $\Delta S_0(T)$ and $C_0(T)$ are the entropy change and heat capacity in the zero magnetic field, and $\Delta S_H(T)$ and $C_H(T)$ are the entropy change and heat capacity in the magnetic field H, then the expression for the magnetic contribution to entropy will be calculated as the difference of entropies in the field H and in the zero field

$$\Delta S_m(T) = \Delta S_H(T) - \Delta S_0(T) \qquad (1.22)$$

For further calculations, formulas 1.21, 1.22 will be used to calculate entropy and magnetic entropy from experimental heat capacity data.

1.3 Measurement methods

The heat capacity of the samples was measured on the system for measuring physical properties of materials *PPMS-9 + Evercool II* manufactured by Quantum Design (USA) in the Resource Centre «Centre for Diagnostics of Functional Materials for Medicine, Pharmacology and Nanoelectronics» of the Research Park SPbU.

The *PPMS* is a sophisticated system for measuring physical quantities. It is equipped with a cryostat with a magnet up to 9 T and a set of electronics that allows to maintain the temperature from 1.9 to 400 K during measurements and to control the magnetic field. Various additional optional modules can be installed to this standard module, which allow measuring various quantities (resistance, heat capacity, thermal conductivity, magnetic susceptibility, etc.), as well as extending the range of operating temperatures [**38**].

Heat Capacity *Heat Capacity (HC) Quantum Design* option was used for the studied samples, which allows heat capacity measurement. In this work, a relaxation microcalorimeter [**39**] was used on a standard calorimetric cell of the Heat Capacity *(HC)* Quantum Design figure 1.2.

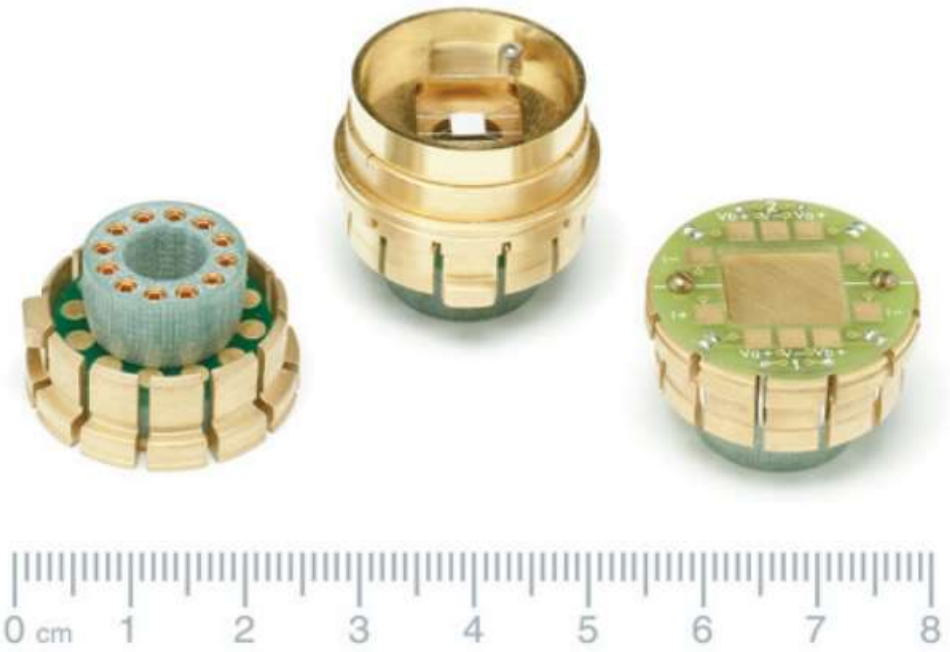

Figure 1.2 — Image of a standard calorimeter cell of the Heat Capacity option *Heat Capacity*.

During the experiments, relaxation curves were analyzed and heat capacity was calculated using *MultiVu* software in automatic mode using the *Two-tau model* ™ *(Quantum Design)* [**38**]. Subsequent analysis of experimental data was performed using *Mathcad* and *OriginPRO* software. The following working ranges were used in the studies: for temperature - from 1,9 to 220 K, for magnetic field - from 0 to 9 T. The standard relative error of measurements did not exceed 5

For measurements, the sample is pre-mounted on the measuring cell platform. The measuring cell has a *Cernox Lake Shore Cryotronics* thermometer (see 1.3)

built into the platform, which requires pre-calibration in working magnetic fields to reveal the dependence of resistance on the magnetic field [**41**]. Also preliminary for each sample it is necessary to measure the hardware function (*addenda*) for its further consideration in measurements of heat capacity of the figure 1.3.

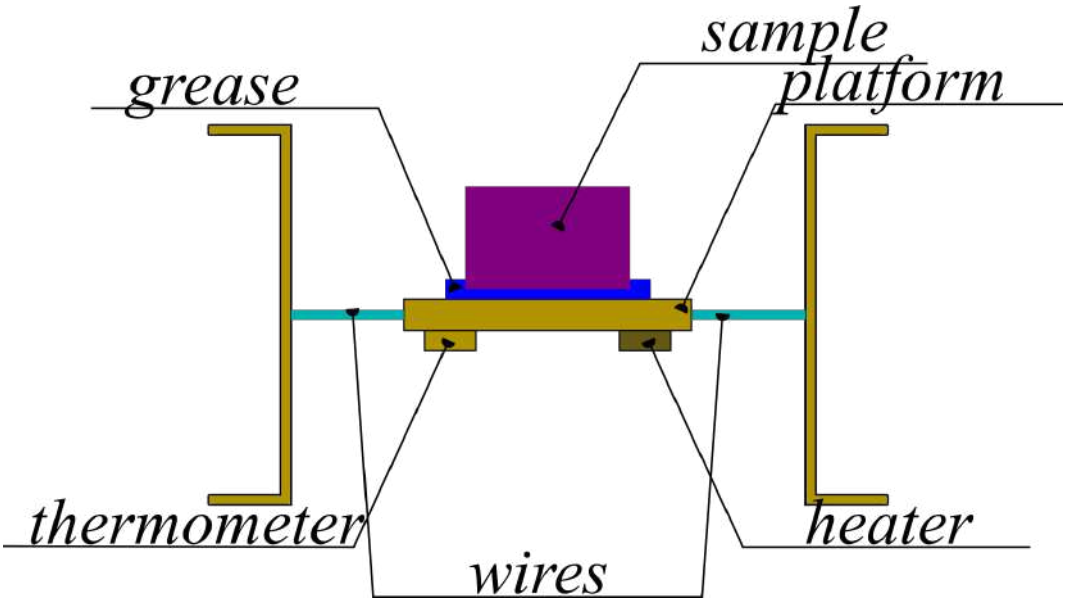

Figure 1.3 — Schematic representation of a heat capacity measuring cell with a sample installed. Eight thin thermally conductive wires suspend the sample platform in the middle of the cell, through which the thermometer and heater are connected. The sample is held on the platform by grease. The lubricant also provides thermal contact between the specimen and the platform and "smooths out"irregularities in the adjacent edge of the specimen.

During the studies, *Apiezon N* vacuum grease, which is standard for low-temperature measurements, was used to fix the sample. This grease has its own heat capacity anomalies at temperatures above 220 K [**42**], which determined the choice of the upper boundary of the operating temperature range. Dependences of the heat capacity of the cell and grease on the magnitude of the magnetic field were absent. For the studied samples, the heat capacity of the measuring cell (the largest contribution to which was made by the cell platform) with the applied *Apiezon N* grease (volume of about 1 mm^3) was used as a hardware function.

After preliminary measurements (without sample), the sample is mounted on the platform. It is important to make sure that the amount of lubricant on the platform does not change during mounting, otherwise the value of the hardware function may change. Then the cell with the sample is placed in the helium-filled chamber of the instrument and a vacuum of the order of 10^{-5} Torr is created. During

measurements in magnetic fields, the field was applied perpendicular to the platform plane, collinear to the crystallographic planes of the studied crystals, the directions of which were previously determined by X-ray phase analysis.

During the measurement process, the temperature of the sample and the cryostat are first equalized. Then a current pulse (heating pulse) is applied to the heater, which is attached to the cell platform, after which the thermometer response is recorded as a function of time

If we assume that there are no thermal losses at the contact between the sample and the platform, the temperature dependence on time is determined by a simple heat balance equation:

$$C_{tot}\frac{dT_p}{dt} = K_W(T_p - T_b) + P(t) \tag{1.23}$$

here C_{tot} is the total heat capacity of the platform with the sample, T_p is the temperature of the platform, K_W is the total thermal resistance of the wires on which the platform is suspended, T_b is the temperature of the cryostat, $P(t)$ is the applied power as a function of time.

At non-ideal thermal contact between the sample and the platform, the temperature of the sample T_S and the platform T_p during the pulse passage may differ and the thermal balance is described by a pair of equations:

$$C_S\frac{dT_S}{dt} = K_{sp}(T_p - T_b) \tag{1.24}$$

$$C_p\frac{dT_p}{dt} = K_g(T_p - T_b) - K_W(T_p - T_b) + P(t) \tag{1.25}$$

here K_g is the thermal conductivity coefficient between the sample and the grease. Rectangular pulses of power $P(t)$ are applied to the heater, the duration and amplitude of which are known. Figure (1.4) shows a typical response curve. The process of heating and cooling of the platform and the sample is similar to charging and discharging of a capacitor in an RC-circuit when a rectangular current pulse passes through it.

In the case of ideal thermal contact, the time dependence of the platform temperature is an exponential dependence:

$$T(t) = \begin{cases} T_{on}(t) = \dfrac{P_0\tau(1 - e^{-t/\tau})}{C_{tot}} + T_b; & (0 \leqslant t \leqslant t_0) \\ T_{off}(t) = \dfrac{P_0\tau(1 - e^{-t/\tau})e^{-(t-t_0)/\tau}}{C_{tot}} + T_b; & (t > t_0). \end{cases} \tag{1.26}$$

in the heating and cooling regions, respectively, where the time constant $\tau = C_{tot}/K_W$. Thus, by approximating the experimental relaxation curves, the temperature dependence of the time constant can be determined. For the case of non-ideal contact the solution has a more complicated form, there appear two characteristic times of equilibrium establishment τ_1 (between the platform and the sample) and τ_2 (between the platform and the cryostat). Then, having found the dependence of the thermal contact resistance on temperature and the dependence of the platform heat capacity on temperature, we can find the heat capacity of the sample [**43**].

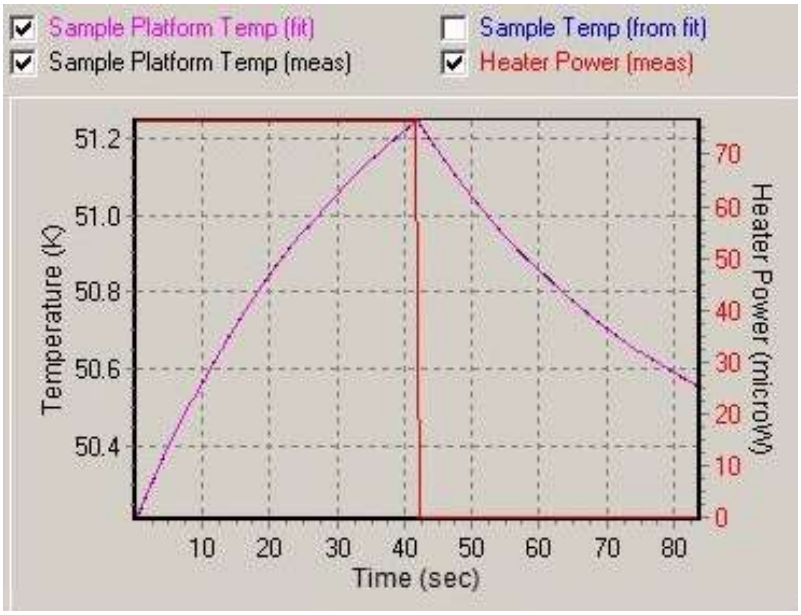

Figure 1.4 — Example of thermometer response curve for heat capacity measurement by relaxation method [**38**].

1.4 Structure and physical properties of pentaphosphates

Since their inception, lasers, in particular solid-state lasers, have been of great interest both scientifically and practically. Thanks to the development of microelectronics, the size and weight of their electronic assemblies have been significantly reduced, making it possible to create portable electro-optical devices for various applications. Such devices include laser rangefinders and levelers, devices for analyzing the composition of the environment, and medical diagnostic devices. Realization of these technologies with the development and improvement of

microelectronics has caused an urgent need in creation of miniature laser radiation sources based on semiconductor lasers and solid-state lasers with pumping by laser diodes. To solve this problem, the research of physical properties of active media of laser radiation sources and the search for optimal functional materials has been actively carried out [**21**; **44**].

Since the beginning of the development of laser electrical engineering, it has been noted that it is most appropriate to use a substance with rare-earth ion impurities as an active medium [**21**]. In the case of small-size solid-state lasers, crystals or glasses doped with rare-earth ions (Nd^{3+}, Er^{3+}, Ho^{3+}, Ce^{3+}, Tm^{3+}, Pr^{3+}, Gd^{3+}, Eu^{3+}, Yb^{3+}, Sm^{2+}, Dy^{3+}, Tm^{2+}) were of most interest. The main problem in selecting the activator ion is that to increase the gain, the concentration of active particles must be increased, which leads to concentration quenching of luminescence. Over the last 35 years, neodymium ions have remained the most common activator ions. The first microlasers based on highly concentrated neodymium crystals NdP_5O_{14}, $LiNdP_4O_{12}$, and $NdAl_3(BO_3)_4$ were developed back in the 1970s [**45**]. Due to the crystal structure of these compounds, concentration quenching at high neodymium concentrations was not observed, which made it possible to achieve large enhancement factors [**44**].

Crystals with high concentrations of active particles $\sim 10^{21} - 10^{22}$ cm^{-3} are required to create microsized solid-state lasers [**46**]. In the case of yttrium aluminum garnet $Y_3Al_5O_{12}$ with an admixture of niodymium *Nd:YAG*, when the neodymium concentration increases above 10^{19} cm^{-3}, a sharp drop in the probability of radiative transitions ${}^4F_{3/2} \rightarrow {}^4I_j$, an increase in the generation threshold, and a strong drop in the efficiency are observed. This problem has led to the necessity to find such crystals in which the crystal electric field strength is minimal in the lattice nodes where neodymium ions are located. In this case, the maximum frequency of crystal lattice vibrations should be small enough to exclude the possibility of resonance of electronic transitions. Studies have shown that in order to reduce the energy splitting of ${}^4I_j$ multiplets, neodymium ions in the crystal lattice should be surrounded by oxygen ions. This kind of structure is characteristic of phosphate, borate, tungstate and other groups. It was also noted that in such crystals the Stark splitting is significantly smaller than in *YAG* crystals.

Among the crystals whose lattice nodes can contain an active neodymium ion, the most suitable are low-symmetric structures in which the maximum phonon energy is low. Such crystals are the most promising for the creation of microscale

lasers, in particular, neodymium pentaphosphate NdP_5O_{14} is of great interest. Rare - earth pentaphosphates are well known as "pure"or stoichiometric active laser materials.

It should be noted that studies of the crystal structure for single-crystal rare-earth pentaphosphates conducted by different authors did not agree with each other at first. In 1969 Jaulmes [**47**] concluded that LaP_5O_{14} has an orthorhombic lattice (lattice symmetry group P_{nc2} or P_{ncm}). In 1970 Bagieu-Beucher and his colleagues [**48**] studied a number of elements from lanthanum to lutetium and showed that these elements form compounds with three different types of crystal structure. The first type from lanthanum to terbium (La, Ce, Pr, Nd, Sm, Eu, Gd and Tb) was monoclinic with lattice symmetry group $P_{21/a}$. The second type of elements (Tb, Dy, Ho, Er, Tm, Yb, Lu) was also monoclinic with space group C_c or $C_{2/c}$. The third group (Dy, Ho, Er) had rhombic cells and corresponded to the symmetry group $P_{c21/m}$ or P_{cmn}.

Danielmeyer and Weber [**49**] also studied NdP_5O_{14} and found that this pentaphosphate has a rhombic crystal structure. Albrand and co-workers [**50**] found a pseudoorthorhombic structure (space group $P_{21/c}$) for NdP_5O_{14} . This latter result is consistent with the conclusions drawn by Danielmeyer and Weber [**49**], but is not consistent with those of Bagier-Beuel [**48**]. Albrand and coworkers proposed that NdP_5O_{14} can be grown in different structural modifications that are determined by the crystal growth temperature, which explains the inconsistency of the data for NdP_5O_{14}. In [**51**], the results of electron paramagnetic resonance studies for samples of pentaphosphates GdP_5O_{14} and EuP_5O_{14}, were presented. It was obtained that gadolinium pentaphosphate has a strongly anisotropic structure, with the observed line widths not allowing a detailed analysis of the local symmetry of gadolinium. The authors calculated the parameters of the spin Hamiltonian and calculated the g - factors at $T = 300$: $g_x = g_y = g_z = 1.995 \pm 0{,}005$.

In addition to the promising application of pentaphosphates in laser electrical engineering, there are other applications of these materials. In general, pentaphosphates are most in demand for the production of fluorescent lamps, plasma panels, luminescent materials, etc. [**49**; **52**; **53**].

In addition to various optical properties, rare-earth metaphosphate compounds exhibit interesting magnetic properties. In [**54**], the magnetic susceptibility of single crystal GdP_5O_{14} was measured using a $SQUID$ magnetometer in the field

of 1,000 Oe. Figure 1.5 shows the temperature dependence of the molar magnetic susceptibility and its inverse.

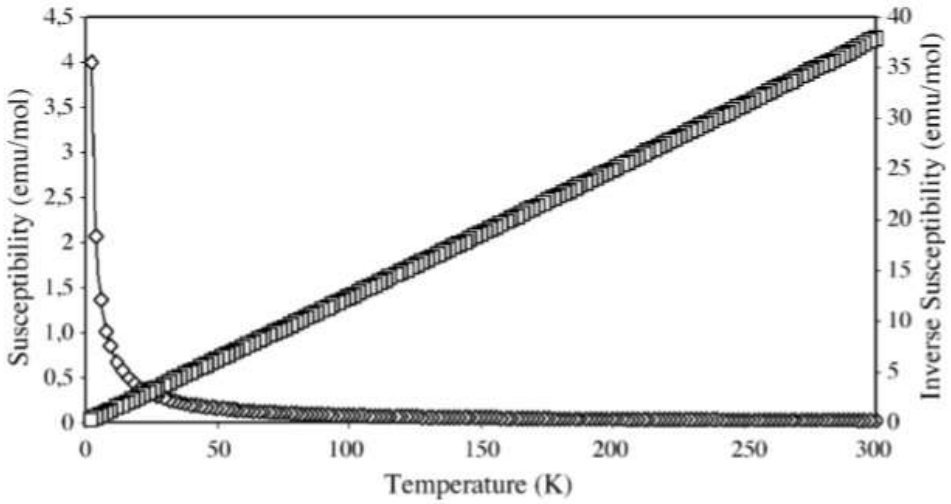

Figure 1.5 — Magnetic susceptibility and its inverse for GdP_5O_{14} as a function of temperature GdP_5O_{14} [**54**].

As can be seen from the results presented in [**54**], the variation of the inverse susceptibility for this material obeys the Curie law. It was found that GdP_5O_{14} is characterized by paramagnetic behavior in the temperature range from 2 to 300 K.

In [**52**], measurements of magnetic susceptibility and magnetization from temperature were carried out for a series of RP_5O_{14} pentaphosphates (R=Nd, Sm, Gd). These results are presented in Figures 1.6, 1.7.

Magnetic susceptibility measurements were carried out in the temperature range from 5 to 350 K at 1,000 Oe using a *Quansum Design MPMS 5 SQUID* magnetometer. Experiments to measure the field dependence of the magnetization were performed in *VSM* mode when a magnetic field up to 6 T was applied at a constant temperature of 2 K. The authors note that all the studied compounds are paramagnetic.

As noted earlier, in addition to the use of crystalline substances, glassy media, which have a number of advantages over crystals, have great potential.

It is known [**55**] that glasses are characterized by two main temperature anomalies, which are universal for all representatives of the amorphous type. First, glasses have a large value of heat capacity compared to the Debye heat capacity; as a rule, this feature is manifested as a peak in the temperature dependence of C/T^3. The second anomaly is the plateauing of the temperature dependence of thermal conductivity $\lambda(T)$ at $T < 10$ K [**56**].

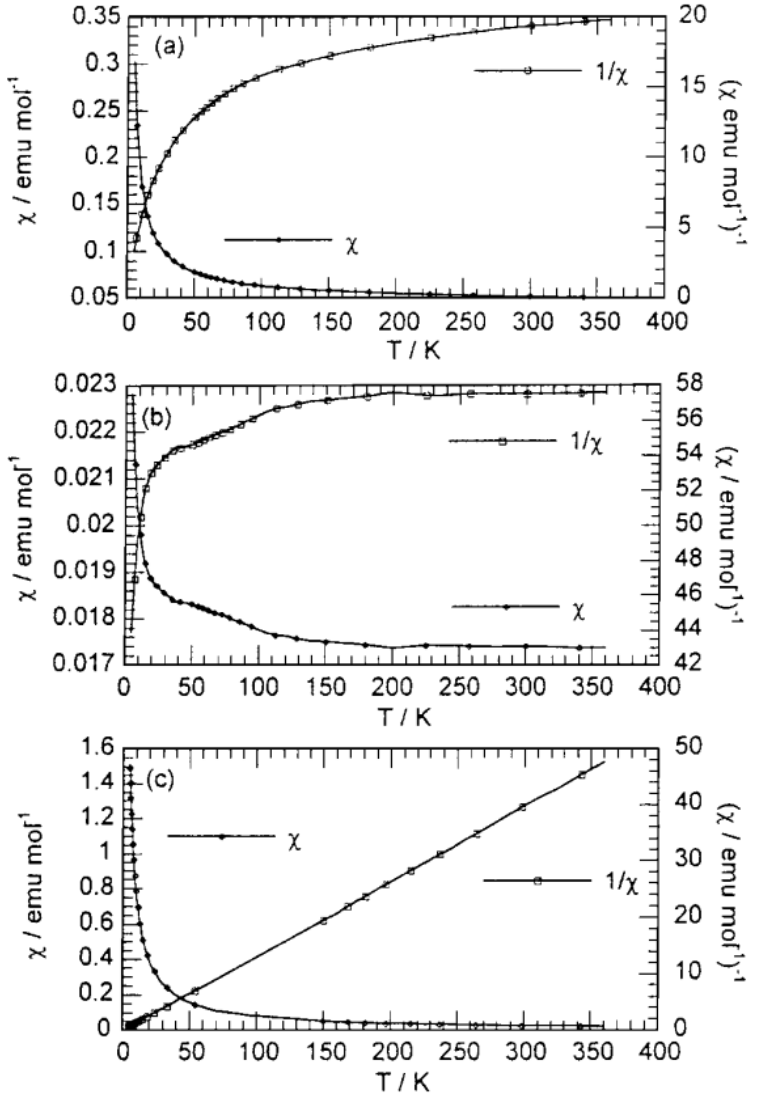

Figure 1.6 — Magnetic susceptibility and inverse magnetic susceptibility as a function of temperature for (a) NdP_5O_{14}, (b) SmP_5O_{14}, (c) GdP_5O_{14} [**52**].

Various phenomenological models have been developed to explain the anomalous behavior of the thermophysical properties of the amorphous state. These models use a number of low-energy elementary excitations for description: two-level systems (TLS) [**12**; **57**] responsible for the properties at $T < 1$, relaxation systems (RS) [**58**] and low-frequency quasi-local vibrational modes [**59**], which are responsible for the formation of plateaus at $T < 10$.

In [**60**], the value of heat capacity for solid alcohols existing in both crystalline and amorphous states was determined. In the amorphous state, the onset of a broad bosonic peak is observed at $T \approx 3$ K, while in the crystalline state – at $T > 10$ K. For crystalline structures, this is due, in the authors opinion, to the "unfreezing"of phonons of narrow optical modes, the contribution to the heat capacity from which can be described as the contribution from Einstein oscillators; similar results were

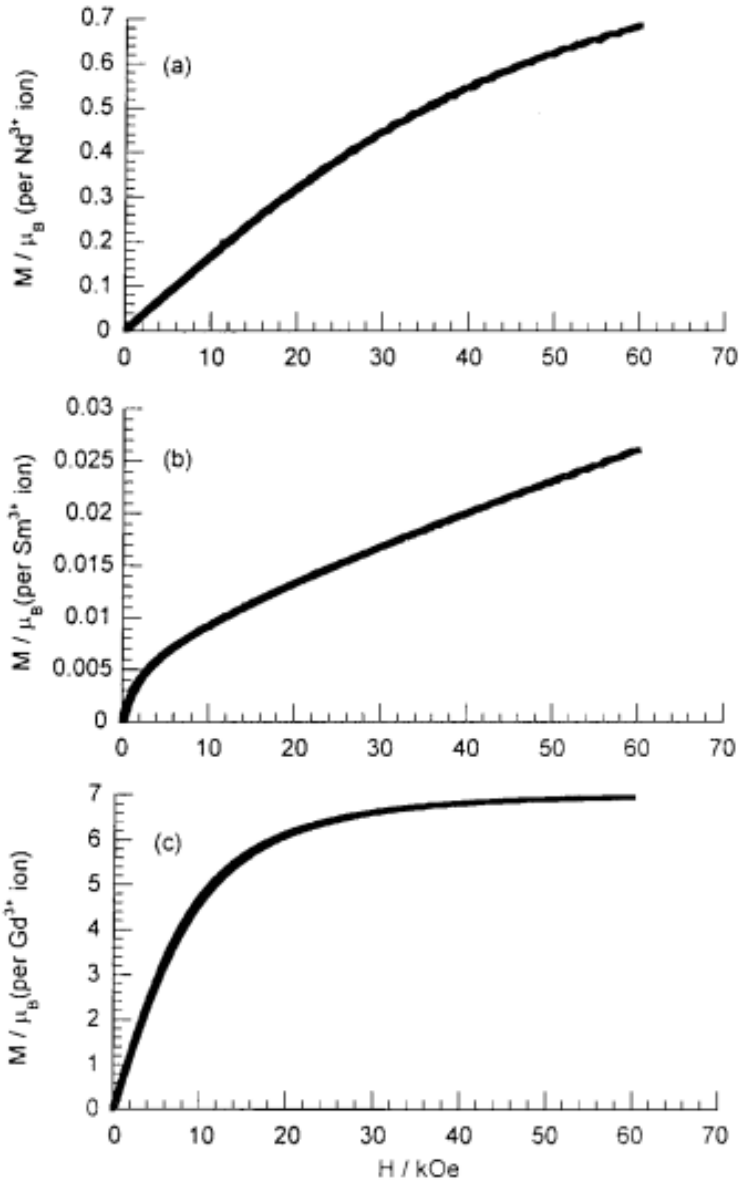

Figure 1.7 — Dependence of magnetization on the magnetic field magnitude at T=2K for (a) NdP_5O_{14}, (b) SmP_5O_{14}, (c) GdP_5O_{14} [**52**].

observed in [**56**]. The results obtained by the authors are presented in Figure 1.8. It can be seen from the figure that the peak of the temperature dependence of the heat capacity in the C/T^3 representation in amorphous structures is shifted to lower temperatures compared to single crystals.

In [**61**], the heat capacity of NdP_5O_{14} and PrP_5O_{14} in the temperature range of 385–440 K. K was measured using a differential scanning calorimeter. The results showed a non-standard behavior of the heat capacity, the temperature dependence of which was not monotonic in this range, but had a ridge-like appearance (1.9). Two peaks could be distinguished in this section for both compounds. The authors

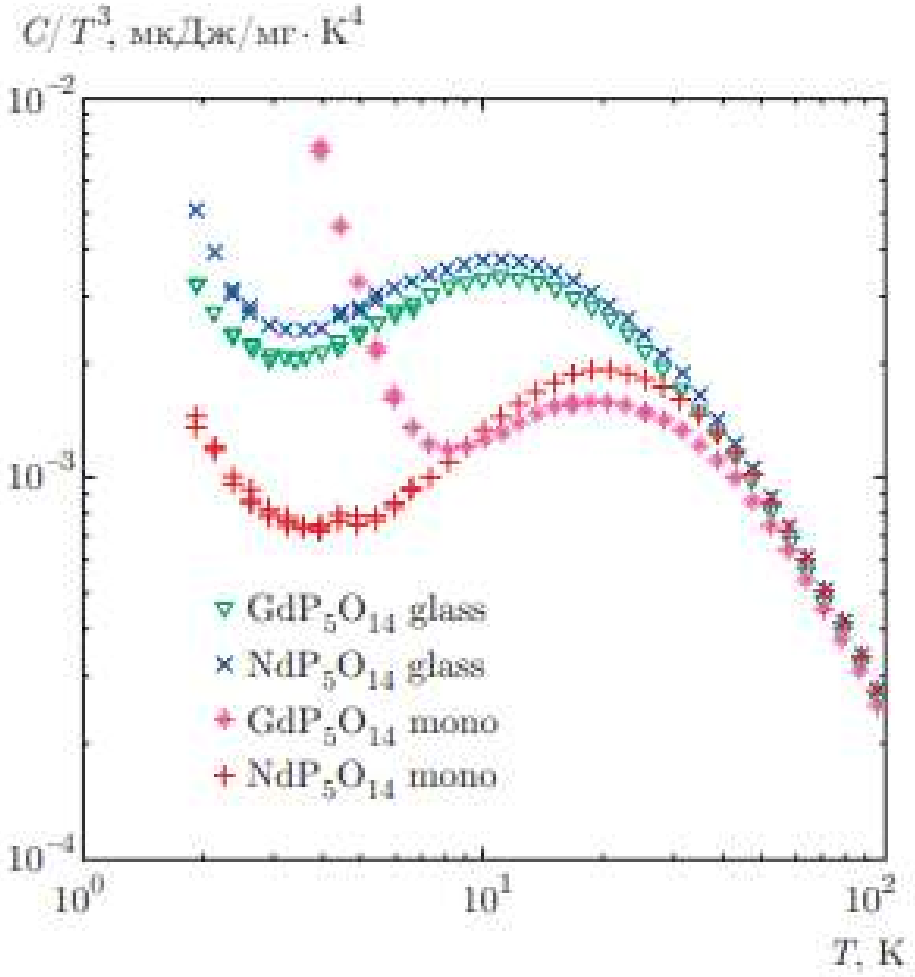

Figure 1.8 — Temperature dependences of heat capacity of single crystals (mono) of pentaphosphates and glasses (glass) of similar composition [**56**].

correlated this behavior with deformation effects arising due to the segmental elastic nature of the materials under consideration.

The authors determined the temperatures of the segmentoelastic phase transition, for NdP_5O_{14} and PrP_5O_{14} they amounted to 426.5 K and 416.5 K, respectively. The peaks of the temperature dependence of the heat capacity were located near the phase transition temperatures. In addition to unique thermal properties, amorphous materials also possess interesting magnetic features. As a consequence, studies of magnetic glasses are of both fundamental interest and have wide potential applications in laser and optoelectronic engineering. In general, the doping impurity of a rare-earth element included in the glass matrix provides the structure of electronic energy levels necessary for nonlinear optical devices.

It is noteworthy that in order to understand and use the magnetic and magneto-optical properties of rare-earth metaphosphate samples, it is necessary to have an idea of the local structure of the materials, since the environment of rare-earth ions is

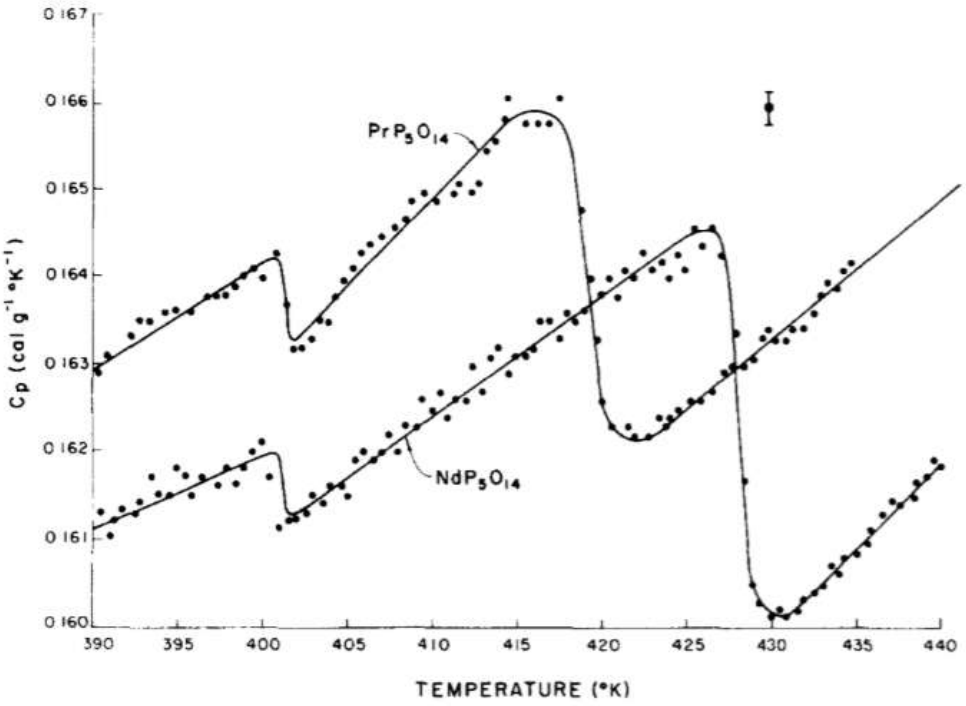

Figure 1.9 — Specific heat capacity of NdP_5O_{14} and NdP_5O_{14} at segmentoelastic phase transitions [**61**].

associated with optical absorption and fluorescence. In [**62**], the unit cell constants of cerium pentaphosphate were determined from X-ray diffraction analysis data. The authors note that such a compound crystallizes in a monoclinic system with the following cell parameters: $a = 8.80(2)$ Å; $b = 9.07(10)$ Å; $c = 13.11(12)$ Å. According to the obtained IR and Raman spectra, the structural environment of atoms was analyzed.

The effect of high pressure and low temperature on the fluorescence spectra of glass of composition $(Sm_2O_3)_{0.248}$ $(P_2O_5)_{0.752}$ and crystalline SmP_5O_{14} was analyzed in [**63**]. It was found that the fluorescence spectrum of samarium in the crystal contains five groups of well separated bands. The number of lines in each band indicated a cubic local symmetry. It was also found that when the crystal temperature decreased below 12 K, some of the fluorescence lines at short wavelengths in each band disappeared. The authors suggested that this is due to a decrease in the population of higher energy levels.

To summarize, it can be noted that despite the widespread popularity and interest in pentaphosphates, the representatives of these compounds are still poorly studied. To date, quite a lot of information on the structure of rare-earth pentaphosphates has been accumulated. There are also some data on the magnetic properties of these materials. However, there have been very few studies of the

heat capacity behavior of pentaphosphates, both for crystals and amorphous forms. There are no data on the effect of magnetic fields on the magnitude of heat capacity for such compounds in the literature, which served as a strong argument in favor of a comprehensive study of the heat capacity of representatives of rare-earth pentaphosphates of crystalline and amorphous forms in different magnetic fields.

1.5 Heat capacity and magnetic properties of rare-earth garnets and aluminates

Aluminum garnets doped with various rare-earth ions with the general chemical formula $RE_3Al_5O_{12}$ (where RE - rare-earth ions) are widely used in laser technology and as phosphors [**21**]. In recent years, much attention has been paid to establishing the possibilities of using these materials in other applied technical fields, for example, as low-temperature magnetic refrigerators. The most common methods in the study of this class of compounds are optical and X-ray studies. It should not be overlooked that the study of thermodynamic properties has previously been carried out only superficially for a limited number of garnets, despite the fact that these studies have a pronounced practical interest [**37**].

Among the investigated rare earth element garnets, as noted earlier, $Y_3Al_5O_{12}$ (YAG) is one of the most studied compounds to date.

YAG is a material with a cubic crystal structure with high chemical stability and excellent optical and thermomechanical properties. This material is optically homogeneous and its thermal expansion is isotropic. The results of numerous studies have shown the promising use of these materials in various applications, in particular, it is used in solid-state lasers, as luminescent materials and scintillators [**21**; **64**]. The relatively high phonon energy of yttrium-aluminum garnets makes it possible to use them as a carrier matrix for various rare-earth metals, which makes it possible to obtain materials with improved optical properties.

Yttrium-aluminum garnets doped with transition metals or lanthanide elements are actively used as solid-state laser materials, in luminescent systems [**64**]. These compounds have good optical and thermal properties and are promising for application in high-power LED devices [**65**; **66**; **67**].

Two most promising applications can be identified for YAG containing the trivalent ion dysprosium Dy^{3+} [**68**]. The first is the possibility of use as an alternative material in optical amplifiers in optical fiber transmission lines instead of YAG with praseodymium. The second promising area is the application in solid-state lasers operating in the visible spectral range [**69**]. In particular, Dy-doped YAG emits blue (470-500 нм) and yellow (570-600) light when excited with ultraviolet light, which makes it a potential white-light phosphor.

In [**70**], the dependence of the heat capacity of pure and yttrium-doped dysprosium-aluminum garnet near the Neel temperature T_N was obtained. No pronounced influence of yttrium doping was found in dysprosium-aluminum garnet. However, the authors of the paper found that the heat capacity peak is unusually rounded, which may mask subtle effects of doping. The authors believe that the rounding of the peak is due to the small size of yttrium particles.

In [**71**], the authors used YAG with 30% substitution of Y ions by Er ions for cooling of X-ray detectors. Figure 1.10 shows the temperature dependences of the heat capacity of the studied garnets in the ranges of magnetic fields of zero to 8,000 Oe.

The results obtained in [**71**] showed that in the absence of a constant magnetic field ($B = 0$), a maximum in the region of 266 mK is observed on the temperature dependence of the heat capacity of the studied garnet (1.10 a). The nature of this behavior was associated with the presence of a local magnetic field formed by neighboring atoms, in connection with which the temperature dependence of the heat capacity shows a blurred peak due to the Schottky contribution from the split Kramers duplet of the ground state of the $4^I_{15/2}$ multiplet. In the range of magnetic fields from 0,5 to 8 T, the temperature dependences of heat capacity were characterized by one main peak (Figure 1.10 b). The dependences obtained by the authors were described by the sum of two contributions: lattice and Schottky contributions from the Kramers duplex split by the external magnetic field. The position of the heat capacity maximum T_{max} was proportional to the magnitude of the magnetic field applied to the sample, which corresponds to the Zeeman effect.

Temperature dependences of the heat capacity of $Y_3Al_5O_{12}$ garnet without additional impurities were investigated in [**72**] (Figure 1.11).

As can be seen from the graph, the heat capacity increases smoothly from 0 to 420 K without anomalies. The authors approximated the experimental data in the temperature region above 20 K by the function $C_p = \alpha T^3$ and obtained

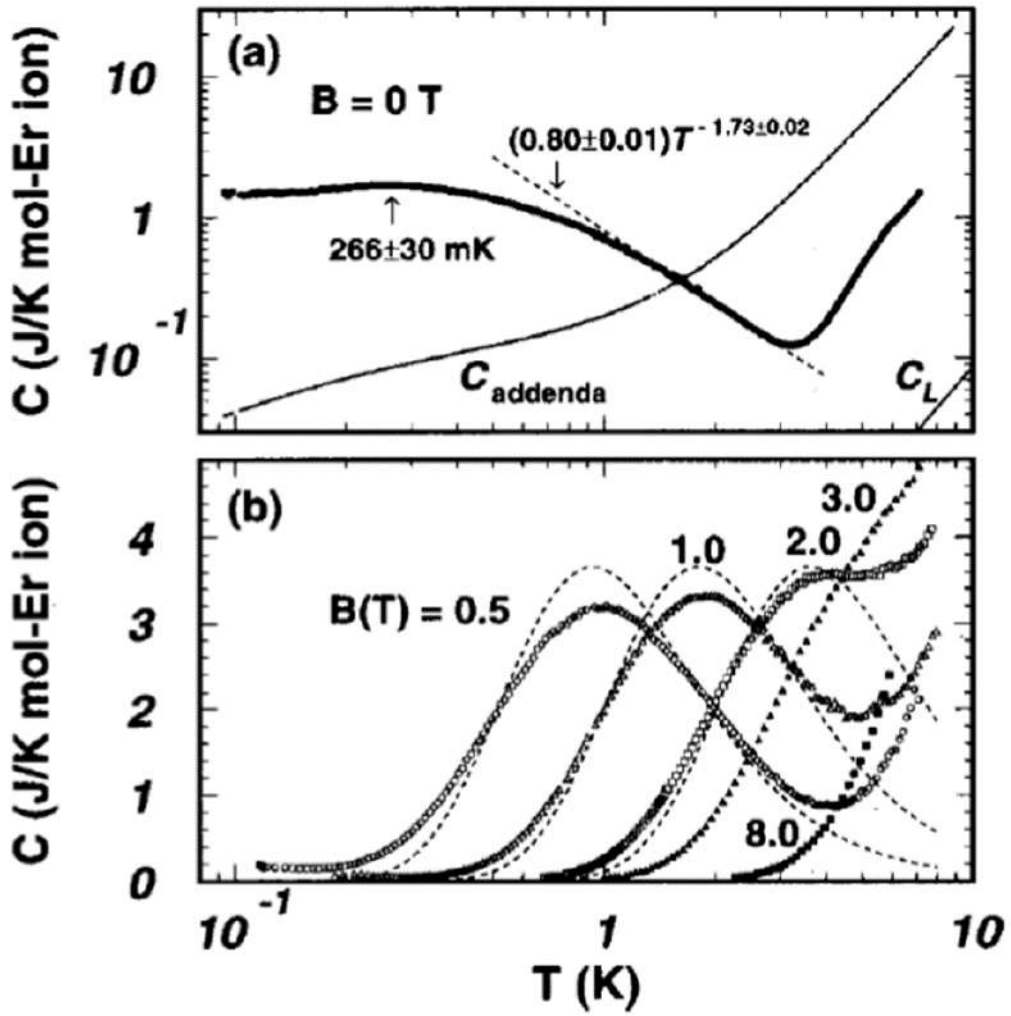

Figure 1.10 — Temperature dependence of heat capacity in mixed yttrium-herbium garnet. (a) Heat capacity at zero magnetic field, C_L is the phonon contribution, $C_{addenda}$ is the hardware function of heat capacity, which is subtracted from the data. (b) Heat capacity at magnetic fields from 0.5 to 8.0 T. The dotted lines are the sum of the Schottky and lattice heat capacity contributions [**71**].

$\alpha = 0.219 \times 10^{-3}$ J*K/Mol. It was also noted that YAG without impurities has diamagnetic properties [**73**].

YAG doped with erbium and neodymium ions can be applied to create a low-temperature cooler operating using the adiabatic demagnetization phenomenon [**73**; **74**].

In [**22**], experimental dependences of heat capacity in a zero magnetic field, as well as experimental dependences at different values of the magnetic field from 0 to 9 T for erbium-yttrium garnets with the formula $Er_xY_{3-x}Al_5O_{12}$ (where $x = 0; 0.6; 1.1; 3$) are presented in Figure 1.12. In crystals containing erbium

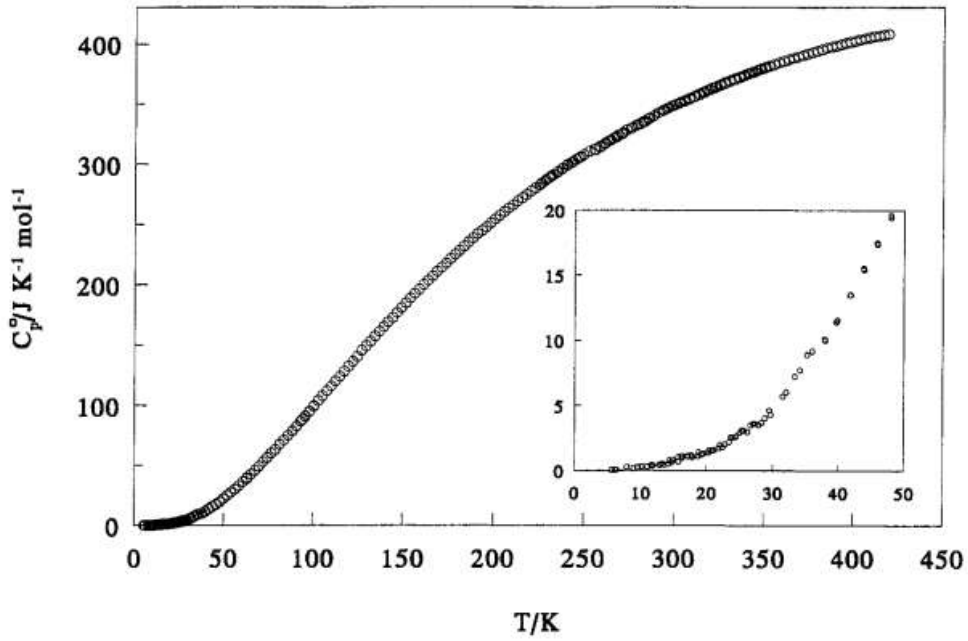

Figure 1.11 — Experimental heat capacity curve for $Y_3Al_5O_{12}$ without impurities [**72**].

($x = 0.6; 1.1; 3$) in the low-temperature region ($T < 5$ K) an increase in heat capacity with decreasing temperature was observed.

The value of heat capacity was approximated by the sum of Debye, Einstein, and Schottky contributions [**22**; **75**]. It was noted that the Schottky contribution dominates at low temperatures for all garnets with magnetic ions. Magnetic fields up to 9 T shifted the Schottky anomalies to high temperature. From the obtained experimental dependences of the heat capacity of garnets, the authors calculated the entropy and isolated the magnetic contribution to the entropy [**22**; **76**]. The authors note the presence of a significant magnetocaloric effect in $Er_{1.1}Y_{1.9}Al_5O_{12}$ garnet, which allows the future use of this material in low-temperature magnetic refrigerators when operating in the adiabatic demagnetization regime.

In the temperature range below 20 K, the thermodynamic Carnot cycle and paramagnetic materials are commonly used. Some success was achieved using gallium-gadolinium garnet and dysprosium-aluminum garnet [**77**].

Gallium-gadolinium garnets $Gd_3Ga_5O_{12}$ (GGG) are among the most well-known and widely used rare-earth garnets [**21**]. GGG single crystals are mainly used as optical and magneto-optical elements, substrates, and in the jewelry industry. GGG crystals, as well as YAG crystals, have been proposed as materials for magnetic refrigerators based on the magnetocaloric effect [**78**] due to the significant magnitude of the magnetic entropy.

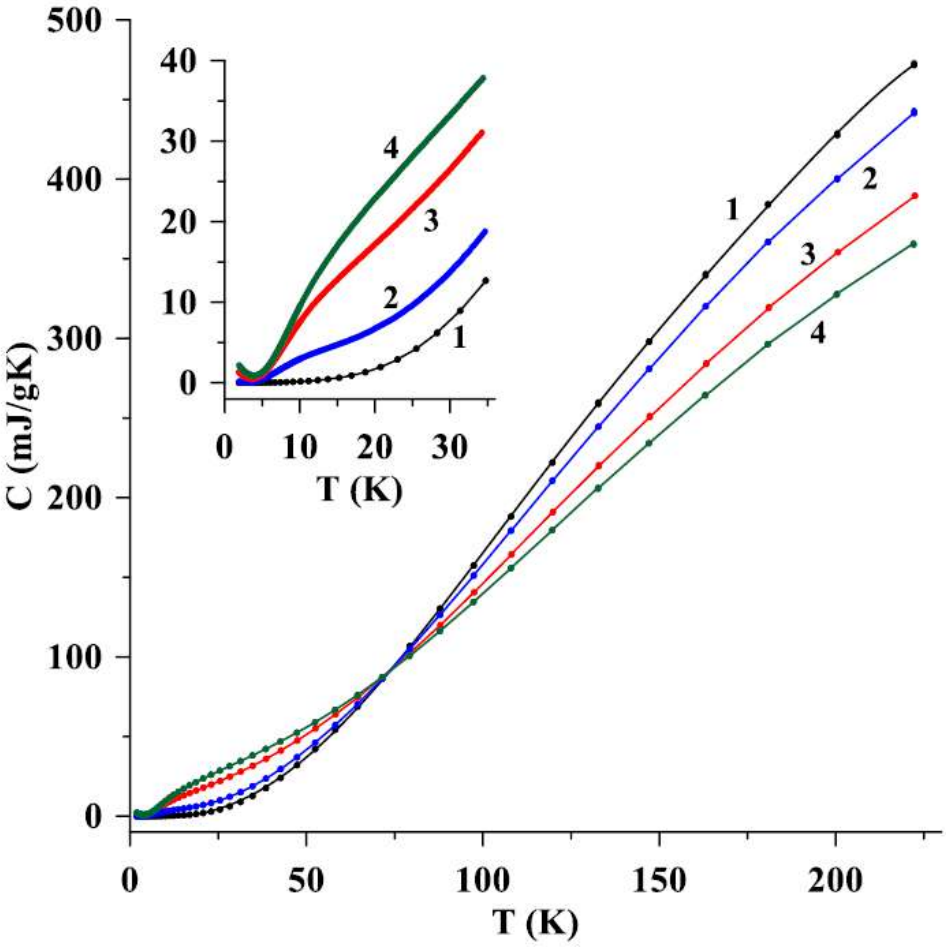

Figure 1.12 — Temperature dependences of heat capacity of garnets $Er_xY_{3-x}Al_5O_{12}$ in a zero magnetic field. Numbers 1, 2, 3, 4 in the figure denote the dependences for $x = 0; 0.6; 1.1; 3$, respectively. The inset shows the value of heat capacity in the interval from 1.9 to 32 K [**22**].

The first detailed studies of the low-temperature properties of *GGG* in a magnetic field were carried out by Prof. Schiffer's group [**79**]. During the experiments, low-temperature dependences of heat capacity in different magnetic fields were obtained (see figure 1.13). The authors noted the presence of a broad peak in the temperature region below 1 K. It was found that at the phase transition from antiferromagnetic to paramagnetic state there is a sharp jump in the value of heat capacity at a transition temperature of 0.375 K in the field 1 T. This jump was not observed far from the phase transition region.

Later, S.R. Dansiger and coworkers conducted similar studies of the heat capacity value in *GGG* [**80**]. The obtained dependences repeated the results of Prof. Schiffer's group. A broad peak was also observed in the zero field (Figure 1.14). At 0.9 and 1.0 T magnetic fields, characteristic peaks were observed as before. To analyze the heat capacity in a zero magnetic field, the authors suggested analyzing

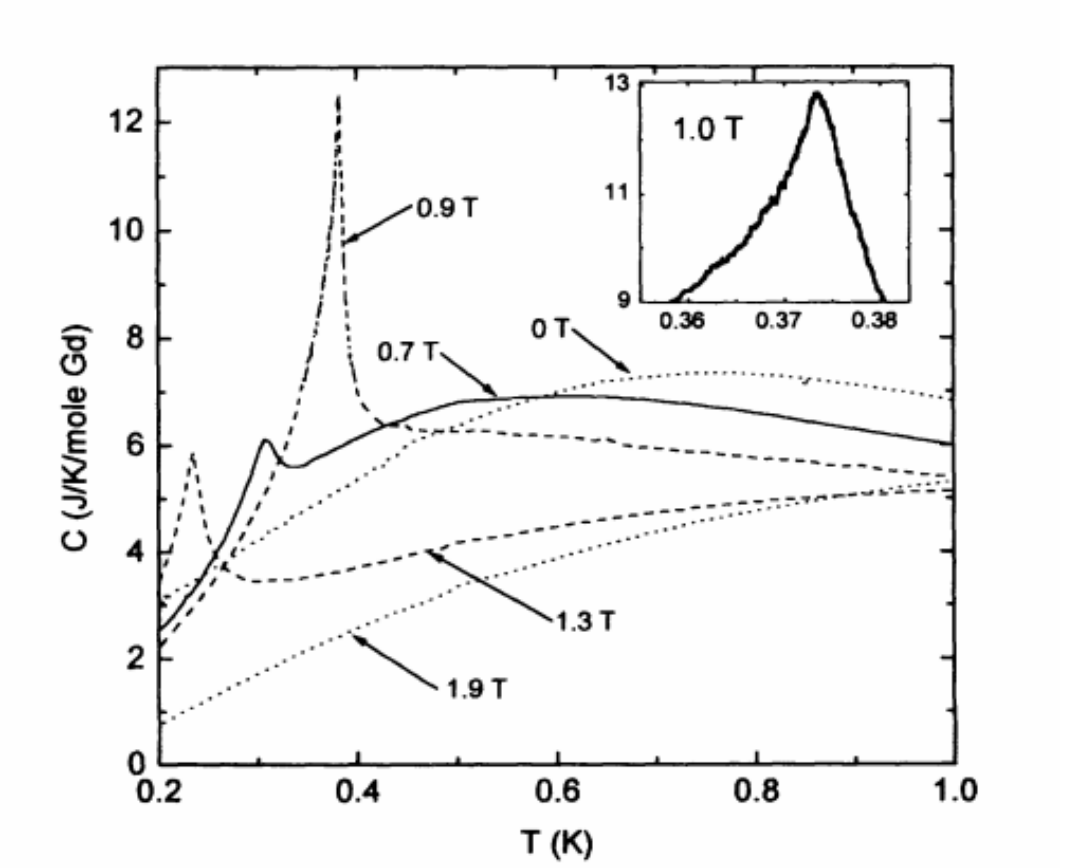

Figure 1.13 — Specific heat capacity of GGG at several magnetic fields. The inset shows the critical behavior at 1 T[**79**].

the temperature dependence of C/T rather than C. The results showed the presence of an additional peak in the region of 0.37 K.

Further studies of the heat capacity of GGG, which were carried out in a wider temperature range (up to 30 K), also showed the presence of a peak [**81**]. The authors note that the specific heat C for GGG at 0 T shows a sharp increase at temperatures below 5 K, but no peak associated with magnetic ordering is observed up to 0.9 K. After 10 K, the heat capacity at 0 T increases with increasing temperature (Figure 1.15).

In a number of later works, it was shown that different substitution variants in the GGG lattice of both gadolinium and gallium ions can lead to some enhancement of the magnetocaloric effect [**81**; **82**; **83**]. In [**82**], it was shown that the change in magnetic entropy of $Gd_3Ga_5O_{12}$ is enhanced by replacing the Gd^{3+} ion with a Dy^{3+} ion for magnetic fields greater than 2 T in the range from 0,5 to 5 K. The authors explain this by the fact that the Dy^{3+} ion is characterized by a strong anisotropic magnetic interaction.

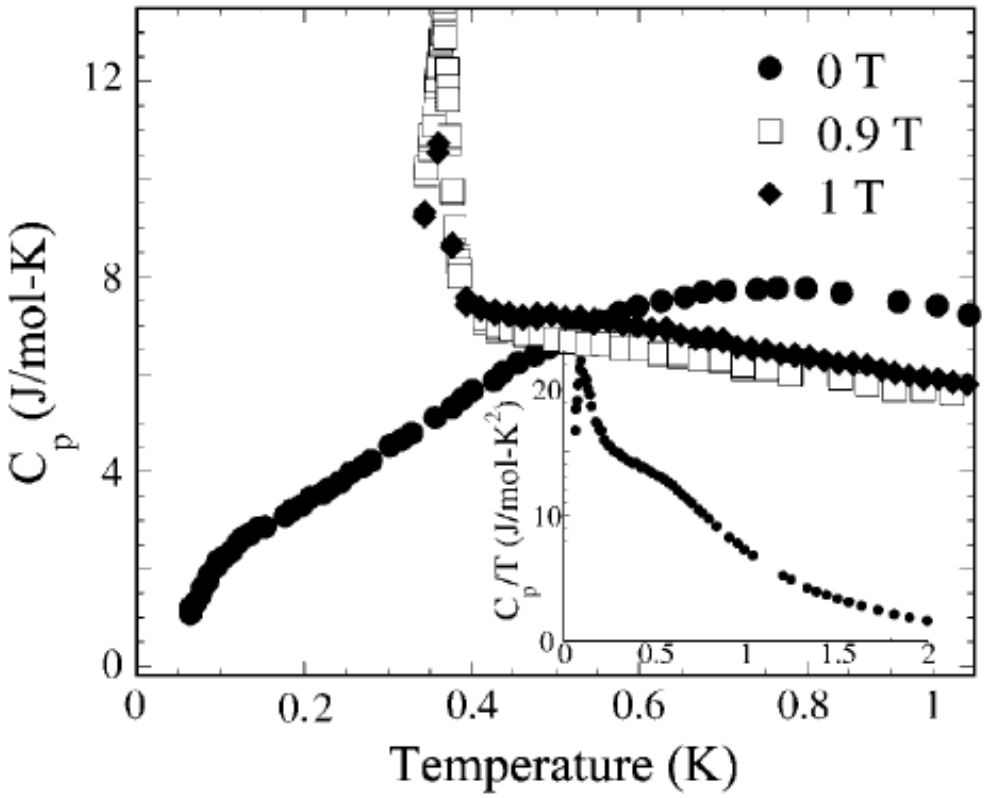

Figure 1.14 — Specific heat capacity of GGG as a function of temperature in magnetic fields of 0, 0.9, and 1 T. The inset shows the temperature dependence of C/T [**80**].

In [**84**], the authors, using the self-consistent field method, revealed that $RAlO_3$ orthoaluminates (perovskites) are superior to RAl_5O_{12} garnets in cooling capacity in the whole range of magnetic fields from 10 to 50 kOe. This phenomenon is explained by both the higher concentration of RE ions and the larger magnetic moments.

In [**85**], single crystals of Ce^{3+} – doped $YAlO_3$ containing other trace elements such as Er^{3+}, Nd^{3+} ,Cr^{3+}, Fe^{3+} were studied by electron paramagnetic resonance (EPR). The EPR measurements were carried out at 9.204 Hz on a standard spectrometer in the temperature range from 4 to 77 K. The obtained spectra are well described by the spin Hamiltonian of rhombic symmetry

$$\mathcal{H} = S \cdot gB + S \cdot A \cdot J$$

where S is the effective spin $S = 1/2$, J is the nuclear spin, B is magnetic field.

The main values of g - tensors were determined from analyzing the angular dependences of EPR spectra. For the value of the average g - factor, the authors obtained the value: $\langle g \rangle = (g_x + g_y + g_z)/3 = 6.61$, which is in good agreement with

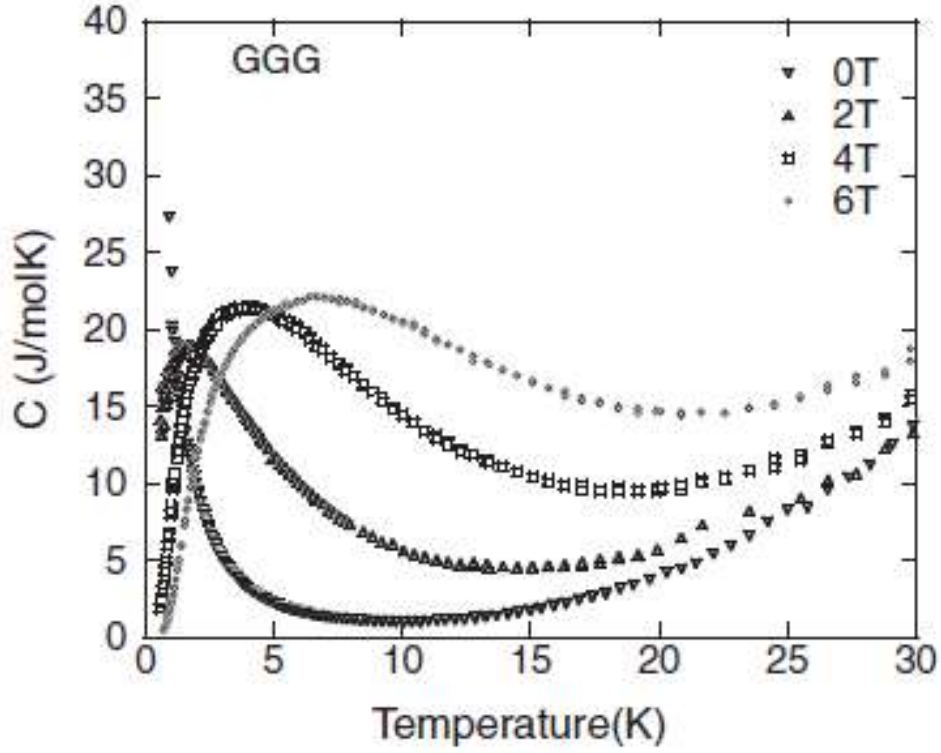

Figure 1.15 — Heat capacity of GGG in 0, 2, 4 and 6 T fields [**81**].

the value of the g - factor obtained for the Kramers doublet G_7 of Er^{3+} ions in the cubic crystal field, which is 6,8 [**86**].

In conclusion of this review, it can be noted the investigation that of the studied aluminates of rare-earth elements erbium aluminate ($ErAlO_3$) is one of the most studied compounds and for this compound many authors note the presence of magnetocaloric effect. In addition, various scientific laboratories have conducted studies of thermal conductivity, calculated g - factor values by the EPR method. However, despite the popularity of this compound and the study of some of its properties, a detailed study of heat capacity, including modeling and studies of contributions of different nature, as well as the influence of magnetic fields on the behavior of heat capacity has not been previously conducted.

Chapter 2. Heat capacity of gallium-gadolinium garnet $Gd_3Ga_5O_{12}$ (*GGG*) and *GGG* crystal with erbium admixture (*GGG:Er*)

This chapter presents the results of experimental studies of heat capacity of *GGG* and *GGG* crystals with Erbium impurity *(GGG:Er)* in the temperature range from 1.9 to 40 K and magnetic fields from 0 to 9 T. The theoretical interpretation of the obtained results is presented. Based on these experimental results, the entropy is calculated and the magnetic contribution to the entropy is determined. Note that measurements of the heat capacity of erbium-doped *GGG* crystals have not been carried out before [**87**].

2.1 Samples and experiment

Pure and erbium-doped *GGG* single crystals were grown by horizontal directional crystallization in a molybdenum container. The concentration of erbium in the doped crystal was 5 at.% of the amount of gadolinium in stoichiometric *GGG*. Samples for heat capacity studies were cut from the middle parts of the boule. They had the form of plates oriented perpendicularly to the cubic axis of the crystals, with a thickness of about 0.3 mm and a cross section of about 20 mm^2.

2.2 Heat capacity of garnets in different magnetic fields

Temperature dependences of heat capacity in different magnetic fields are shown in Figure 2.1 for crystals of *GGG:Er* (a) and pure *GGG*(b). The unusual behavior of the heat capacity value in the low temperature region and a maximum characteristic of the Schottky anomaly can be noted.

The results show that for *GGG:Er* and pure *GGG* crystals, the magnitude of the heat capacity is markedly affected by the magnetic field in the temperature range up to 80 K. In the numerical analysis of the heat capacity of dielectric crystals with paramagnetic ions, several contributions were taken into account, including the

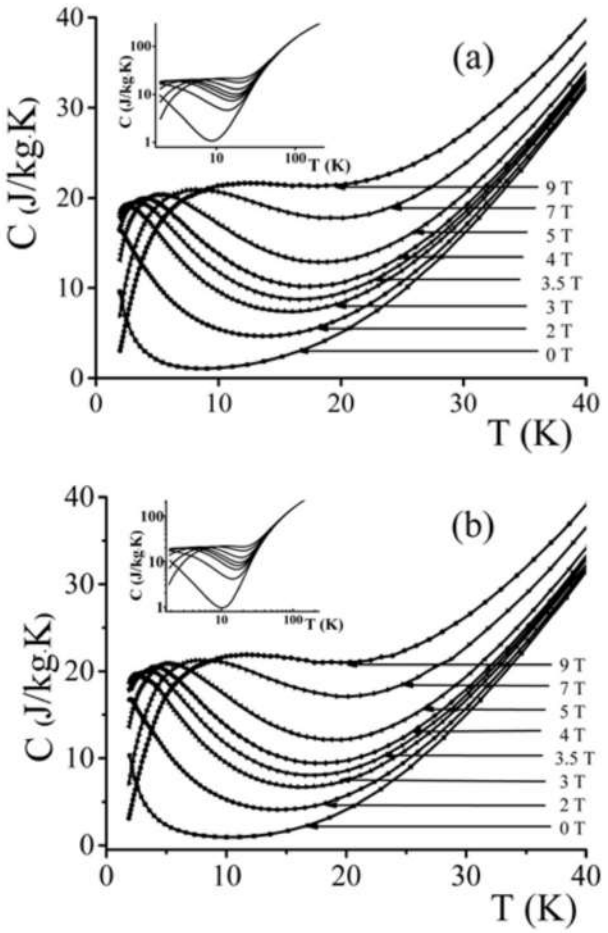

Figure 2.1 — Temperature dependences of the heat capacity for *GGG:Er* (a) and *GGG* (b) below 40 K in the different magnetic fields indicated. The insets show the heat capacity in the same magnetic fields over the whole temperature range from 1.9 to 220 K in double logarithmic scale

Debye, Einstein, and Schottky anomalies [**31**]. The Schottky anomaly prevails in the temperature dependence of the heat capacity at temperatures up to 30 K due to the influence of Gd^{3+} and Gd^{3+} ions [**88**]. Increasing the magnetic field changes the appearance of Schottky anomalies due to the shift and splitting of ion energy levels in the crystal field. Above 30 K the lattice (phonon) contribution dominates [**31**].

At temperatures below the melting point, structural phase transitions do not occur in gallium-gadolinium garnets. The unusual appearance of the magnetic phase diagram of *GGG* crystals can be noted. The formation of the far antiferromagnetic order occurs only in the presence of external magnetic fields belonging to a certain range [**79**; **89**; **90**]. However, only at temperatures well below 1.9 K do the magnetic singularities arise, so they do not affect the heat capacity measurements that were carried out in this work. Consequently, the temperature dependences of the heat

capacity can be described using the sum of the Debye, Einstein, and Schottky contributions.

An expression is used to account for the of Debye's contribution:

$$C_D(T) = 3r_D R \left(\frac{T}{\theta}\right)^3 \int_0^{\theta/T} \frac{x^4 e^x}{(e^x - 1)^2} dx \tag{2.1}$$

where r_D is the number of vibrational modes interpreted within the Debye model, R is the gas constant, θ is the Debye temperature.

The Einstein contribution calculated per mole of matter is represented as:

$$C_E(T) = 3r_E R \left(\frac{\theta_E}{T}\right)^2 \frac{e^{\theta_E/T}}{(e^{\theta_E/T} - 1)^2} \tag{2.2}$$

where θ_E is the Einstein temperature and r_E is the number of vibrational modes considered within this model.

The presence of Schottky anomalies has a connection with the Stark levels of paramagnetic ions in the crystal field. The Schottky contribution according to [**31**] has the form:

$$C_S = \frac{nR}{T^2} \left[\frac{\sum \Delta_i^2 g_i e^{-\Delta_i/T}}{g_0 + \sum g_i e^{-\Delta_i/T}} - \left(\frac{\sum \Delta_i g_i e^{-\Delta_i/T}}{g_0 + \sum g_i e^{-\Delta_i/T}} \right)^2 \right] \tag{2.3}$$

where n is the number of paramagnetic ions of a certain kind in the molecular formula, Δ_i is the energy difference in K between the ground level and the excited level with number i, g_0 and g_i are the degree of degeneracy of the ground and excited states, i=1 corresponds to the lower excited level.

The structure of the levels of Gd^{3+} ions is necessary in order to analyse the Schottky contribution to the heat capacity of a pure GGG crystal. In accordance with the work [**91**] $^8S_{7/2}$ - the lowest spin multiplet. The difference between the energy level of the main multiplet and the rest is more than 30,000 cm^{-1}. There is a weak interaction of the lower multiplet with the crystal field. Based on theoretical estimates [**91**], the eightfold degenerate lower state splits into four Kramers doublets with energies 0; 0.3, 0.5, 0.6 cm^{-1} (0; 0.43; 0.72; 0.86 K, respectively).

The paper [**88**] presents experimentally determined energy levels of low-lying states of trivalent erbium in gallium-gadolinium garnet. It was found that there is a splitting of the main $^4I_{15/2}$ multiplet into eight Kramers doublets. The four lower doublets have energies of 0, 31, 44, and 63 cm^{-1} (0; 44.6; 63.3 and 90.6 K), while the

remaining levels are at temperatures above 380 K. Note that the energy values of the three lower excited doublets are close to the Kramers states of erbium in garnets $Y_3Sc_2Ga_3O_{12}$ [**92**] and $Y_3Al_5O_{12}$ [**93**]. In spite of this, recent works have noted the necessity of assuming additional splitting of the lower Kramers doublet of the Er^{3+} ion by magnetic fields from neighbouring ions [**71**; **22**] for numerical interpretation of experimentally obtained heat capacity values in mixed alumina-erbium garnets. The magnitude of the additional splitting into two singlet was of the order of 1 K.

Let us consider the temperature dependence of the heat capacity of the investigated GGG crystals. Let us determine the value of the total heat capacity $C_{th}(T)$ represented as the sum of the Debye contribution, two Einstein and Schottky contributions from paramagnetic ions:

$$C_{th}(T) = \alpha_D C'_D(T) + \alpha_{E_1} C'_{E_1}(T) + \alpha_{E_2} C'_{E_2}(T) + \sum C_S(T) \qquad (2.4)$$

In fitting the total heat capacity to experimental values, we will restrict ourselves to temperatures lying in the range 1.9 - 40 K, in which the use of only two Einstein contributions is justified. In the cases of pure and erbium-doped garnets, the Debye temperature was found to be 500 K [**94**; **95**]. To calculate the Einstein contribution, fitting parameters such as: temperatures θ_{E1} and θ_{E2} and coefficients r_D, r_{E_1}, r_{E_2} were used. For pure GGG crystal, the Schottky contribution from gadolinium ions was taken into account. The fitting parameters were the energy differences Δ_i (i = 1, 2, 3) between the excited and main Kramers doublets. For doped garnet, the contribution of erbium ions was taken into account. A weak influence of the additional splitting of the lower Kramers doublet on the quality of the fit was found, due to the presence of local fields. For this reason it was set to 1 K, the same as in [**22**]. The energies of the other Kramers doublets were equal to the values determined in [**88**]. The approximation results are shown in 2.2. The figure shows the individual contributions to the heat capacity and their sum. From figure (2.2 a, b) it follows that at low temperatures the heat capacity can be fully determined using Schottky anomalies. The values of all fitting parameters are given in Table 1.

It should be emphasised that the calculated values of the splitting of the basic multiplet of trivalent gadolinium ions exceed the theoretical estimates by almost an order of magnitude. It can be assumed that magnetic fields from neighbouring paramagnetic gadolinium ions play a significant role in the splitting, as has been shown in the case of alumina-erbium garnets [**71**; **22**]. Table 1 shows that doping with erbium leads to weak changes in the fitting parameters for the heat capacity,

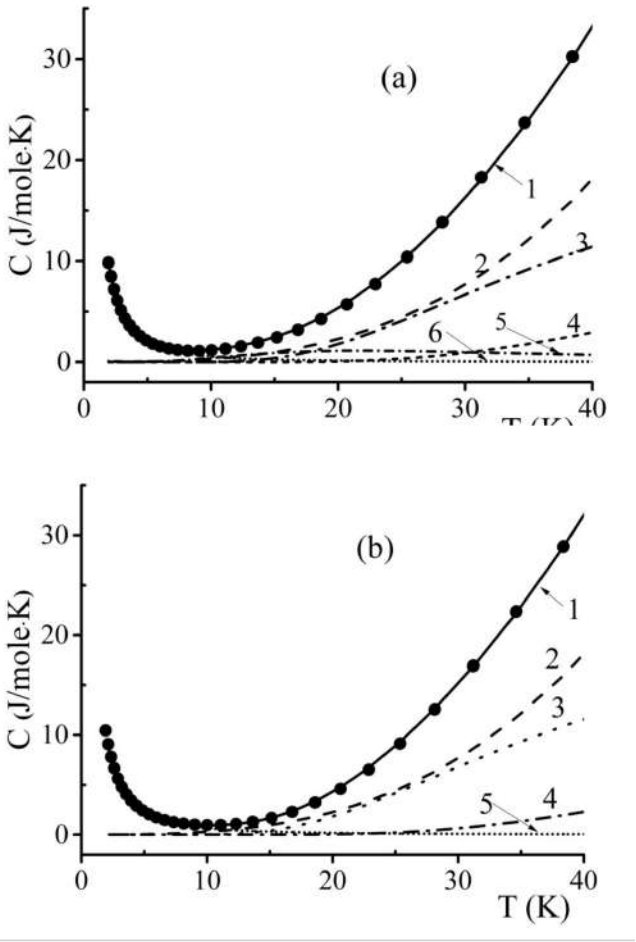

Figure 2.2 — Approximation of heat capacity in *GGG:Er* (a) and *GGG* (b) crystals below 40 K. Circles are experimental data. Solid lines show the full calculated heat capacity (1); Debye contribution (2); Einstein contributions (3,4); Schottky anomalies induced by Gd (5) and Er (6) ions.

but even at low erbium concentration the Schottky contribution due to the presence of erbium is appreciable.

The application of an external magnetic field causes the splitting of Kramers doublets, which should be proportional to the field. As a result, the growth of heat capacity with decreasing temperature becomes more pronounced at first, and then maxima appear on the heat capacity curves, which shift towards high temperatures with further increase of the field. The dependences of the position of the heat capacity maxima on the field for doped and undoped *GGG* crystals are shown in Figure 2.3. The value of the splitting can be calculated by the formula:

$$\Delta_m = \hbar g \mu_B B \tag{2.5}$$

Table 1 — Fitting coefficients r_D, r_{E_1}, r_{E_2} from relations (2.1 and 2.2), Einstein temperatures θ_{E_1} and θ_{E_2}, the splitting of the main gadolinium ion multiplet into Kramers doublets Δ_1, Δ_2, Δ_3

Sample	r_D	$\theta_{E_1}(K)$	r_{E_1}	$\theta_{E_2}(K)$	r_{E_2}	$\Delta_1(K)$	$\Delta_2(K)$	$\Delta_3(K)$
GGG	54,6	126	3	230	2.4	1.5	2.4	4.4
GGG:Er	54,6	127	3	210	2.4	1.5	2.4	4.2

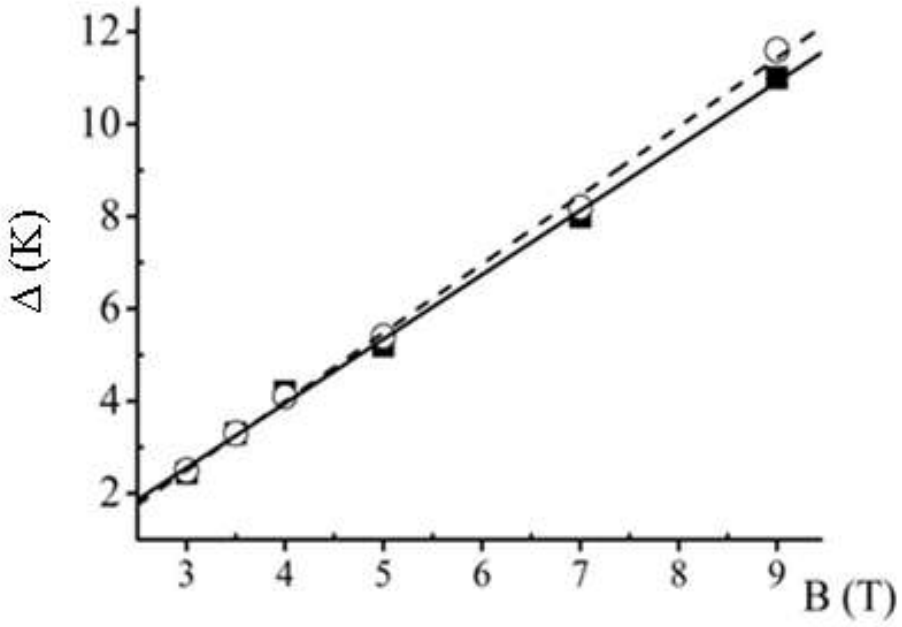

Figure 2.3 — Temperature dependences of heat capacity max Δ on magnetic field for *GGG:Er* (open symbols) and *GGG* (filled symbols) crystals. Straight lines show linear approximations.

As expected, the shift of the heat capacity maximum depends approximately linearly on the applied field. The construction of these dependences allowed us to calculate the g - factor for the studied samples. However, the shift values slightly exceed the estimates made taking into account the g - factor value for gadolinium ions corresponding to the lower spin multiplet ($g = 2$) and electron paramagnetic resonance data in pure *GGG* [**96**]. The obtained values are summarised in Table 2.

Table 2 — g - factor values for *GGG:Er* and *GGG*

Sample	*GGG* : *Er*	*GGG*
g – factor	2.8	2.5

2.3 Magnetic entropy

The conducted measurements of heat capacity in external magnetic fields allow us to calculate the change of entropy and magnetic entropy from 1.9 K to some temperature T. These experimental dependences are shown in Figure 2.4 (a). In the case where the contribution to entropy below 1.9 K is negligible, the calculation of the entropy change provides a good approximation for estimating both the total entropy and the total magnetic entropy at T $>$ 1.9 K. However, in pure and doped *GGG* crystals, the increase in heat capacity as the temperature decreases below 10 K in zero and weak magnetic fields indicates a significant role of the low-temperature contribution to entropy. Therefore, the theoretical dependences obtained above can be used to estimate the entropy increase in the interval from 0 to 1.9 K, although such estimates do not include the contributions of short and long-range magnetic correlations.

The results of calculation of temperature dependences of entropy up to 8 K are presented in Figure 2.4. The entropy in the zero field was calculated by formula 1.20. The entropy $S_B(T)$ was found in a similar way in the field B. The magnetic contribution to the entropy was calculated as the difference between the entropies in the field and in the absence of the field (formula 1.22). The magnetic entropy for the three fields is shown in figure 2.4 (b).

It can be seen that weak doping with erbium leads to entropy changes comparable to the effect of significant gallium substitution with aluminium [**96**]. Note that in the range from 0 to 8 K the magnetic entropy is negative in pure and doped *GGG*. At the same time, doping with erbium has the most significant effect on the magnetic entropy value for fields around 5 T.

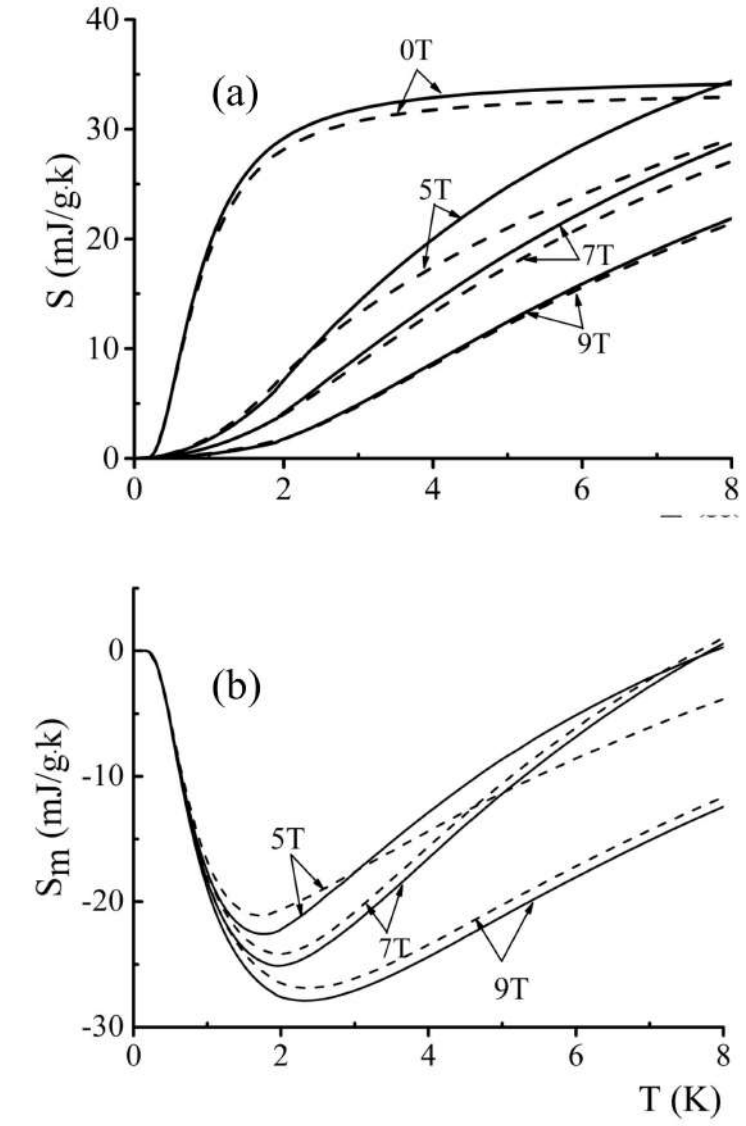

Figure 2.4 — Results of calculation of temperature dependences of entropy up to 8 K for *GGG:Er* (dashed lines) and *GGG:Er* (solid lines) crystals at magnetic fields indicated in the figure. Calculated magnetic entropy for *GGG:Er* (dashed lines) and *GGG:Er* (solid lines) crystals at magnetic fields indicated in the figure

2.4 Chapter 2 Conclusions

In this chapter, the heat capacity value of *GGG:Er* and pure *GGG* crystals was investigated. The results of measuring the heat capacity value showed the following:

– in the range from 1.9 to 40 K, the temperature dependence of the heat capacity obtained from the experiment for pure and erbium-doped *GGG* is

represented as the sum of the contributions of the Schottky anomalies, as well as the contributions of Debye and Einstein. The presence of Schottky anomaly is associated with the presence of gadolinium and erbium ions in the GGG composition.

– splittings of the gadolinium basic spin multiplet have values an order of magnitude higher than the theoretical estimates.
– Entropy and magnetic entropy were calculated using the heat capacity analysis performed.

As part of the work, it should be noted that erbium-doped GGG crystals can be proposed as materials for magnetic refrigerators due to the higher value of magnetic entropy.

Chapter 3. Heat capacity of mixed yttrium-disperse aluminium garnets

This chapter presents the results of experimental studies of the heat capacity of mixed garnet single crystals with the general formula $Dy_xY_{3-x}Al_5O_{12}$ ($x = 0; 0.15; 0.50; 1.00; 1.50, 2.25; 3.00$). The measurements were carried out in the temperature range from 1.9 to 80 K in the absence of a magnetic field applied to the samples and in fields up to 6 T. Similarly to the results of Chapter 2, various contributions to the heat capacity in the absence of an external magnetic field were calculated. Based on the experimental data obtained, the entropy and magnetic entropy values of yttrium-disprosium aluminium garnets have been calculated. The nature of the heat capacity anomalies in the magnetic field related to the peculiarities of the structure of mixed garnets is discussed [**97**].

3.1 Samples for research.

Mixed single crystals of $Dy_xY_{3-x}Al_5O_{12}$ garnet (DAG) were grown by vertical directional crystallisation in a molybdenum crucible using the Bridgman method [**98**]. To measure the heat capacity, plates orientated perpendicular to the [111] crystal axis were cut from the grown boules. The thickness of the plates was ≈ 0.3 mm and the surface area was ≈ 4 mm^2. During the heat capacity measurements, the magnetic field was applied perpendicular to the plate surfaces.

3.2 Heat capacity in zero field

Figure 3.1 shows the experimental dependences of the heat capacity of a series of $Dy_xY_{3-x}Al_5O_{12}$ samples in zero magnetic field: in double logarithmic scale in the temperature range from 1.9 to 80 K and in linear scale at temperatures below 30 K.

As can be seen from Figure 3.1, for all samples except $Y_3Al_5O_{12}$, a pronounced growth of heat capacity at temperatures below 10 K is observed, with the low-temperature contribution to the heat capacity increasing with increasing yttrium

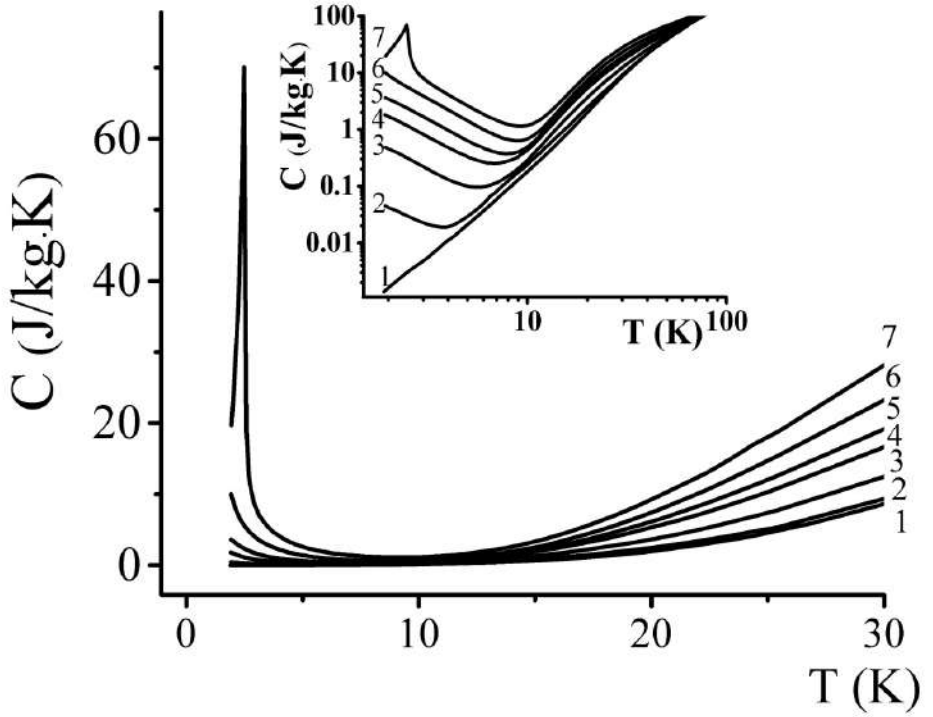

Figure 3.1 — Temperature dependences of heat capacity for $Dy_xY_{3-x}Al_5O_{12}$ below 30 K in zero magnetic field with different yttrium concentration. Numbers 1,2,3,4,5,6 in the figure correspond to dysprosium concentrations $x = 0; 0.15; 0.50; 1.00; 1.50, 2.25; 3.00$, respectively. The inset shows the heat capacity over the whole temperature range from 1.9 to 80 K in double logarithmic scale

concentration. Antiferromagnetic anomalies of λ-type heat capacity characteristic of similar compounds were observed only in single crystal $Dy_3Al_5O_{12}$. For this compound, the peak in the temperature dependence of the heat capacity corresponds to a temperature of 2.48 K, which agrees well with the temperature of the antiferromagnetic phase transition obtained in [**99**; **100**]. For mixed garnets, the anomaly associated with the antiferromagnetic transition is not observed in the investigated range. It can be assumed that the transition is below the temperature limit of measurements, i.e., below 1.9 K.

As noted earlier in 1 and 2, the heat capacity of single crystals with paramagnetic ions can be described as a combination of the phonon contribution and Schottky anomalies. The heat capacity of yttrium-aluminium garnet with no magnetic ions in its lattice ($x = 0$) is entirely due to the phonon contribution, which at a sufficiently low temperature can be described by the Debye model. Analysis of the experimental data allows us to estimate the Debye temperature by

approximating the temperature dependence of the heat capacity for YAG using the usual relation for the molar Debye contribution. The approximation at temperatures up to 15 K allowed us to determine the Debye temperature for yttrium-aluminium garnet equal to 730 K (see formula 2.1). The Debye temperature for dysprosium-aluminium garnet was about 500 K [**99**].

Many physical properties of mixed rare-earth aluminium garnets are well described by Wegard's law [**101**], so it can be assumed that the Debye temperature for mixed dysprosium-yttrium garnets varies linearly with the composition of the garnet. Thus, knowing the temperatures for pure aluminium garnets, it is possible to estimate the temperatures for dysprosium-yttrium garnets as well. The calculated values of Debye temperatures are given in Table 3. The obtained values are necessary for further calculation of fitting parameters of the heat capacity value.

Table 3 — Debye temperature of the investigated samples

Sample	θ, (K)
$Y_3Al_5O_{12}$	730
$Dy_{0.15}Y_{2.85}Al_5O_{12}$	719
$Dy_{0.5}Y_{2.5}Al_5O_{12}$	692
$Dy_1Y_2Al_5O_{12}$	653
$Dy_{1.5}Y_{1.5}Al_5O_{12}$	615
$Dy_{2.25}Y_{0.75}Al_5O_{12}$	556
$Dy_3Al_5O_{12}$	500

The appearance of dysprosium ions in the garnet lattice leads to Schottky anomalies in the heat capacity. To calculate the Schottky contribution, we will use formula 1.14, where Δ is the magnetic splitting of the main doublet. Similarly to the previously described gallium-gadolinium garnet $Gd_3Ga_5O_{12}$ doped with erbium, we carry out a full calculation of the heat capacity in a zero magnetic field.

The energy levels of trivalent dysprosium ions in DAG and in some mixed yttrium-dysprosium garnets are presented in [**102**; **103**; **104**]. The main $^6H_{15/2}$ multiplet is split by the crystal field into eight Kramers doublets. The energies of the excited doublets change weakly with the Dy concentration. The first and second excited doublets were recorded at 101 K and around 168 K relative to the main

doublet in *DAG* single crystals. In dilute *Dy*: *Dy:YAG* and *YAG* doped with 5 and 10% *Dy*, the corresponding gaps were 87 and 146 K, 88 and 145 K, 82 and 141 K, respectively. The higher doublets (above 200 K) are insignificantly populated at low temperatures and cannot noticeably affect the magnitude of the heat capacity. Since the lowest excited doublet is separated by more than 80 K from the main doublet, it and higher doublets cannot be responsible for the strong increase in heat capacity shown in Figure 3.1 at temperatures below 8 K. An increase in heat capacity with decreasing temperature has also been previously reported for erbium-yttrium garnets [**22**; **71**]. Er^{3+} erbium ions in the garnet lattice have twice degenerate levels, and the distance between the main and first excited doublets is 32 K. Thus, the Stark splitting of degenerate levels in the crystal field does not cause a low-temperature increase in heat capacity in erbium garnets, as well as in dysprosium garnets. To explain the anomalous behaviour of heat capacity in erbium yttrium garnets, it was suggested in [**22**; **71**] that the main Kramers doublet is split by local magnetic fields caused by neighbouring magnetic ions. The distance between the two singlet can be of the order of 1 K. In this case, the heat capacity increase is also described by formula 1.4.

In Chapter 2 part 2.1 the results of the study of erbium-doped garnets were discussed. In further analyses of the results obtained, a similar approach was used. The temperature dependence of the zero-field heat capacity for all investigated dysprosium-yttrium garnets at temperatures below 15 K was approximated by the sum of Debye and Schottky contributions. The approximation parameters for such data processing are the splitting of the main doublet Δ and the difference between the lowest energy levels and the first excited Kramers doublet Δ_1. Figures 3.2 (a – f) show the approximations for mixed yttrium-dysprosium garnets with dysprosium concentrations $x = 0.15; 0.50; 1.00; 1.50; 2.25; 3.00$. Since the heat capacity of *DAG* is affected by the λ – anomaly at the antiferromagnetic phase transition, the experimental data for DAG were approximated in the range from 5.5 to 15 K. For the other samples, the approximation was carried out at temperatures from 1.9 K.

The figures show that the fitting by two contributions, Debye and Schottky, gives very good results in the range from 1.9 and up to 15 K. Thus, the parameter Δ was determined during the approximation.

Figure 3.3 shows the dependence of Δ on the composition x. As can be seen from Figure 3.3, the value of the splitting value increases with increasing x. This behaviour is natural, since the splitting of levels is carried out by magnetic

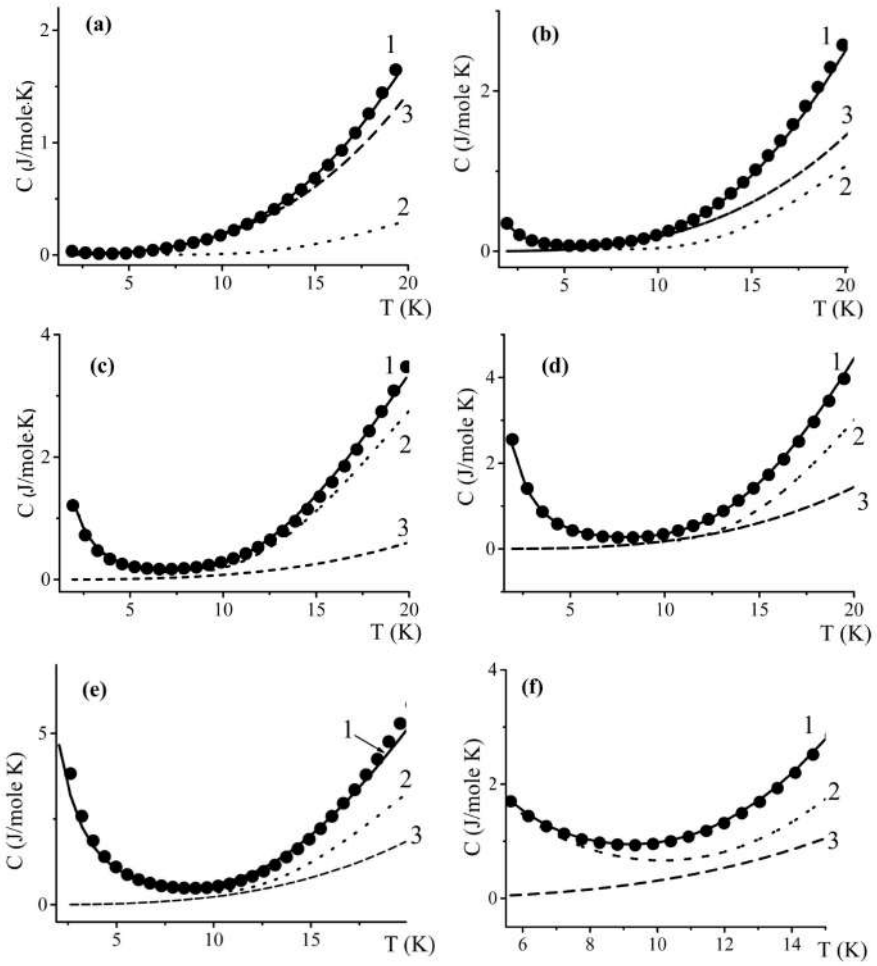

Figure 3.2 — Approximation of the heat capacity in the $Dy_xY_{3-x}Al_5O_{12}$ (where x = 0.15 (a); 0.50 (b); 1.00 (c); 1.50 (d), 2.25 (e); 3.00 (f)). The circles are the experimental data. The solid line shows the full calculated heat capacity (1), the dashed line shows the Schottky anomalies (2), and the dashed line shows the Debye contribution (3).

coupling with neighbouring dysprosium ions. In the case of the dipole-dipole interaction, which plays an important role for *DAG* [**99**; **105**], the splitting should be proportional to x.

Analyses of the dependence of Δ on x on a double logarithmic scale allowed us to determine that $\Delta \sim x^{0.57}$.

Parameters of approximation of the experimental temperature dependences of heat capacity were also energy differences: Δ splitting of the main Kramers doublet, Δ_1 difference between the main and the first excited levels. The Einstein contribution for $Dy_xY_{3-x}Al_5O_{12}$ was not taken into account. When calculating Schottky contributions, the values of energy levels were slightly corrected depending on the concentration of yttrium and dysprosium.

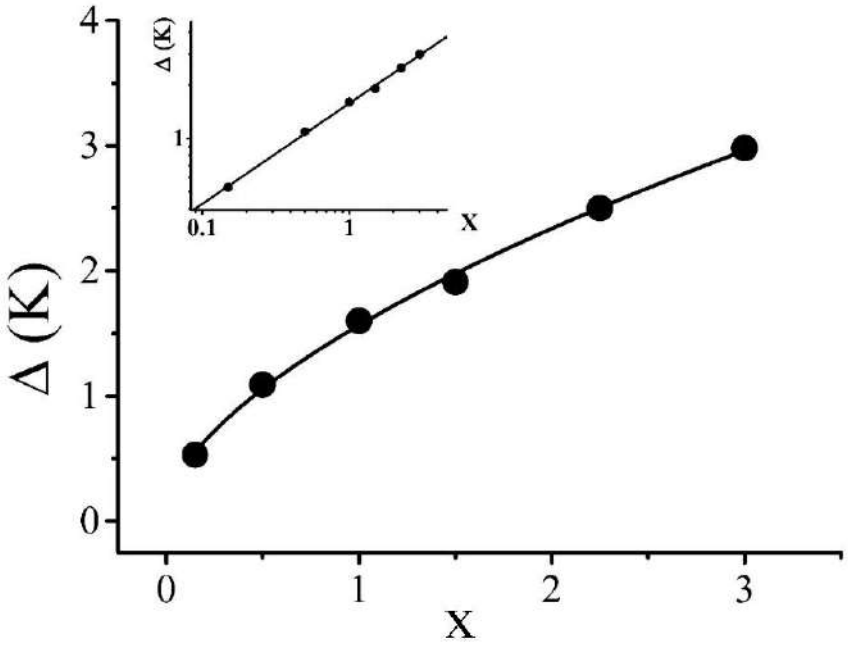

Figure 3.3 — Dependence of Δ on the amount of dysprosium ions. The inset shows this dependence in double logarithmic scale.

The estimated values of Δ and Δ_1 are given in Table 4 for pure DAG and for mixed garnets. The obtained data are in good agreement with the results of [**102**; **103**; **104**].

According to the data presented in the table, it can be seen that with increasing dysprosium concentration, there is a slight increase in the values of Δ and Δ_1.

Table 4 — Corrected values of the main doublet splitting for $Dy^{3+}(\Delta)$ and the energy of the first excited level (Δ_1)

Sample	Δ, K	Δ_1, K
$Y_3Al_5O_{12}$	0.53	75
$Dy_{0,5}Y_{2,5}Al_5O_{12}$	1.09	88
$Dy_1Y_2Al_5O_{12}$	1.60	90
$Dy_{1,5}Y_{1,5}Al_5O_{12}$	1.91	97
$Dy_{2,25}Y_{0,75}Al_5O_{12}$	2.50	103
$Dy_3Al_5O_{12}$	2.98	103

3.3 Heat capacity in magnetic field

After studying the heat capacity in the absence of an external magnetic field, studies were carried out in different magnetic fields. It is known that the effect of the magnetic field on the system of Stark levels in the lattice of dysprosium garnet is strongly anisotropic [**106**; **107**]. The dysprosium ions in the unit cell are divided into 3 groups with the principal axes of the gz tensor oriented along three crystallographic axes.

EPR studies have shown that the parallel component g_z in the g-tensor is close to 18, while the two perpendicular components g_x and g_y are much smaller and approximate 0.5 [**106**]. Since the investigated garnet samples were plates whose faces were cut perpendicular to the direction [111], the splitting of doublets in them should be determined by the same g - factor for the three groups of dysprosium ions:

$$g = \sqrt{g_z^2 + g_x^2 + g_y^2}/3 \approx 10{,}4 \tag{3.1}$$

This means that on the temperature dependence of the heat capacity at the application of a magnetic field one maximum associated with the splitting of the main doublet with $g \approx 10$ should be observed.

The obtained experimental dependences of heat capacity at different values of magnetic field from 0 to 6 T in the temperature range from 1.9 to 20 K are presented in Figures 3.4 (a – f). As can be seen from the results, a strong dependence of the heat capacity on the magnetic field is observed. When a magnetic field of 1 T was applied, a pronounced maximum was observed. With increasing applied magnetic field, the position of the maximum shifted towards higher temperatures. In addition to the displacement of the maximum, its blurring occurred. Also, the shape of the peak was slightly different from the dependence described by relation 1.4, which is related to the splitting of the main Kramers doublet in the magnetic field B.

The splitting value was calculated by formula (2.5). As an example, Figure 3.5 shows the dependence of Δ_m on B for the sample $Dy_{2.25}Y_{0.75}Al_5O_{12}$.

The construction of these dependences allowed us to calculate the g - factor for garnets with $x = 0.15; 0.50; 1.00; 1.50, 2.25; 3.00$. The obtained values are given in Table 5. The value of g - factor ranges from 8.4 to 10.4. The g - factor value for *DAG* was 10.4, which is in good agreement with the above estimate and the results of [**106**]. For the other samples, deviations of the g - factor can be caused

by distortions of the maximum due to disordered substitution in mixed crystals, as well as deviations in the orientations of the samples in the magnetic field.

Table 5 — Value of g - factor for Dy^{3+} ions in c-positions in $Dy_xY_{3-x}Al_5O_{12}$

x	0.15	0.5	1	1.5	2.25	3
g - factor	8.4	10.2	10.3/∼5	10.4	10.1	10.3

Deviations from the random distribution of ions in crystalline solid solutions affect the practical application of these compounds. To obtain information on the

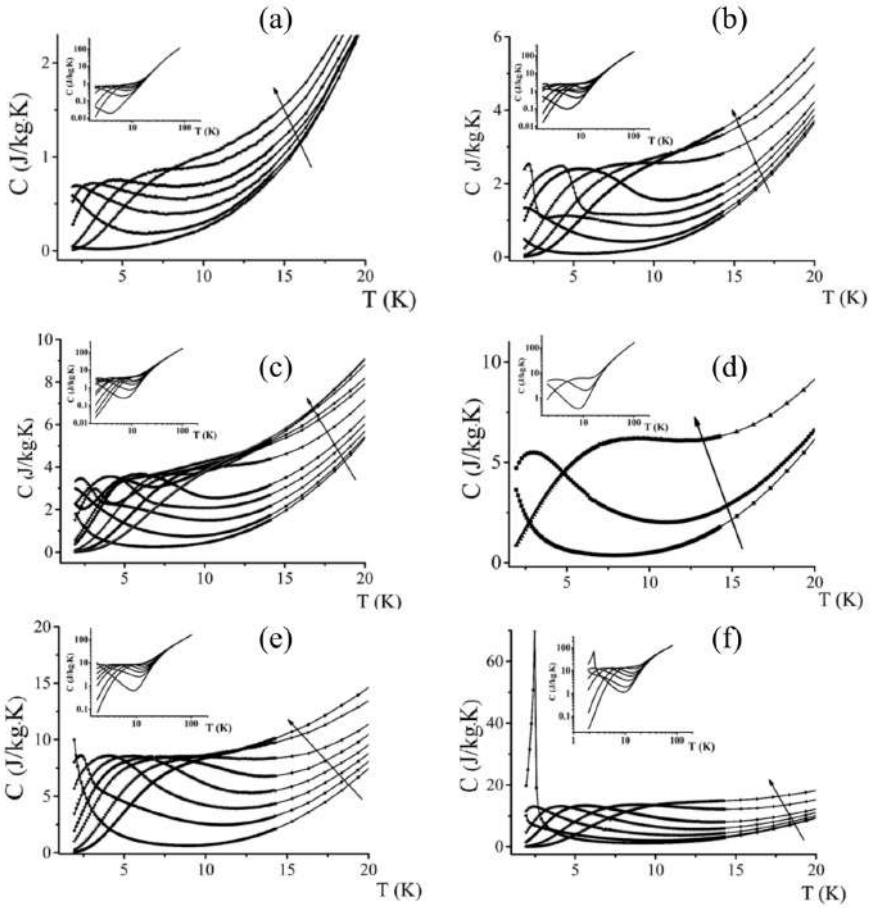

Figure 3.4 — Temperature dependences of heat capacity for $Dy_xY_{3-x}Al_5O_{12}$ (where x = 0.15 (a); 0.50 (b); 1.00 (c); 1.50 (d), 2.25 (e); 3.00 (f)) in different magnetic fields at temperatures from 1.9 to 20 K. The insets show these dependences in the temperature range from 1.9 to 100 K in double logarithmic scale. The magnitudes of magnetic fields in these measurements were: 0; 0.5; 1.0; 1.0; 1.5; 2.0; 3.0; 4.0 T. The arrow shows the direction of magnetic field increase.

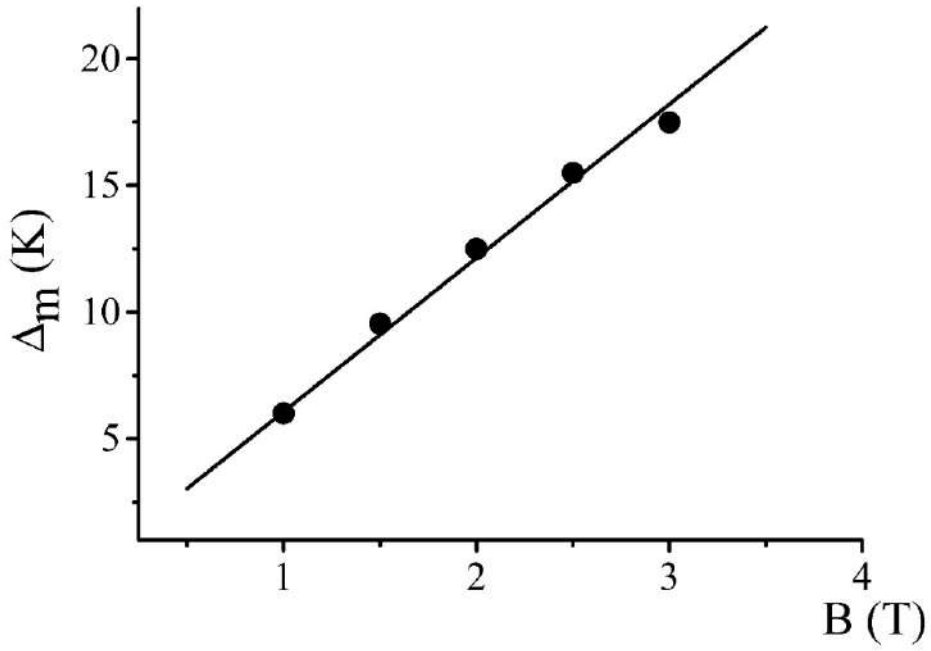

Figure 3.5 — Dependence of the splitting of the main Kramers doublet on the magnetic field B for the crystal $Dy_{2.25}Y_{0.75}Al_5O_{12}$. The solid line corresponds to the linear approximation of this dependence.

order of substitution and stoichiometry in the mixed crystals, additional analysis of the obtained experimental data of heat capacity in a magnetic field was carried out.

DAG single crystals have known stoichiometry defects when dysprosium ions fall into octahedral *a*-positions [**21**]. These features give weak additional lines in the EPR spectra of dysprosium with g - factors different from the g - factors of Dy^{3+} in stoichiometric crystals [**106**]. It can be assumed that the dysprosium ions in the a-position are the cause of side high-temperature peaks, which are superimposed on the main peaks of the heat capacity value in *DAG* and mixed crystals studied in this work. The value of the g - factor for these peaks is 18.

The heat capacity in magnetic fields observed for mixed garnet with $x = 1$ is markedly different. In addition to the weak shoulder associated with $g \sim 18$, two pronounced peaks of similar intensity are observed, which is non-standard for this type of dependence.

The position of the first maximum found on the temperature dependence of the heat capacity for $Dy_1Y_2Al_5O_{12}$, which is clearly visible at the application of a magnetic field from 1 to 3 T, agrees with the positions of the maximum in other mixed garnets with $g \sim 10$. The second maximum is clearly visible in fields from 3 to 6 T and is consistent with $g \sim 10$. Since the peaks corresponding to $g \sim 5$ and

$g \sim 10$ have comparable intensities, the peak with $g \sim 5$ cannot be associated with Dy ions in positions different from the c-position in the lattice. Therefore, it can be assumed that the anomalous behaviour of the temperature dependence of the heat capacity in the magnetic field is due to the inhomogeneity of the distribution of Dy^{3+} and Y^{3+} ions in the c-positions. The appearance of the second peak may arise due to the appearance of groups of Dy^{3+} ions characterised by $g \sim 5$, i.e. clustering in the solid solution for a particular composition with $x = 1$ occurs. Figure 3.6 shows the dependences of the g - factor value on the amount of the ratio of yttrium and dysprosium ions in the mixed garnet $Dy_xY_{3-x}Al_5O_{12}$.

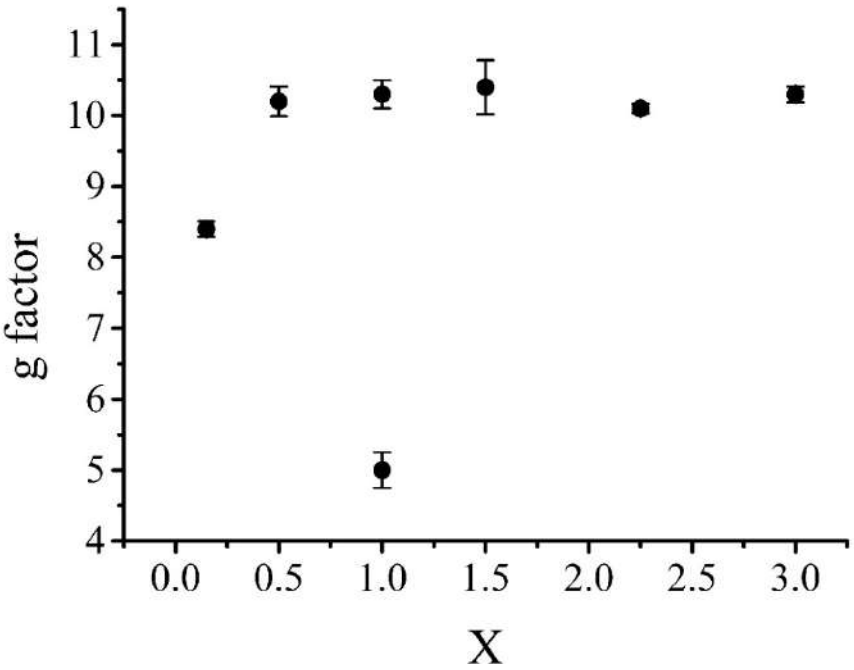

Figure 3.6 — Dependences of the g - factor value on the composition of single crystal $Dy_xY_{3-x}Al_5O_{12}$. The solid line corresponds to a linear approximation of this dependence.

3.4 Magnetic entropy

The values of entropy and magnetic entropy were calculated for dysprosium-yttrium garnets. The obtained dependences are presented in Figures 3.7 (a – f).

As can be seen from the results, with increasing dysprosium concentration, an increase in entropy is observed in all investigated magnetic fields. It can also be

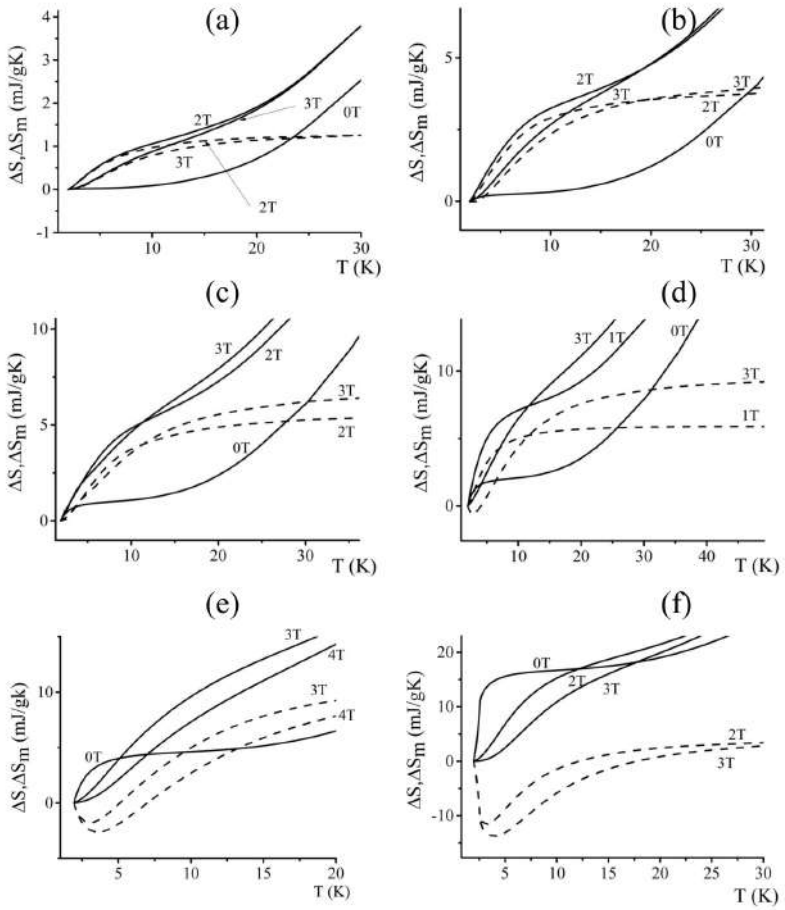

Figure 3.7 — Entropy change (solid lines) and magnetic entropy change (dashed lines) for $Dy_xY_{3-x}Al_5O_{12}$ $(x = 0.15(a); 0.50(b); 1.00(c); 1.50(d), 2.25(e); 3.00(f))$. The values of magnetic fields are indicated in the figure.

noted that at x greater than 1.5 the value of magnetic entropy is positive, and at x equal or less than 1.5 the values of magnetic entropy become negative.

The magnetic entropy in the investigated garnets can be compared with the entropy in some magnetocaloric materials that are being investigated for magnetic refrigerator applications [**108**]. The difference between the entropy in a non-zero and zero magnetic field found for dysprosium-yttrium garnets is only slightly smaller than in chromium-potassium-quartz and dysprosium-gallium garnets [**109**], and about three times smaller than the maximum magnetic entropy in a magnetic field in anhydrous gadolinium phosphate [**110**]. Since the calculated magnetic entropy for mixed dysprosium-yttrium-aluminium garnets is of the same order of magnitude as for known magnetocaloric materials, the applicability of these garnets for the development of adiabatic magnetic refrigerators can be assumed.

3.5 Chapter 3 Conclusions

In this chapter, the heat capacity of $Dy_xY_{3-x}Al_5O_{12}$ (x = 0; 0.15; 0.50; 1.00; 1.50, 2.25; 3.00) crystals was investigated. The results of the crystal heat capacity studies showed the following:

- at zero external magnetic field, the heat capacity value can be described by the sum of the phonon contribution and the contribution of Schottky anomalies due to the population of level splitting and the split main Kramers doublet.
- the splitting was caused by the interaction with neighbouring magnetic ions and increased with increasing dysprosium concentration (x) according to the law $\Delta \sim x^{0,57}$.
- the dependences of heat capacity in the magnetic field for garnets containing dysprosium, except for the sample with $x = 1$, are characterised by the presence of a maximum caused by the splitting of the Kramers doublet, and a shoulder associated with Dy^{3+} ions in the a - position is revealed.
- appearance of two intense maxima in the $Dy_xY_{3-x}Al_5O_{12}$ (where $x = 1.00$), with corresponding g - factors $g \cong 10.7$ and $g \sim 5$.

The presented results demonstrated the potential ability of magnetocalorimetry to study the order of substitution and stoichiometry in crystalline solutions. The calculated magnetic entropy for mixed yttrium-aluminium dysprosium garnets was of the same order of magnitude as for known magnetocaloric materials, suggesting the applicability of these garnets in magnetic refrigerators.

Chapter 4. Heat capacity measurements in single crystals and glasses of a number of rare earth pentaphosphates (NdP_5O_{14}, GdP_5O_{14}, YbP_5O_{14}, SmP_5O_{14}, CeP_5O_{14})

In the present chapter, the features of low-temperature heat capacity in single crystals and glasses of a number of rare-earth pentaphosphates (NdP_5O_{14}, GdP_5O_{14}, YbP_5O_{14}, SmP_5O_{14}, CeP_5O_{14}) will be considered.

The measurements were carried out in the temperature range from 1.9 to 100 K in the absence of a magnetic field applied to the samples and in fields up to 9 T. The values of entropy and magnetic entropy in single crystals and glasses of a number of rare-earth pentaphosphates were calculated on the basis of the experimental data obtained [**111**].

4.1 Heat capacity in zero magnetic field

The temperature dependence of the heat capacity in zero magnetic field is shown in 4.1 for single crystal NdP_5O_{14} The inset to the figure shows the dependence of heat capacity in double logarithmic scale. As can be seen from Figure 4.1, the value of heat capacity in the logarithmic scale in the region of low temperatures (up to 10 K) has a small "tail". This "tail"has a weak intensity and is not associated with paramagnetic ions Nd^{3+}. The obtained curve is probably related to defects in the crystal.

For single crystal and glass containing gadolinium GdP_5O_{14} the obtained experimental dependences of heat capacity in zero magnetic field are presented in Figure 4.2. Both in monocrystal and glass of gadolinium pentaphosphate, the obtained results at low temperature can be described by a combination of phonon contribution and Schottky anomalies. However, the heat capacity of glasses at $T \approx 10$ K exceeds the heat capacity of single crystals of the corresponding composition. That is explained by the contribution to the heat capacity of two-level systems.

Figure 4.3 shows the temperature dependence of the heat capacity value for single crystal YbP_5O_{14}. The inset shows this dependence in double logarithmic

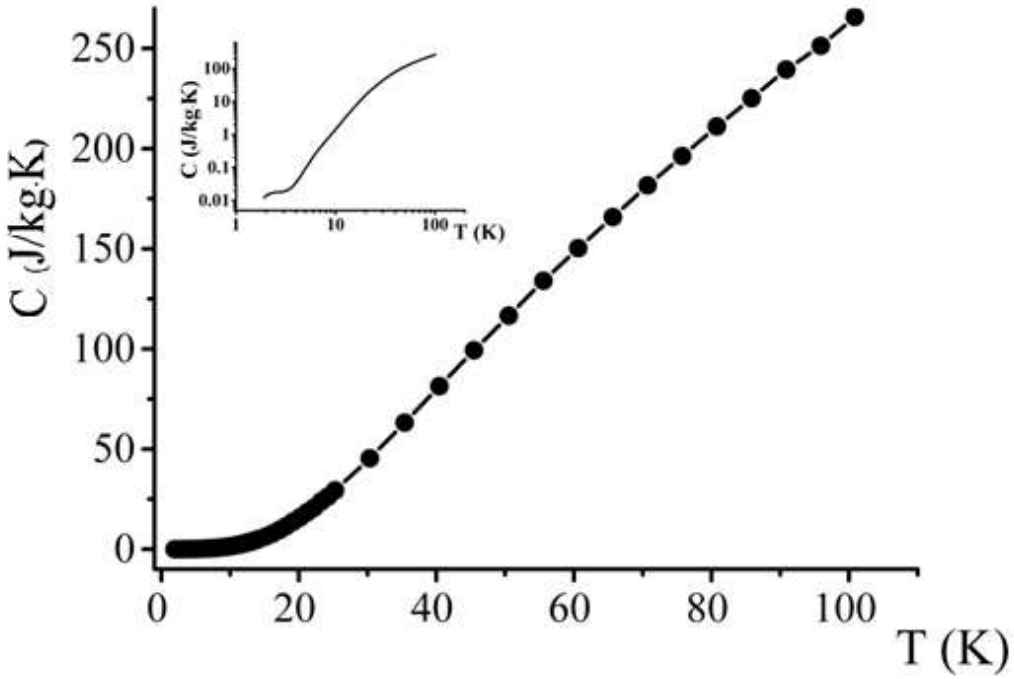

Figure 4.1 — Temperature dependences of heat capacity for NdP_5O_{14} single crystal in zero magnetic field.

scale. In the low temperature range (1.9-10 K) there is a kink in the temperature dependence. This kink is not related to the Debye contribution and appears also due to the influence of uncontrolled impurities. Temperature dependences of the heat capacity value for ReP_5O_{14} ($Re = Sm$, Ce, Gd) pentaphosphate glasses are shown in Figure 4.4 in double logarithmic scale.

As mentioned earlier in Chapters 1 and 2, the heat capacity of single crystals (NdP_5O_{14}, GdP_5O_{14}, YbP_5O_{14}) can be described by the phonon contribution, Schottky anomaly, and features caused by magnetic and structural phase transitions [**31**]. In the case of studies of pentaphosphate glasses, theoretical estimates of heat capacity in the temperature range from 1.9 to 15 K are complicated by the blurring of energy levels due to local inhomogeneities of the structure.

To describe the heat capacity of pentaphosphates, we will use the same method as in the case of describing the heat capacity of garnets: pure and erbium-doped GGG and DAG in a zero magnetic field. The theoretical calculation of the total heat capacity will be performed according to expression (2.4). For the Debye and Schottky contributions, we will use formulas (2.1) and (2.3), respectively. Figures 4.5 (a – c) show approximations of the heat capacity value for single crystals NdP_5O_{14}, GdP_5O_{14}, YbP_5O_{14}. It can be seen from the figures that the fitting by two contributions, Debye and Schottky, gives good results in the range from 1.9 and

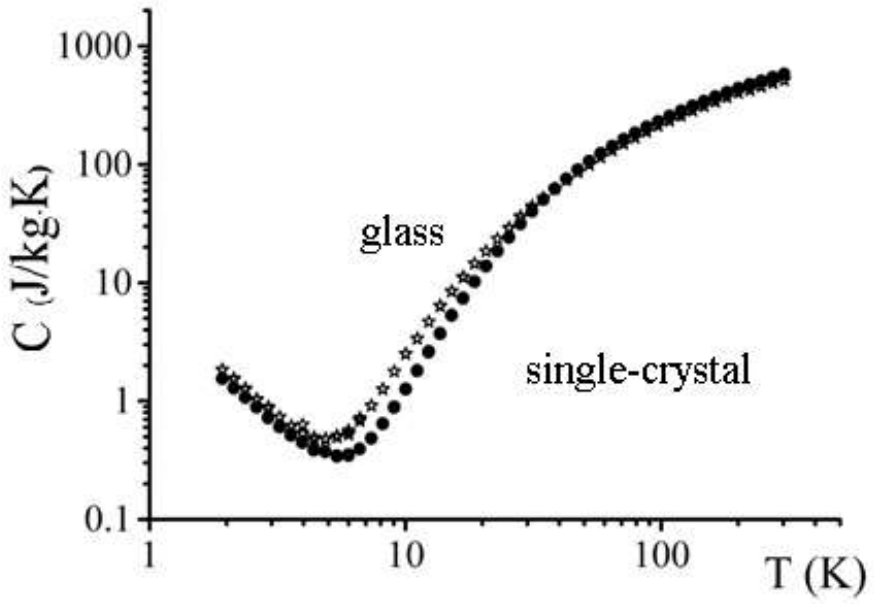

Figure 4.2 — Temperature dependences of heat capacity for GdP_5O_{14} single crystal and GdP_5O_{14} pentaphosphate glass in zero magnetic field.

up to 15 K for NdP_5O_{14}, YbP_5O_{14} single crystals and in the range from 1.9 to 10 K for GdP_5O_{14} single crystal. The approximation parameter of the experimental temperature dependences of heat capacity was the splitting of the main doublet Δ. The Einstein contribution for these samples was not taken into account. For pentaphosphate glasses ReP_5O_{14} ($Re = Sm$, Ce, Gd no approximation of the heat capacity value was carried out due to the disruption of the structure and, consequently, a strong blurring of energy levels.

In a single crystal of neodymium pentaphosphate, the main $^4I_{9/2}$ multiplet is split by the crystal field into five Kramers doublets. The first doublet has an energy of 84 cm^{-1} (121 K) with respect to the main doublet. The next two doublets have energies of 305 and 369 K [**112**]. Neodymium pentaphosphate crystal belongs to monoclinic symmetry. In terms of structure, the single crystal NdP_5O_{14} consists of cross-linked double chains of PO_4 tetrahedrons with common angles running parallel to the crystallographic a-axis. Each Nd atom is coordinated by eight O atoms [**113**]. The molecular weight of NdP_5O_{14} = 523,10 g/mol. From the slope of the curve at temperatures less than 10 K, where Schottky anomalies do not yet appear, the Debye temperature can be determined. This approximation allowed us to calculate that for single crystal NdP_5O_{14} the Debye temperature is 375 K .

In single crystal GdP_5O_{14}, in order to analyse the Schottky contribution to the heat capacity, it is necessary to know the level structure of the Gd^{3+} ions.

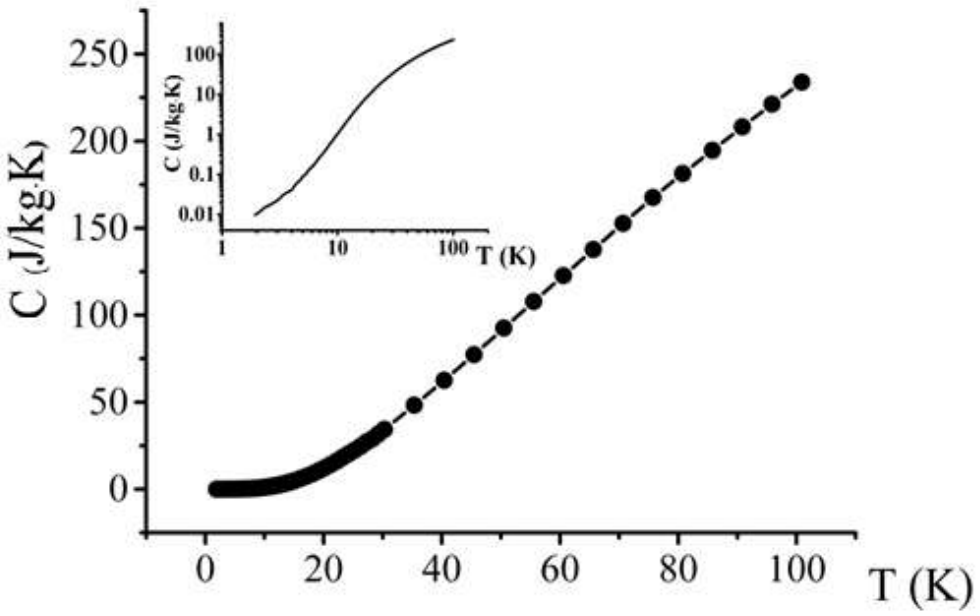

Figure 4.3 — Temperature dependences of heat capacity for YbP_5O_{14} single crystal in zero magnetic field. The inset shows the heat capacity over the entire temperature range from 1.9 to 100 K in double logarithmic scale.

According to [**52**] the lowest one is the spin multiplet. The other energy levels are more than 30000 cm^{-1} away from the main multiplet. The lower multiplet weakly interacts with the crystal field. The obtained values of the energy of low-energy excitations for the Gd^{3+} ion in single crystal GdP_5O_{14} were $\Delta = 1.3$ K and glass $\Delta = 1.4$ K. The obtained value reflects only the average character of Δ values, since, for example, for the Gd^{3+} ion in gallium-gadolinium garnet (GGG), the structure of levels with energies of 0; 0.43; 0.72; 0.86 K was observed [**114**]. When calculating the Δ values, the best agreement between the calculated and experimental temperature dependences was achieved at a Debye temperature value of 400 K. The molecular weight of GdP_5O_{14} was 536.11 g/mol.

The monocrystal YbP_5O_{14} also has a monoclinic structure. The lattice parameters are: $a = 12.830(3)$, $b = 12.676(3)$, $c = 12.337(3)$, $S = 91.25(2)$, $z = 8$ [**115**]. The $4f^{13}$ electron configuration for the free Yb^{3+} ion has only two levels: $^2F_{5/2}$ and $^2F_{7/2}$. These levels are separated by an energy interval of ~ 10000 cm^{-1} [**116**]. Under the action of the crystal field, the degeneracy is removed, leading to the splitting of the $^2F_{5/2}$ state into four sublevels and the $^2F_{5/2}$ state into three sublevels [**116**]. As well as for the single crystal NdP_5O_{14}, for the sample YbP_5O_{14} the Debye temperature was determined from the slope of the heat capacity curve at low temperatures (less than 10 K), where there is still no influence of Schottky

anomalies. The molecular mass of YbP_5O_{14} = 552 g/mol. The fitting parameters for the sample YbP_5O_{14}, were as follows: Debye temperature = 420 K, Δ = 90 K.

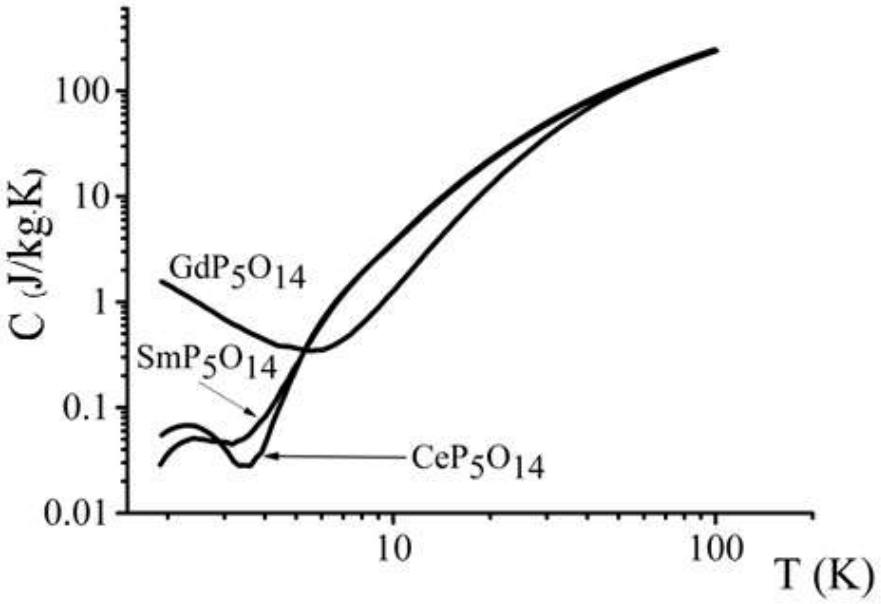

Figure 4.4 — Temperature dependences of the heat capacity of ReP_5O_{14} ($Re = Sm$, Ce, Gd) pentaphosphate glasses in zero magnetic field.

Table 6 summarises the fitting parameters for samples of a range of rare earth pentaphosphates (NdP_5O_{14}, GdP_5O_{14}, YbP_5O_{14}) at which the calculated and experimental curves best matched each other.

Table 6 — Debye temperature and low energy excitation energy values for the investigated samples

Single sample	θ, K	Δ, K
NdP_5O_{14}	375	121
GdP_5O_{14}	400	1.3
YbP_5O_{14}	420	90

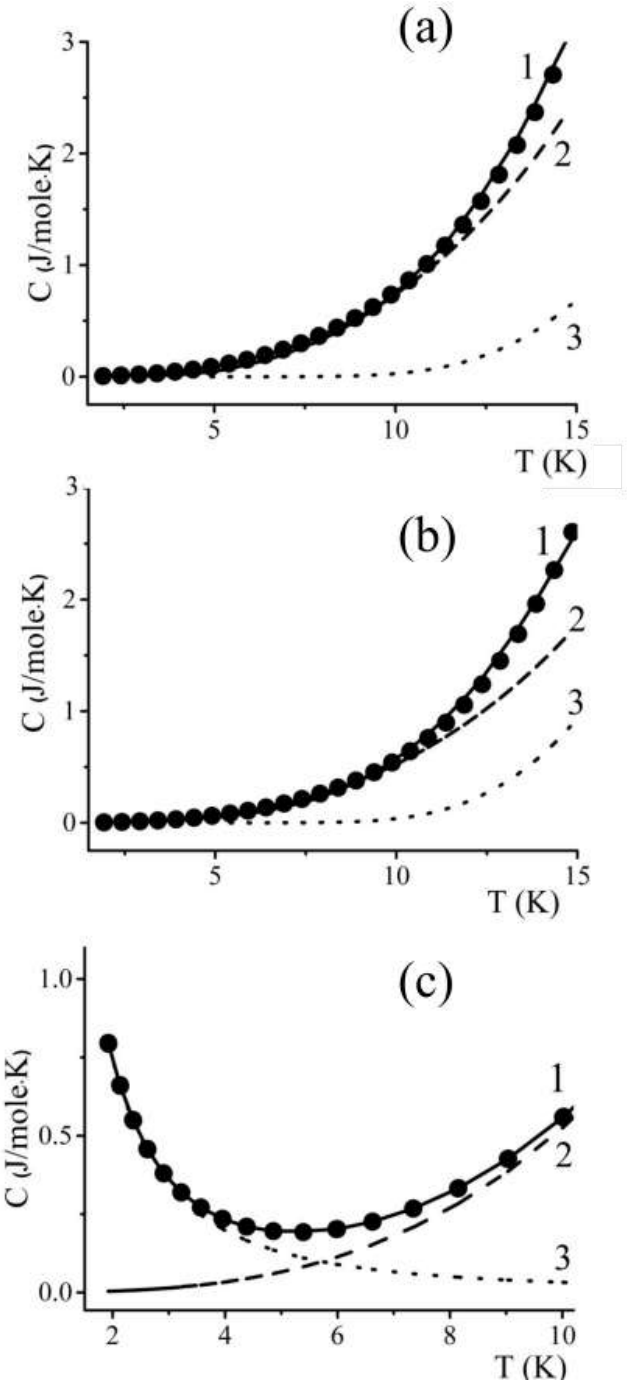

Figure 4.5 — Heat capacity approximation in single crystal NdP_5O_{14} (a); YbP_5O_{14} (b); GdP_5O_{14} (c). The circles are experimental data. The solid line shows the total calculated heat capacity (1), the dashed line is the Debye contribution (2), and the dotted line is the Schottky anomaly (3).

4.2 Heat capacity of pentaphosphates in magnetic field

This chapter presents the results of measurements of the temperature dependences of the heat capacity of pentaphosphate single crystals and glasses at different values of the external magnetic field from 0 to 9 T.

The obtained dependences for ReP_5O_{14} ($Re = Nd$, Yb, Gd) pentaphosphate single crystals in the temperature range from 1.9 to 15 K are presented in Figures 4.6 (a – c), respectively.

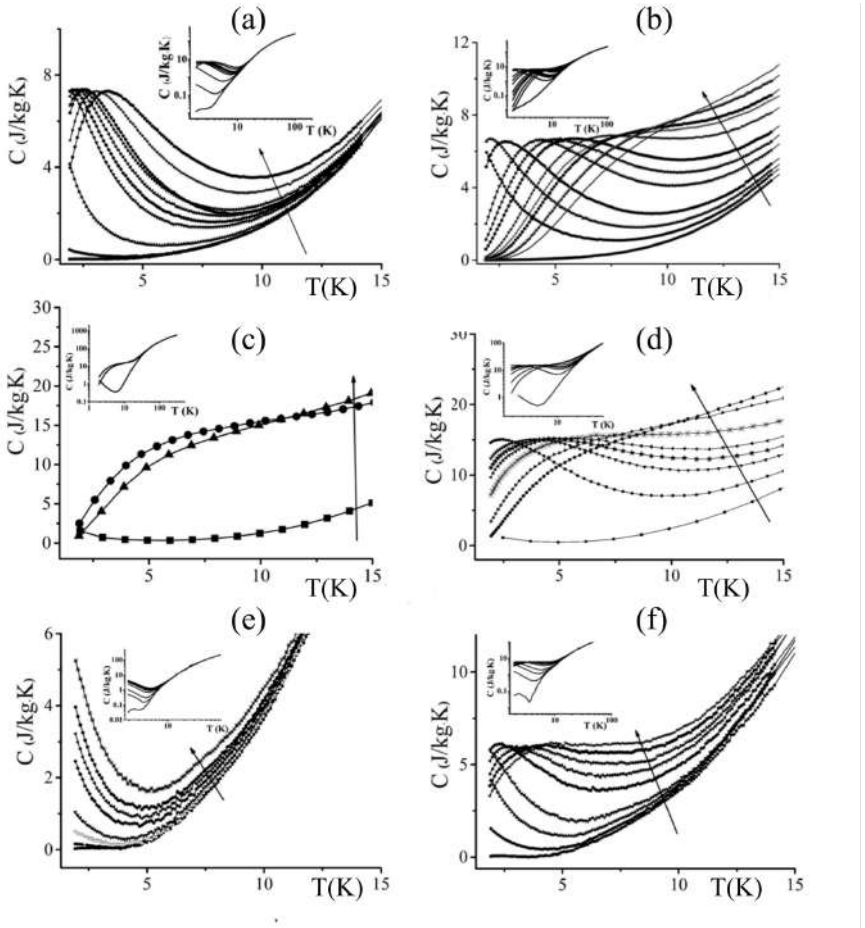

Figure 4.6 — Temperature dependences of heat capacity for single crystal ReP_5O_{14} where ($Re = Nd$ (a), Yb (b), Gd (c)) and pentaphosphate glass ReP_5O_{14} where ($Re = Gd$ (a), Sm (b), Ce (c)) below 15 K. The magnitudes of the magnetic fields in these measurements were: 0; 1.0; 3.0; 5.0; 5.5; 6.0; 6.5; 7.0; 8.0; 9.0 T, the arrow shows the direction of increase in the magnitude of the magnetic field. The insets show the heat capacity in the same magnetic fields in the whole temperature range from 1.9 to 100 K in double logarithmic scale.

Temperature dependences of heat capacity at different values of external magnetic field for ReP_5O_{14} (Re = Gd, Sm, Ce,) pentaphosphate glasses are presented in Figures 4.6 – (d – f).

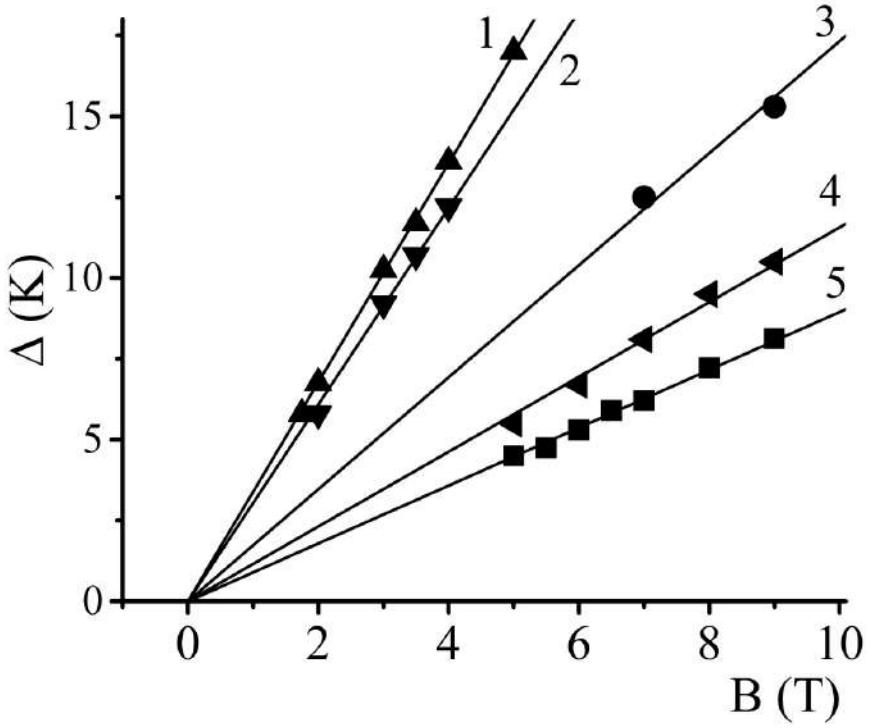

Figure 4.7 — Dependence of the cleavage of the main Kramers doublet on the magnetic field B for all pentaphosphate samples. Numbers in the figure indicate the following samples: 1 - YbP_5O_{14}, 2- pentaphosphate glass GdP_5O_{14}, 3 - GdP_5O_{14}, 4 - pentaphosphate glass CeP_5O_{14}, 5 - NdP_5O_{14}. The straight line shows the linear approximation.

The results show that for both NdP_5O_{14}, GdP_5O_{14}, YbP_5O_{14}, single crystals and SmP_5O_{14}, CeP_5O_{14}, GdP_5O_{14} pentaphosphate glasses, the magnitude of heat capacity is markedly influenced by the magnetic field at temperatures below 15 K.

In general, low-energy excitations having a wide energy distribution due to random structural disorder are a universal feature distinguishing the glassy state from the crystalline state.

An ion of a rare-earth element embedded in a glass or crystal matrix is exposed to the crystal field of the surrounding ions, so that the Stark effect splits each single level of the free ion into a group of levels. The application of an external magnetic field leads to the displacement of singlet and splitting with the removal of

degeneracy of doublet Stark levels. The magnitude of the splitting is proportional to the magnitude of the applied field.

Table 7 — Value of g - factor for single crystals

Sample	g - factor
NdP_5O_{14}	1.3
GdP_5O_{14}	2.5
YbP_5O_{14}	5

In the case of samarium pentaphosphate glass, fluorescence and optical absorption studies in the previously cited literature showed that samarium enters the lattice as a trivalent Sm^{3+} [**117**]. As can be observed from Figure 4.6 on the experimentally obtained temperature dependence of heat capacity for this sample, the value of the maximum is in the temperature region below 1.9 K. The technical possibility to conduct measurements at such low temperatures was not available. It was not technically possible to carry out measurements at such low temperatures.

The energy splitting Δ for non-zero applied fields caused by the Zeeman effect is expressed by the same formula as in Chapter 3. In addition to the displacement of the maximum, its blurring occurred. From the value of the magnitude of the maximum, we can calculate the magnitude of the splitting of the main Kramers doublet in the magnetic field B, according to formula 2.5. Figure 4.7 shows the dependence of the magnitude of the splitting energy on the magnetic field for all pentaphosphate samples. As could be expected, the shift of the heat capacity maximum depends linearly on the applied field.

The construction of these dependences allowed us to calculate the g-factor for the investigated pentaphosphate samples, except for the sample of samarium pentaphosphate glass. The obtained values are given in Tables 7 – 8.

Table 8 — Value of g-factor for pentaphosphate glasses

Sample	g - factor
SmP_5O_{14}	–
CeP_5O_{14}	1.7
GdP_5O_{14}	4.5

4.3 Magnetic entropy

The performed measurements of heat capacity in external magnetic fields allow us to calculate the change of entropy and magnetic entropy from 1.9 K to a certain temperature T.

The entropy and magnetic entropy values were calculated for ReP_5O_{14} ($Re = Nd$, Yb, Gd) pentaphosphate single crystals and ReP_5O_{14} ($Re = Sm$, Ce, Gd) pentaphosphate glasses. The obtained dependences are presented in Figures 4.8 (a – f).

As can be seen from the figures for all pentaphosphate samples in the temperature range from 1.9 K to 20 K the magnetic entropy is negative. The magnetic entropy of the investigated pentaphosphates can be compared with the magnetic entropy in some magnetocaloric materials, which earlier publications suggested for application in magnetic refrigerators. The entropy value found for a number of rare-earth pentaphosphates, as well as for the investigated dysprosium garnets, is slightly smaller than that of chromium-potassium alum and dysprosium-gallium garnet [**109**], and several times smaller than the magnetic entropy in the same magnetic field in gadolinium phosphate [**110**]. It can be noted that the magnetocaloric effect associated with Schottky anomalies is quite strong with respect to crystal defects and impurities. Therefore, single crystals and glasses of a number of rare-earth pentaphosphates can be recommended for use in adiabatic magnetic refrigerators.

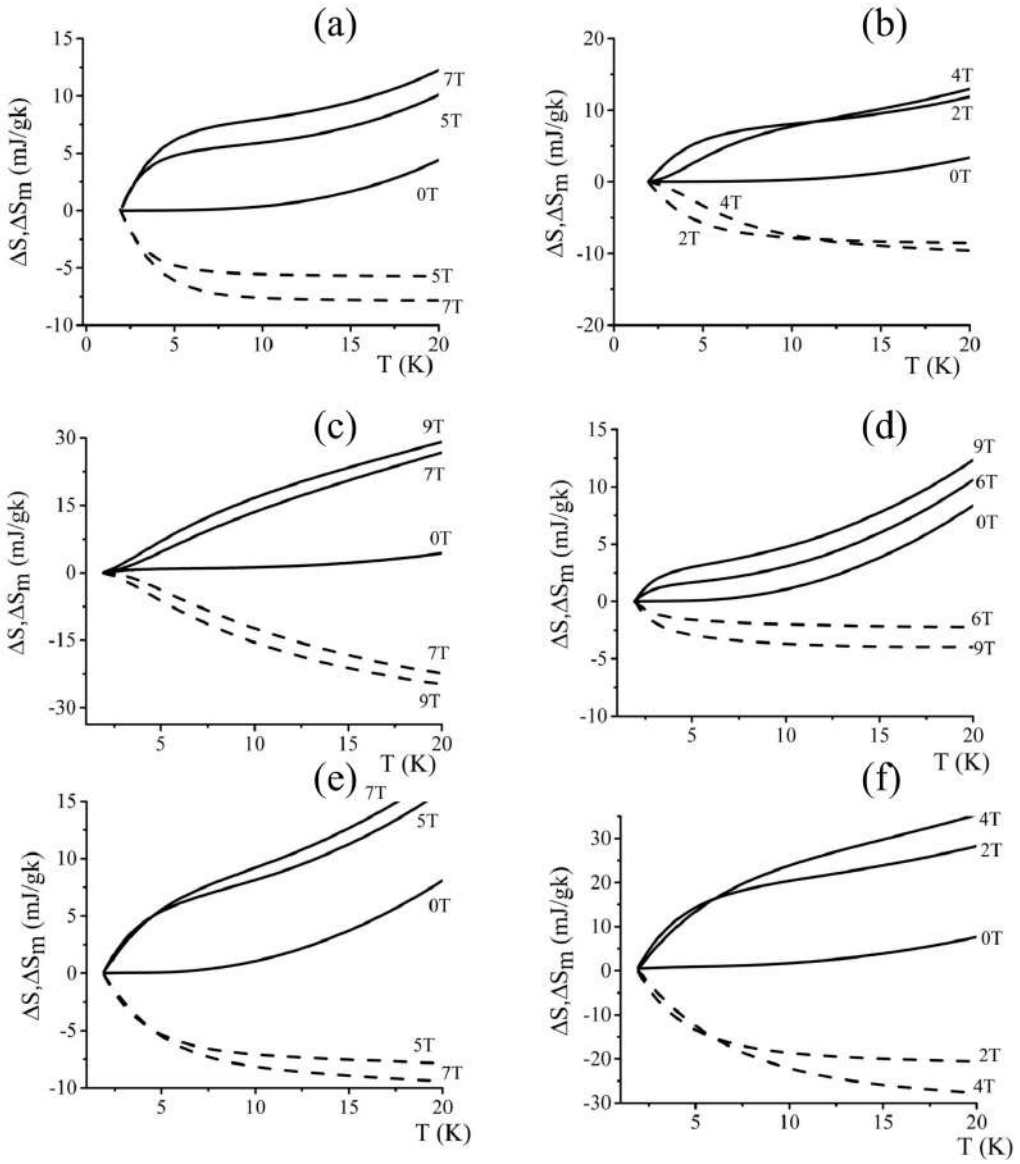

Figure 4.8 — Entropy change (solid lines) and magnetic entropy change (dashed lines) for NdP_5O_{14} (a); YbP_5O_{14} (b); GdP_5O_{14} (c); SmP_5O_{14} (d); CeP_5O_{14} (e); glass GdP_5O_{14} (f). The values of magnetic fields are indicated in the figure.

4.4 Chapter 4 Conclusions

The following conclusions were drawn from the results of the study in Chapter 4:

– For single crystals and glasses of pentaphosphates (NdP_5O_{14}, GdP_5O_{14}, YbP_5O_{14}, SmP_5O_{14}, CeP_5O_{14}) experimental temperature dependences of the heat capacity in the temperature range from 1.9 to 100 K and various magnetic fields from 0 to 9 T were obtained. For single crystal samples, the

experimental value of the heat capacity was described by the sum of the phonon (Debye) contribution and the contribution of the Schottky anomaly due to the population of Starkov levels and the split main Kramers doublet. For pentaphosphate glasses the calculation was not carried out due to the strong blurring of energy levels. The difference of heat capacities of the material in the glassy and crystalline states can be related to the glass structure.

– After the approximation, the Debye temperatures and low-energy excitation energy values were calculated for a number of rare-earth pentaphosphates (NdP_5O_{14}, GdP_5O_{14}, YbP_5O_{14}). Using experimental data of heat capacity values obtained in magnetic fields, magnetic entropy was calculated.
– The obtained values of magnetic entropy allow us to propose the use of single crystals and glasses of a number of rare-earth pentaphosphates as elements for low-temperature magnetic refrigerators.

Chapter 5. Heat capacity of solid solutions of aluminates($Y_{1-x}Er_xAlO_3$)

This chapter presents the results of experimental studies of the heat capacity of mixed aluminate single crystals with the general formula $Y_{1-x}Er_xAlO_3$ ($x = 0; 0.07; 0.1; 0.15; 0.2; 0.45$). The measurements were carried out in the temperature range from 1.9 to 100 K in the absence of a magnetic field applied to the samples and in fields up to 6 T. Similar to the results of Chapter 2, the various contributions to the heat capacity in the absence of an external magnetic field were calculated. Based on the experimental data obtained, entropy and magnetic entropy values for aluminates were calculated. The nature of heat capacity anomalies in the magnetic field related to the peculiarities of the structure of mixed aluminates is discussed [**118**].

5.1 Samples for research

Yttrium aluminates $YAlO_3$ have high mechanical strength, good thermal conductivity, and high transparency [**119**]. Aluminates are synthesized on the basis of yttrium oxide Y_2O_3 and aluminium oxide Al_2O_3 in the ratio of 1:1 and 1:3, respectively. When yttrium is substituted with paramagnetic rare earth ions, these materials have a successful combination of spectral properties [**119**]. The aluminates have a rhombic lattice ($a = 0.5179$; $b = 0.5329$; $c = 0.77370$ nm) and are optically biaxial [**120**]. To measure the heat capacity, plates were cut from these samples with orientation [111]. $YAlO_3 : Er$ single crystals are opaque at $\nu > 35.000$ cm^{-1} [**121**], which appears to be due to the formation of colouring centres.

5.2 Heat capacity in the zero field

Figure 5.1 shows the experimental dependences of the heat capacity of a series of $Y_{1-x}Er_xAlO_3$ samples ($x = 0; 0.07; 0.1; 0.15; 0.2; 0.45$) in a zero magnetic field: in double logarithmic scale in the temperature range from 1.9 to 100 K and in a linear scale at temperatures below 20 K. The dependence of the heat capacity is

determined by the presence of low-energy excitations. It follows from the nature of the dependences that in the helium temperature region the heat capacity is determined by the presence of low-energy excitations. The energy of the lowest excited level of the ${}^4I_{15/2}$ multiplet of the Er^{3+} ion in $YAlO_3$: $\sim$ 51 K [**122**], i.e., the energies are too high for the observed features. This level position cannot explain the observed features at helium temperatures.

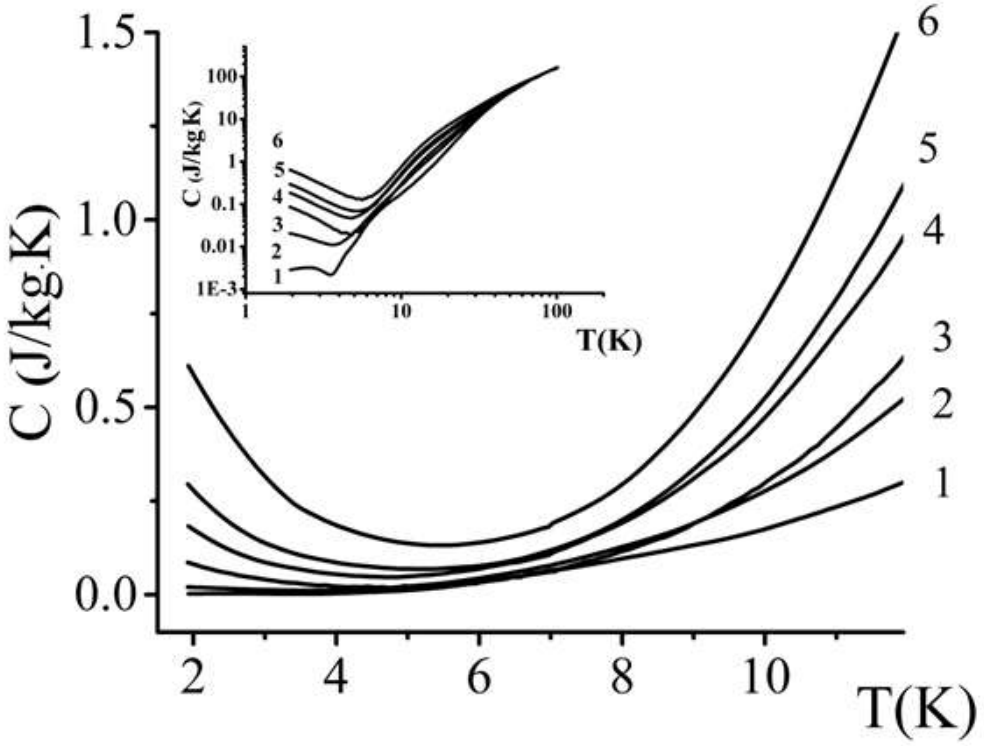

Figure 5.1 — TTemperature dependences of heat capacity for $Y_{1-x}Er_xAlO_3$ below 20 K with different yttrium concentration. Numbers 1, 2, 3, 4, 5, 6 in the figure correspond to yttrium concentrations x =0; 0.07; 0.1; 0.15; 0.2; 0.45 respectively. The inset shows the heat capacity over the entire temperature range from from 1,9 to 100 K in double logarithmic scale.

The approximation at temperatures up to 10 K allowed us to determine the Debye temperature for yttrium aluminate $YAlO_3$ equal to 710 K (see formula 1.10). In yttrium aluminate, the temperature dependence of the heat capacity was described only by the Debye contribution (Figure 5.2).

It can be assumed that the Debye temperature for mixed erbium aluminates $YAlO_3 : Er$ varies linearly with the composition of the aluminate. Thus, knowing the temperature for pure yttrium aluminate, it is possible to estimate the temperatures for mixed erbium aluminates as well. The calculated values of the

Debye temperatures are given in Table 9. The obtained values are necessary for further calculation of fitting parameters of the heat capacity value.

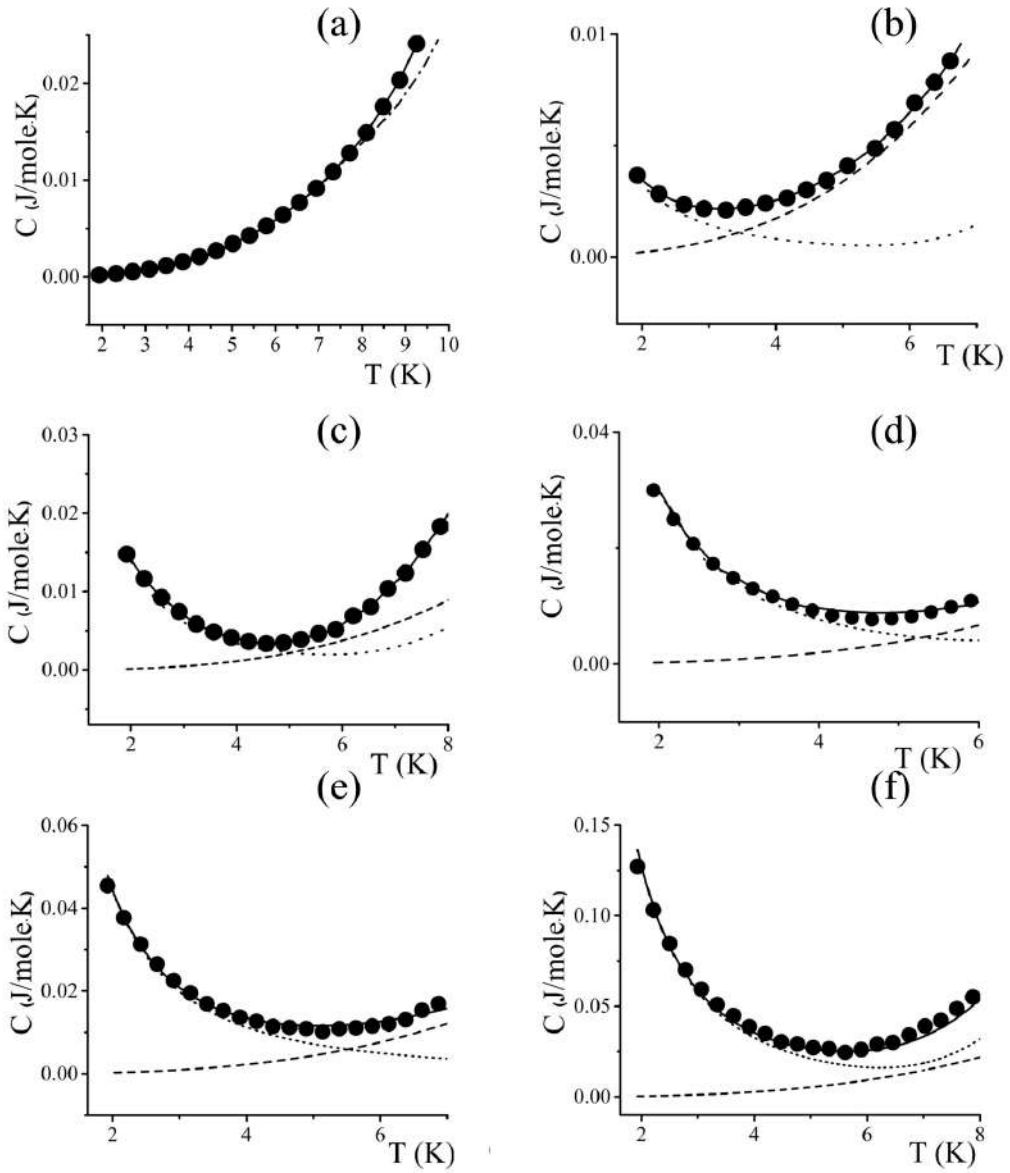

Figure 5.2 — Approximation of heat capacity in $Y_{1-x}Er_xAlO_3$ crystal (where x = 0 (a); 0.07 (b); 0.1 (c); 0.15 (d); 0.2 (e); 0.45 (f)). The circles are experimental data. The solid line shows the total calculated heat capacity, the line with a dot - Debye contribution.

In Chapter 2 (see Part 2.3), the results of the study of erbium-doped garnets were discussed. When analysing the dependences of heat capacity obtained for aluminates, a similar approach was used.

Microscopic regions with different concentrations of erbium are formed in solid solutions [**123**].

Table 9 — Debye temperature of tested samples

Sample	θ, K
$YAlO_3$	710
$Y_{0,93}Er_{0.07}AlO_3$	700
$Y_{0,9}Er_{0.1}AlO_3$	695
$Y_{0,85}Er_{0.15}AlO_3$	680
$Y_{0,8}Er_{0.2}AlO_3$	650
$Y_{0,55}Er_{0.45}AlO_3$	610

The dependence of the total heat capacity as a function of temperature for $Y_{1-x}Er_xAlO_3$ crystals ($x = 0; 0.07; 0.1; 0.15; 0.2; 0.45$), as well as for GGG crystals (Chapter 2), was approximated by the sum of two contributions: Debye and Schottky (equation 2.4). When approximating the experimental dependence of the total heat capacity, we limit ourselves to temperatures lying in the range of 1.9 - 8 K.

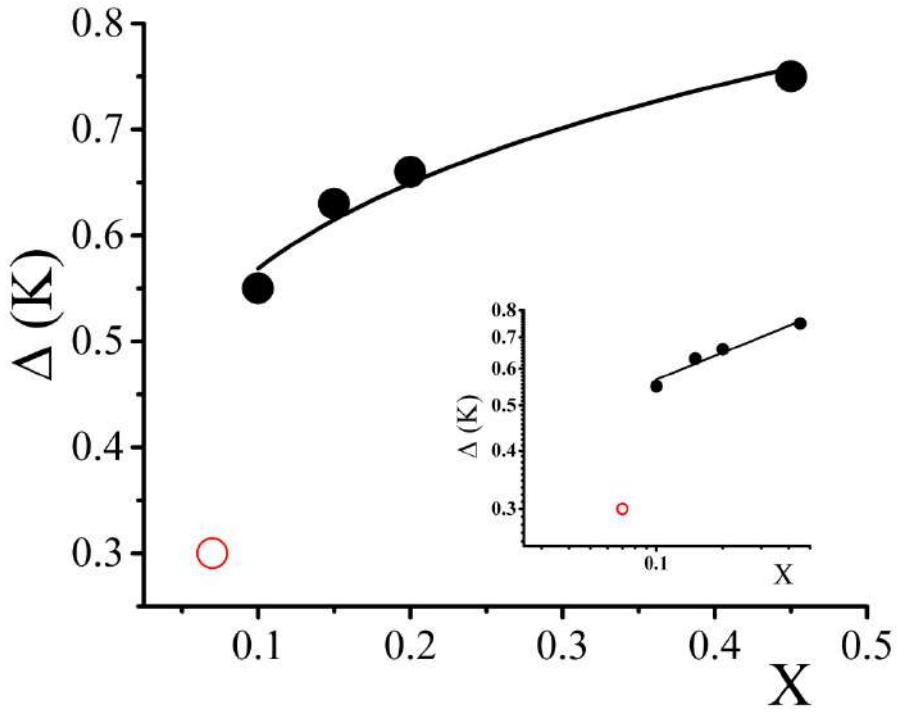

Figure 5.3 — Dependence of Δ on the amount of erbium ions. The inset shows this dependence in double logarithmic scale. The filled symbols participate in the approximation, and the unfilled symbol does not participate

The approximation parameters for such data processing are the splitting of the ground doublet Δ and the difference between the lowest energy levels and the first excited Kramers doublet Δ_1. This splitting is related to the Kramers nature of the ion, when it is possible to remove the degeneracy of the ground level in a zero external magnetic field due to the interaction of magnetic moments of neighbouring ions. The energy of the corresponding ground level splitting in $YAlO_3 : Er$ $\Delta < 1$ K in the studied concentration range of erbium in the solid solution.

Figures 5.2 (a – e) show approximations for mixed erbium aluminates, with erbium concentration $x = 0; 0.07; 0.1; 0.15; 0.2; 0.45$. It is clear from the figures that the approximation to two contributions - Debye and Schottky - gives very good results in the range from 1.9 to 8 K.

Figure 5.3 shows the dependence of the parameter Δ on the composition x, obtained from the study of a series of mixed aluminate samples. For the sample $Y_{1-x}Er_xAlO_3$ ($x = 0.07$), the value of the splitting value Δ is noticeably smaller than Δ determined for the other studied samples. Apparently, the presence of strong inhomogeneity of the erbium concentration in the solid solution, which was discussed above, significantly affected the experimentally determined value of Δ. When approximating the dependence of $\Delta(x)$ by a step function, the value of Δ at $x = 0.07$ was not taken into account. Analyses of the dependence of Δ on x in a double logarithmic scale allowed us to determine that $\Delta \sim x^{0,2}$.

The evaluation of Δ and Δ_1 values is given in Table 10 aluminate samples $Y_{1-x}Er_xAlO_3$ ($x = 0.07; 0.1; 0.15; 0.2; 0.45$). According to the data presented in the table, it can be seen that with increasing erbium concentration there is a slight increase in the values of Δ_1.

Table 10 — Adjusted values of the main doublet splitting for Er^{3+} (Δ) ions and energy of the first excited level (Δ_1)

Sample	Δ, K	Δ_1, K
$Y_{0,93}Er_{0,07}AlO_3$	0.3	71
$Y_{0,9}Er_{0,1}AlO_3$	0.55	72
$Y_{0,85}Er_{0,15}AlO_3$	0.63	76
$Y_{0,8}Er_{0,2}AlO_3$	0.66	77
$Y_{0,55}Er_{0,45}AlO_3$	0.75	77

5.3 Heat capacity of aluminates in magnetic field

This chapter presents the results of measurements of the temperature dependences of the heat capacity of yttrium aluminates at different values of the external magnetic field from 0 to 9 T.

The results of studies have shown that for single crystals of yttrium aluminates doped with erbium the value of heat capacity is significantly influenced by the magnetic field at temperatures below 15 K.

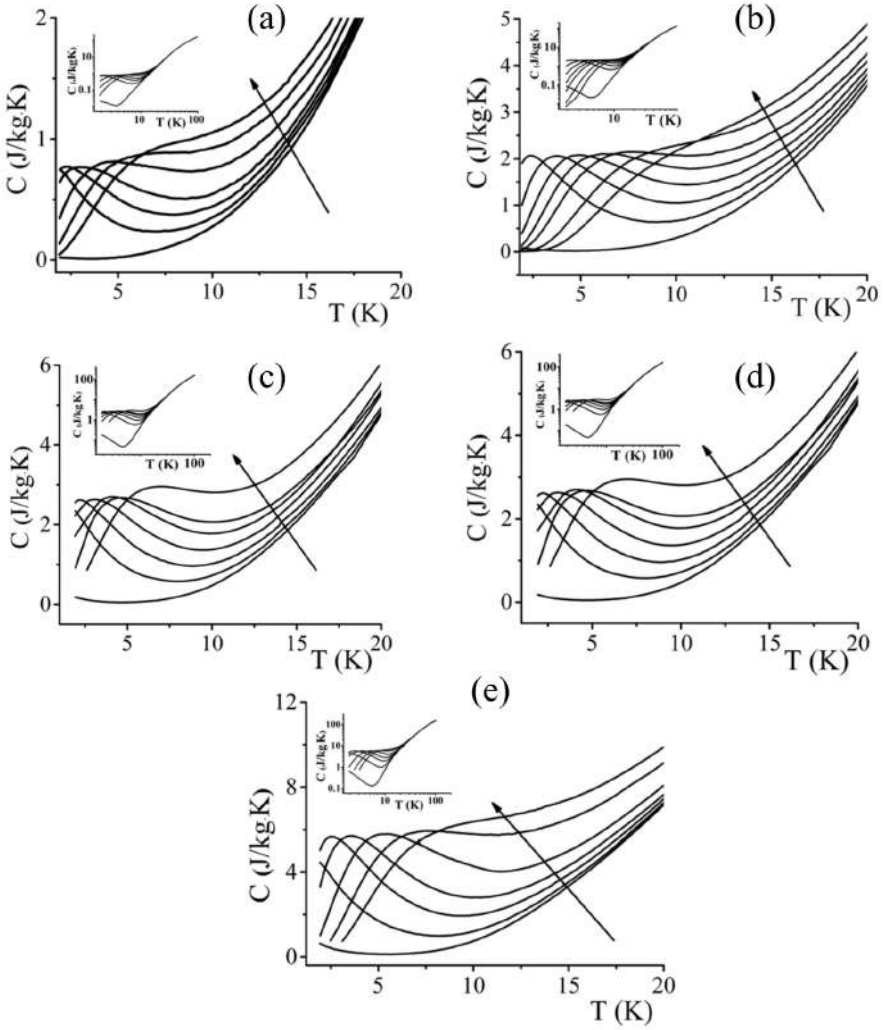

Figure 5.4 — Temperature dependences of heat capacity for $Y_{1-x}Er_xAlO_3$ (where $x = 0.07; 0.1; 0.15; 0.2, 0.45$) in different magnetic fields at temperatures from 1.9 to 20 K. The insets show these dependences in the temperature range from 1.9 to 100 K in double logarithmic scale. The magnitudes of magnetic fields in these measurements were: 0; 1,0; 1,5; 2,0; 3,0; 4,0; 5,0 T. The arrow shows the direction of magnetic field increase.

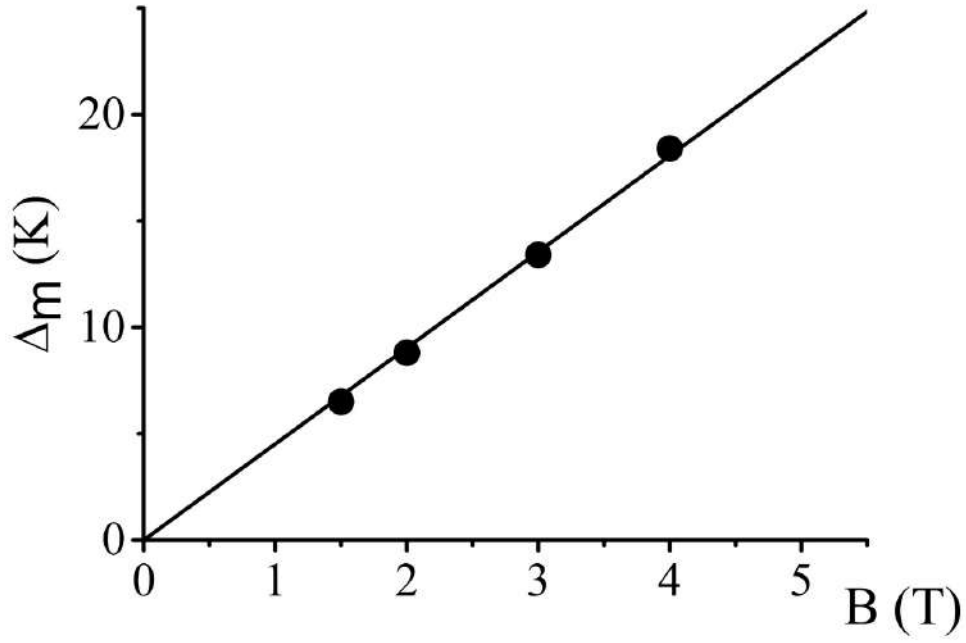

Figure 5.5 — Dependence of the splitting of the main Kramers doublet on the magnetic field B for the crys $Y_{0.55}Er_{0.45}AlO_3$. The solid line corresponds to the linear approximation of this dependence.

Table 11 — Value of g-factor for Er^{3+} ions in crystals $Y_{1-x}Er_xAlO_3$

x	g - factor
0.07	5.4
0.1	5.7
0.15	6.1
0.2	6.5
0.45	6.8

Similarly to Chapter 3, a pronounced maximum was observed on the experimental dependence of heat capacity when a magnetic field of 1 T was applied (see Figure 5.4 (a-e)). With increasing applied magnetic field, the position of the maximum shifted towards higher temperatures. In addition to displacement of the maximum, its blurring occurred. Figure 5.5 shows the dependence of the magnitude of the splitting energy of the main duplex on the magnetic field for the aluminate sample $Y_{0.55}Er_{0.45}AlO_3$. For the other samples these dependences also had linear character. As could be expected, the shift of the heat capacity maximum depends linearly on the applied field.

From the value of the maximum value we can calculate the value of the splitting of the main Kramers doublet in the magnetic field B, according to formula 2.5: the construction of these dependences allowed us to calculate the g-factor for aluminates with $x = 0.07; 0.1; 0.15; 0.2, 0.45$. The obtained values are given in Table 11. As can be seen from Table 11, the value of g-factor increases with increasing erbium concentration.

5.4 Magnetic entropy

The entropy and magnetic entropy values were calculated for erbium aluminates. The obtained dependences are presented in Figures 5.6 (a – e).

As can be seen from the results, with increasing erbium concentration, an increase in entropy is observed in all investigated samples. The temperature dependences of entropy (Figure 5.6) at temperatures below 10 K clearly show the magnetocaloric effect. It should also be noted that the results obtained indicate that all of the studied aluminate samples can be used for adiabatic magnetic refrigerators. A comparison of the magnitude of this effect with substances already used in magnetic refractors [**110**], as well as with the results for garnet samples with dysprosium (Chapter 3), allows us to conclude that garnet samples with dysprosium are more promising than aluminate samples with erbium.

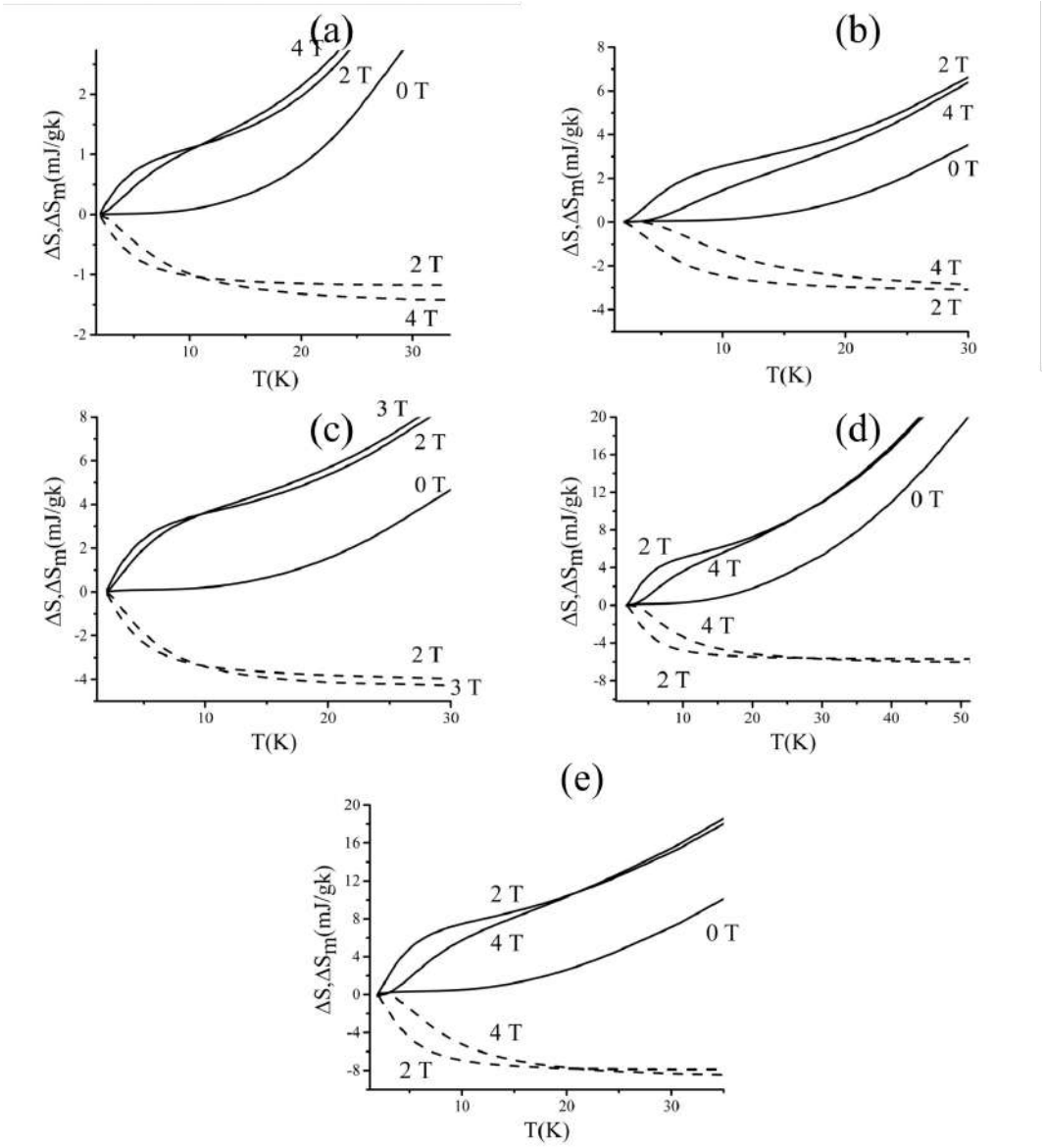

Figure 5.6 — Entropy change (solid lines) and magnetic entropy change (dashed lines) for $Y_{1-x}Er_xAlO_3$ ($x = 0.07(a); 0.1(b); 0.15(c); 0.2(d); 0.45(e)$). The values of magnetic fields are indicated in the figure.

5.5 Chapter 5 Conclusions

According to the results of the study in Chapter 5, the following conclusions can be drawn.

– For single crystals $Y_{1-x}Er_xAlO_3$ ($x = 0; 0.07; 0.1; 0.15; 0.2; 0.45$) experimental temperature dependences of heat capacity in the temperature range from 1.9 to 100 K and different magnetic fields from 0 to 9 T were obtained. Also, for these samples, the experimental value of heat capacity

was described by the sum of the phonon (Debye) contribution and the contribution from the Schottky anomaly due to the population of the levels and the split main Kramers doublet.

– After the approximation, the Debye temperature was calculated and the values of low-energy excitation energies were calculated for single crystals of $Y_{1-x}Er_xAlO_3$ aluminates ($x = 0.07; 0.1; 0.15; 0.2; 0.45$). The splitting was caused by interaction with neighbouring magnetic ions and increased with increasing erbium concentration (x) according to the law (with the exception of the sample with equal to $= 0.07$) $\Delta \sim x^{0.2}$.

– Using experimental data of heat capacity values obtained in magnetic fields, magnetic entropy was calculated. The obtained values of magnetic entropy allow us to propose the use of single crystals of aluminates as elements for low-temperature magnetic refrigerators.

Conclusions

The following main results have been obtained in this thesis work:

1. In the erbium-doped single crystal of gallium-gadolinium garnet, in a series of $Dy_xY_{3-x}Al_5O_{12}$ garnet single crystals (x = 0; 0.15; 0.50; 1.00; 1.50, 2.25; 3.00), in single crystals and glasses of pentaphosphates (NdP_5O_{14}, GdP_5O_{14}, YbP_5O_{14}, SmP_5O_{14}, CeP_5O_{14}), and in single crystals of aluminates with the general formula $Y_{1-x}Er_xAlO_3$ ($x = 0; 0.07; 0.1; 0.15; 0.2; 0.45$) temperature dependences of heat capacity in magnetic fields in the range from 0 to 9 T were experimentally obtained.
2. It is shown that for the interpretation of the temperature dependences of heat capacity in the studied single crystals in the zero magnetic field at low temperatures it is sufficient to take into account the contribution of lattice vibrations and Schottky anomalies due to paramagnetic ions. The experimental heat capacity of pure and erbium-doped GGG crystals was approximated by the sum of the contributions of Schottky anomalies associated with gadolinium and erbium ions and the Debye and Einstein lattice contributions. For the other studied samples, only the Debye and Schottky anomalies contributions were taken into account. A multilevel model was used to calculate the Schottky heat capacity, which takes into account the contribution from a set of excited levels. It is demonstrated that in the low-temperature region the Schottky contribution dominates over the lattice contribution for most of the samples with paramagnetic ions
3. 3. For garnets, aluminates and pentaphosphates containing paramagnetic ions, a strong dependence of heat capacity on the applied magnetic field due to the splitting and displacement of Stark levels and the corresponding shift of Schottky anomalies to high temperatures has been demonstrated. The values of the corresponding g-factors are calculated.
4. On the basis of measurements of heat capacity in magnetic fields, the magnetic contribution to entropy was calculated. Significant magnetocaloric effect was revealed for all images containing paramagnetic ions, which allows the use of the investigated crystals in magnetic refrigerators. It is shown that the use of GGG crystal doped with erbium is preferable

in comparison with pure GGG crystal. For the series of garnets with dysprosium $Dy_xY_{3-x}Al_5O_{12}$, it is reasonable to use crystals with x larger than 1.5. It was found that single crystals of pentaphosphates also have a rather strong magnetocaloric effect. The weakest magnetocaloric properties were established for solid solutions $Y_{1-x}Er_xAlO_3$.

5. It is shown that in garnet with dysprosium $Dy_1Y_2Al_5O_{12}$ an anomalous behavior of heat capacity is observed, consisting in the appearance of two heat capacity peaks when a magnetic field is applied. The revealed anomaly is most probably a consequence of the clustering of the solid solution of this composition. This result shows that the heat capacity is sensitive to the change of the order of substitution in crystalline solutions.

References

[1] Baryshevsky, V.G. YAlO3:Ce-fast-acting scintillators for detection of ionizing radiation / V.G. Baryshevsky, M.V. Korzhik, V.I. Moroz, V.B. Pavlenko, A.A. Fyodorov, S. A. Smirnova, O. A.Egorycheva, V. A. Kachanov // Nuclear Instruments and Methods in Physics Research Section B: Beam Interactions with Materials and Atoms. – 1991. – Vol.58. – №2. – P. 291-293.

[2] van Loef, E.V. Scintillation Properties of $SrHfO_3$: Ce^{3+} and $BaHfO_3$: Ce^{3+} Ceramics / E.V. van Loef, W.M. Higgins, J. Glodo, C. Brecher, A. Lempicki, Venkat Venkataramani, W. W. Moses, E. S. Derenzo, S. Kanai Shah // Transactions on Nuclear Science. – 2007. – Vol.54. – №3. – P. 741-743.

[3] Zhang, L. Fast fluorescence and scintillation properties of cerium and praseodymium doped lutetium orthoborates / L. Zhang, C. Pedrini, C. Madej, C. Dujardin, J.C. Gacon, [et al.] // Radiation Effects and Defects in Solids. – 1999. – Vol.150. – №1-4. – P. 47-52.

[4] Knitel, M.J. Photoluminescence, and scintillation/thermoluminescence yields of several Ce^{3+} and Eu^{2+} activated borates / M.J. Knitel, P. Dorenbos, C.W.E. van Eijk, B. Plasteig, B. Viana, A. Kahn-Harari, D. Vivien // Nuclear Instruments and Methods in Physics Research Section A: Accelerators, Spectrometers, Detectors and Associated Equipment. – 2000. – Vol.443. – №2. – P. 364-374.

[5] Yanagida, T. Improvement of ceramic YAG(Ce) scintillators to (YGd)3Al5O12(Ce) for gamma-ray detectors / T. Yanagida, T. Itoh, H. Takahashi, S. Hirakuri, M. Kokubun, [et al.] // Nuclear Instruments and Methods in Physics Research Section A: Accelerators, Spectrometers, Detectors and Associated Equipment. – 2007. – Vol.579. – №1. – P. 23-26.

[6] Kamada, K. Crystal Growth and Scintillation Properties of Ce Doped $Gd_3(GaAl_5)O_{12}$ Single Crystals / K. Kamada, T. Yanagida, J. Pejchal, M. Nikl, T. Endo, K. Tsutsumi; Y.Fujimoto, A.Fukabori, A.Yoshikawa // Transactions on Nuclear Science. – 2012. – Vol.59. – №5. – P. 2112-2115.

[7] Fukabori, A. Optical and scintillation characteristics of Y_2O_3 transparent ceramic / A. Fukabori, T. Yanagida, J. Pejchal, S. Maeo, Y. Yokota, A. Yoshikawa, T. Ikegami, F. Moretti, K. Kamada // Journal of Applied Physics. – 2010. – Vol.107. – №7. – P. 073501.

[8] Fukabori, A. Scintillation Characteristics of Undoped Sc_2 O_3 Single Crystals and Ceramics / A. Fukabori, L. An, A. Ito, V. Chani, K. Kamada, T.i Goto, A. Yoshikawa // IEEE Transactions on Nuclear Science. – 2012. – Vol.59. – №5. – P. 2594-2600.

[9] Shmurak, S.Z. Studies of nanocrystalline rare earth gallate and aluminate scintillators prepared by a new method / S.Z. Shmurak, G.K. Strukova, I.M. Smyt'ko, N.V. Klassen, N.P. Kobelev, S. E. Derenzob, M. J. Weberb // Nuclear Instruments and Methods in Physics Research Section A: Accelerators, Spectrometers, Detectors and Associated Equipment. – 2005. – Vol.537. – №1. – P. 149-153.

[10] Akhtar, M.N. Structural elucidation and magnetic behaviour evaluation of gallium substituted garnet ferrites / M.N. Akhtar, S.N. Khan, H. Ahmad, M.S. Nazir, M.A. Khan // Ceramics International. – 2018. – Vol T.44. – №18. – P. 22504-22511.

[11] Alekseev, N.E. Laser phosphate glasses / N.E. Alekseev, V.P. Gapontsev, M.E. Jabotinsky. - Moscow: Science, 1980. - 352 p.

[12] Phillips, W.A. Tunneling states in amorphous solids / W.A. Phillips // Journal of Low Temperature Physics. – 1972. – Vol.7. – №3. – P. 351-360.

[13] Tegus, O. Transition-metal-based magnetic refrigerants for room-temperature applications / O. Tegus, E. Brück, K.H.J. Buschow, F.R. de Boer // Nature. – 2002. – Vol.415. – №6868. – P. 150-152.

[14] Pecharsky, V.K. Magnetocaloric effect and magnetic refrigeration / V.K. Pecharsky, K.A.G. Jr // Journal of Magnetism and Magnetic Materials. – 1999. – Vol.200. – №1. – P. 44-56.

[15] Debye, P. Zur Theorie der spezifischen Wärmen / P. Debye // Annalen der Physik. – 1912. – Vol.344. – №14. – P. 789-839.

[16] Giauque, W.F. Attainment of Temperatures Below 1° Absolute by Demagnetization of Gd2(SO4)3 8H2O / W.F. Giauque, D.P. MacDougall // Phys. Rev. – 1933. – Vol.43. – №9. – P. 768-768.

[17] W.J.D. Haas, E.C. Wiersma, H.A. Kramers : Haas, W.J.D., E.C. Wiersma, H.A. Kramers. Experiments on adiabatic cooling of paramagnetic salts in magnetic fields / W.J.D. Haas, E.C. Wiersma, H.A. Kramers // Physica. – 1934. – Vol T.1. – №1. – P. 1-13.

[18] KURTI, N. Nuclear Cooling / N. KURTI, F.N.H. ROBINSON, F. SIMON, D.A. SPOHR // Nature. – 1956. – Vol.178. – №4531. – P. 450-453.

[19] KURTI, N. Further Experiments with the Magnetic Cooling Method / N. KÜRTI, F. SIMON // Nature. – 1935. – Vol.135. – №3401. – P. 31-31.

[20] Gorter, C.J. Zur Thermodynamik des Supraleitenden Zustandes / C.J. Gorter, H. Casimir // Archives du Musee Teyler: Serie III, Vol. VIII Fascicule 1. – Dordrecht: Springer Netherlands, 1935. – P. 55-60.

[21] Kaminskii A.A. Laser Crystals: Their Physics and Properties. — 2nd ed.. — Springer, 1990.– 256 p.

[22] Shevchenko, E.V. Heat capacity of rare-earth aluminum garnets / E.V. Shevchenko, E.V. Charnaya, E.N. Khazanov, A.V. Taranov, A.S. Bugaev // Journal of Alloys and Compounds. – 2017. – Vol.717. – P. 183-189.

[23] Lezova, I.E. Features of low-temperature heat capacity and phonon kinetics in single crystals and glasses of a number of pentaphosphates / I.E. Lezova, E.I. Salamatov, A.V. Taranov, E.N. Khazanov, E.V. Charnaya, E.V. Shevchenko. – 2019. – T.156. – No. 5. – P. 918-924.

[24] Kittel, P. Magnetic refrigeration in space - Practical considerations / P. Kittel. – 1980. – Vol. 4. – № 6. – P. 266-272.

[25] Callen, H.B. Thermodynamics / H.B. Callen. – Wiley & Sons, New York, 1981.

[26] Einstein, A. Theorie der Strahlung und die Theorie der Spezifischen Warme / A. Einstein. – 1907. – Vol.327. – №1. – P. 180-190.

[27] Born, M. Uber Schwingungen im Raumgittern. / M. Born, T. von Karman. – Vol.13. – P. 297-309.

[28] Asplund, M. Heat capacity and thermodynamic functions of γ - Al_2O_3 synthesized from $Al(NO_3)_3$ / M. Asplund, J.J. Calvin, Y. Zhang, B. Huang, B.F. Woodfield // The Journal of Chemical Thermodynamics. – 2019. – Vol.132. – P. 295-305.

[29] Goel, P. Lattice dynamics and Born instability in yttrium aluminum garnet, $Y_3Al_5O_{12}$ / P. Goel, R. Mittal, N. Choudhury, S.L. Chaplot // Journal of Physics: Condensed Matter. – 2010. – Vol.22. – №6. – P. 065401.

[30] Wieckowski, J. Thermal properties of layered cobaltites $RBaCo_2O_{5.5}$ ($R = Y$, Gd, and Tb) / J. Wieckowski, M.U. Gutowska, A. Szewczyk, S. Lewinska, K. Conder, E. Pomjakushina, V. P. Gnezdilov, S. L. Gnatchenko // Phys. Rev. B. – 2012. – Vol.86. – №5. – P. 054404.

[31] Tari, A. The Specific Heat of Matter at Low Temperatures / A. Tari – Imperial College Press, 2003. – 352 p.

[32] Steinkemper, H. Stark level analysis of the spectral line shape of electronic transitions in rare earth ions embedded in host crystals / H. Steinkemper, S. Fischer, M. Hermle, J.C. Goldschmidt // New Journal of Physics. – 2013. – Vol.15. – №5. – P. 053033.

[33] Karlin, R. Magnetochemistry / R. Karlin. - 1980. - 400 p.

[34] Gopal, E.S.R. Specific Heats at Low Temperatures / E.S.R. Gopal. – New York: Plenum Press., 1966. – 240 p.

[35] Gutowska, M.U. Thermal properties of the $Nd_{1-x}Ca_xBaCo_2O_{5.5}$ compositions ($0 \leqslant x \leqslant 0.2$) / M.U. Gutowska, J. Wieckowski, A. Szewczyk, S. Kolesnik, B. Dabrowski, M. Kowalczyk, J. Pietosa, N. Nedelko, R. Minikayev // Journal of Alloys and Compounds. – 2016. – Vol.670. – P. 175-181.

[36] Andreenko, A.S. Magnetocaloric effects in rare-earth magnets / A.S. Andreenko, K.P. Belov, S.A. Nikitin, A.M. Silence. – 1989. – T.158. – No. 4. – P. 553. [In Russian]

[37] Tishin, A.M. The Magnetocaloric Effect and its Applications / A.M. Tishin, Y.I. Spichkin. – Bristol and Philadelphia: Institute of Physics Publishing, 2003. – 475 p.

[38] Physical Property Measurement System Heat Capacity Option User's Manual. – San Diego: Quantum Design., 2015.

[39] Hwang, J.S. Measurement of heat capacity by fitting the whole temperature response of a heat-pulse calorimeter / J.S. Hwang, K.J. Lin, C. Tien // Review of Scientific Instruments. – 1997. – Vol.68. – №1. – P. 94-101.

[40] Lashley, J.C. Critical examination of heat capacity measurements made on a Quantum Design physical property measurement system / J.C. Lashley, M.F. Hundley, A. Migliori, J.L. Sarrao, P.G. Pagliuso, [et al.] // Cryogenics. – 2003. – Vol.43. – №6. – P. 369-378.

[41] Brandt, B.L. Low temperature thermometry in high magnetic fields. VII. CernoxTM sensors to 32 T / B.L. Brandt, D.W. Liu, L.G. Rubin // Review of Scientific Instruments. – 1999. – Vol.70. – №1. – P. 104-110.

[42] Bunting, J.G. The specific heat of apiezon N grease / J.G. Bunting, T. Ashworth, H. Steeple. – 1969. – Vol.9. – №5. – P. 385-386.

[43] Non-smooth Specific Heat Between 200 K and 300 K due to Anomalous Specific Heat of Apiezon N-grease: Application Note. – San Diego: Quantum Design, 2014.

[44] Weber, H.P. Nd-ultraphosphate laser / H.P. Weber, T.C. Damen, H.G. Danielmeyer, B.C. Tofield // Applied Physics Letters. – 2003. – Vol.22. – №10. – P. 534-536.

[45] Van Wazer, J.R. Phosphorus and Its Compounds / J.R. Van Wazer. – Interscience Publishers, 1958. – 2046 p.

[46] Drozd, A.N. Diode-pumped solid-state lasers. / A.N. Drozd, I.S. Manak. – 2003. – No. 2. – P. 96-160.[In Russian]

[47] Jaulmes, S. Comptes Rendus / S. Jaulmes. – Acad. Sci, 1969. – 268 p.

[48] Bagieu-Beucher, M. Bull. Soc. Fr. Miner / M. Bagieu-Beucher, D. Tranqui. – 1970. – Vol.93. – P. 505.

[49] Danielmeyer, H. Fluorescence in neodymium ultraphosphate / H. Danielmeyer, H. Weber // IEEE Journal of Quantum Electronics. – 1972. – Vol.8. – №10. – P. 805-808.

[50] Albrand, K.-R. Crystal structure of the laser material NdP_5O_{14} / K.-R. Albrand, R. Attig, J. Fenner, J.P. Jeser, D. Mootz // Materials Research Bulletin. – 1974. – Vol.9. – №2. – P. 129-140.

[51] Parrot, R. Electron paramagnetic resonance of Gd^{3+} in CS symmetry and crystallographic study of rare-earth ultraphosphates. Case of Gd^{3+},Eu^{3+}, and Gd_xEu_{1-x} ultraphosphates / R. Parrot, C. Barthou, B. Canny, B. Blanzat, G. Collin // Phys. Rev. B. – 1975. – Vol.11. – №3. – P. 1001-1012.

[52] Cole, J.M. Crystal Structures and Magnetic Properties of Rare-Earth Ultraphosphates, RP_5O_{14} (R=La, Nd, Sm, Eu, Gd) / J.M. Cole, M.R. Lees, J.A.K. Howard, R.J. Newport, G.A. Saunders, E. Schönherr // Journal of Solid State Chemistry. – 2000. – Vol.150. – №2. – P. 377-382.

[53] ZHANG, H.-Y., Laser behavior and the optics and spectroscopy of a new laser medium $La_{1-x}Nd_xP_5O_{14}$ glass / H.-Y. ZHANG, L. ZHAO, Y.-B. LIU // Conference on Lasers and Electro-Optics / journalAbbreviation: Conference on Lasers and Electro-Optics. – Optica Publishing Group, 1988. – P. THP5.

[54] Ettis, H. Reinvestigation of the GdP_5O_{14} crystal structure at room temperature and magnetic properties / H. Ettis, H. Naïli, T. Mhiri // Materials Chemistry and Physics. – 2007. – Vol.102. – P. 275-280.

[55] Zeller, R.C. Thermal Conductivity and Specific Heat of Noncrystalline Solids / R.C. Zeller, R.O. Pohl // Phys. Rev. B. – 1971. – Vol.4. – №6. – P. 2029-2041.

[56] Salamatov, E.I. Transport characteristics of phonons and heat capacity of single crystals of Y_2O_3 : ZrO_2 solid solutions / E.I. Salamatov, A.V. Taranov, E.N. Khazanov, E.V. Charnaya, E.V. Shevchenko. – 2017. – T.151. – No. 5. – P. 910-917.

[57] Anderson, B.I.H. P. w. Anomalous low-temperature thermal properties of glasses and spin glasses / B.I.H. P. w. Anderson, c M. Varma // The Philosophical Magazine: A Journal of Theoretical Experimental and Applied Physics. – 1972. – Vol.25. – №1. – P. 1-9.

[58] Tielbürger, D. Thermally activated relaxation processes in vitreous silica: An investigation by Brillouin scattering at high pressures / D. Tielbürger, R. Merz, R. Ehrenfels, S. Hunklinger // Phys. Rev. B. – 1992. – Vol.45. – №6. – P. 2750-2760.

[59] Elliott, S.R. A Unified Model for the Low-Energy Vibrational Behaviour of Amorphous Solids / S.R. Elliott // Europhysics Letters. – 1992. – Vol.19. – №3. – P. 201.

[60] Hassaine, M. Low-temperature thermal and elastoacoustic properties of butanol glasses: Study of position isomerism effects around the boson peak / M. Hassaine, M.A. Ramos, A.I. Krivchikov, I.V. Sharapova, O.A. Korolyuk, R. J. Jiménez-Riobóo // Phys. Rev. B. – 2012. – Vol.85. – №10. – P. 104206.

[61] Loiacono, G.M. Specific heats of NdP_5O_{14} and PrP_5O_{14} near their ferroelastic phase transitions / G.M. Loiacono, M. Delfino, W.A. Smith // Applied Physics Letters. – 2008. – Vol.32. – №10. – P. 595-596.

[62] Mesfar, M. Synthesis, crystal structure and vibrational spectra characterization of CeP_5O_{14} / M. Mesfar, M. Abdelhedi, M. Dammak, M. Ferid // Journal of Molecular Structure. – 2012. – Vol.1028. – P. 196-199.

[63] Farok, H.M. Comparison between crystal field effects on the fluorescence spectra of crystalline SmP_5O_{14} and vitreous $(Sm_2O_3)_{0.248}(P_2O_5)_{0.752}$ / H.M. Farok, G.A. Saunders, W.C.K. Poon, J. Crain, H. Vass, W. Hönle, E. Schönherr // Journal of Materials Science. – 1999. – Vol.34. – №10. – P. 2389-2400.

[64] Ikesue, A. Fabrication and Optical Properties of High-Performance Polycrystalline Nd:YAG Ceramics for Solid-State Lasers / A. Ikesue, T. Kinoshita, K. Kamata, K. Yoshida // Journal of the American Ceramic Society. – 1995. – Vol.78. – №4. – P. 1033-1040.

[65] Liu, F. White light emission from $NaLa(PO_3)_4 : Dy^{3+}$ single-phase phosphors for light-emitting diodes / F. Liu, Q. Liu, Y. Fang, N. Zhang, B. Yang, [et. all.] // Ceramics International. – 2015. – Vol.41. – P. 1917-1920.

[66] Rajagopal, V. Structural and Luminescence studies on Dy^{3+} doped Borophosphate glasses for white LED's and Laser applications / V. Rajagopal, G. Venkataiah, K. Marimuthu // Journal of Alloys and Compounds. – 2015. – P. 652.

[67] Vijayakumar, M. Structural and optical properties of Dy^{3+} doped Aluminofluoroborophosphate glasses for white light applications / M. Vijayakumar, K. Mahesvaran, D.K. Patel, S. Arunkumar, K. Marimuthu // Optical Materials. – 2014. – Vol.37. – P. 695-705.

[68] Yu, M. Survivability of thermographic phosphors (YAG:Dy) in a combustion environment / M. Yu, G. Särner, C. Luijten, M. Richter, M. Aldén, [et. all.] // Measurement Science and Technology. – 2010. – Vol.21. – P. 037002.

[69] Almessiere, M. Dielectric and Microstructural Properties of $YAG : Dy^{3+}$ Ceramics / M. Almessiere, B. Unal, A. Baykal // Journal of Rare Earths. – 2018. – Vol.36.

[70] Ramirez A.P. Specific heat of pure and yttrium-doped dysprosium aluminum garnet (DAG) powder near TN / A.P. Ramirez // Phys. Rev. B. – 1987. – Vol.35. – №10. – 5254-5256 p.

[71] Kushino, Akihiro. Erbium-doped yttrium aluminum garnet as a magnetic refrigerant for low temperature x-ray detectors / Akihiro Kushino, Y. Aoki, N.Y. Yamasaki, T. Namiki, Y. Ishisaki, Tatsuma D. Matsuda, Takaya Ohashi, Kazuhisa Mitsuda, Takashi Yazawa // Journal of Applied Physics. – 2001. – Vol.90. – №11. – 5812-5818 p.

[72] Konings, R.J.M. The heat capacity of $Y_3Al_5O_{12}$ from 0 to 900 K / R.J.M. Konings, R.R. van der Laan, A.C.G. van Genderen, J.C. van Miltenburg. – 1998. – Vol.313. – P. 201-206.

[73] Alekseevskii, N.E. Adiabatic demagnetization of Er^3+ or Nd^3+ substituted YAG / N.E. Alekseevskii, A.P. Dodokin, C. Bazan, K.S. Bagdasarov, E.A. Fedorov, // Cryogenics. – 1981. – Vol.21. – №10. – P. 598-600.

[74] Yazawa, T. Adiabatic demagnetization cooler for infrared detector / T. Yazawa, A. Sato, J. Yamamoto // Cryogenics. – 1990. – Vol.30. – №3. – P. 276-280.

[75] Shevchenko, E.V. Low-temperature heat capacity of aluminum-rare-earth garnets / E.V. Shevchenko // International youth scientific forum "LOMONOSOV-2018. – I.A. Aleshkovsky, A.V. Andriyanov, E.A. Antipov [Electronic resource] - M.: MAKS Press, 2018.

[76] Shevchenko, E.V. Low-temperature heat capacity of aluminum-rare-earth garnets in magnetic fields / E.V. Shevchenko // Twenty-fourth All-Russian scientific conference of physics students and young scientists. – 2018. – P. 117.

[77] Spichkin, Y. Magnetic molecular clusters as promising materials for refrigeration in low-temperature regions / Y. Spichkin, A. Zvezdin, S. Gubin, A. Mischenko, A. Tishin // Journal of Physics D: Applied Physics. – 2001. – Vol.34. – P. 1162.

[78] Hakuraku, Y. A rotary magnetic refrigerator for superfluid helium production / Y. Hakuraku, H. Ogata // Journal of Applied Physics. – 1986. – Vol.60. – №9. – P. 3266-3268.

[79] Schiffer, P. Investigation of the Field Induced Antiferromagnetic Phase Transition in the Frustrated Magnet: Gadolinium Gallium Garnet / P. Schiffer, A.P. Ramirez, D.A. Huse, A.J. Valentino // Physical Review Letters. – 1994. – Vol. 73.– № 18. – P. 2500-2503.

[80] Dunsiger, S.R. Low Temperature Spin Dynamics of the Geometrically Frustrated Antiferromagnetic Garnet $Gd_3Ga_5O_{12}$ / S.R. Dunsiger, J.S. Gardner, J.A. Chakhalian, A.L. Cornelius, M. Jaime, R. F. Kiefl, R. Movshovich, W. A. MacFarlane, R. I. Miller, J. E. Sonier, B. D. Gaulin // Phys. Rev. Lett. – 2000. – Vol.85. – №16. – P. 3504-3507.

[81] Matsumoto, K. Specific Heat, and Entropy of Iron-Substituted Gadolinium Gallium Garnets $Gd_3(Ga_{1-x}Fe_x)_5O_{12}$ / K. Matsumoto, A. Matsuzaki, K. Kamiya, T. Numazawa // Japanese Journal of Applied Physics. – 2009. – Vol.48.

[82] Numazawa, T. Magneto caloric effect in $(Dy_xGd_{1-x})_3Ga_5O_{12}$ for adiabatic demagnetization refrigeration / T. Numazawa, K. Kamiya, T. Okano, K. Matsumoto // Physica B-condensed Matter. – 2003. – Vol.329. – P. 1656-1657.

[83] Hamilton, A.C. S. Enhancement of the magnetocaloric effect driven by changes in the crystal structure of Al-doped GGG, $Gd_3Ga_{5-x}Al_xO_{12}$ $(0 \leqslant x \leqslant 5)$ / A.C.S. Hamilton, G.I. Lampronti, S.E. Rowley, S.E. Dutton // Journal of Physics: Condensed Matter. – 2014. – Vol.26. – №11. – P. 116001.

[84] Kuz'min, M.D. Magnetic refrigerants for the 4.2-20 K region: garnets or perovskites? / M.D. Kuz'min, A.M. Tishin // Journal of Physics D: Applied Physics. – 1991. – Vol.24. – №11. – P. 2039.

[85] Asatryan, H.R. EPR studies of Er^{3+}, Nd^{3+} and Ce^{3+} in $YAlO_3$ single crystals / H.R. Asatryan, J. Rosa, J.A. Mares // Solid State Communications. – 1997. – Vol.104. – №1. – P. 5-9.

[86] Abragam, A. Electron Paramagnetic Resonance of Transition Ions / A. Abragam, B. Bleaney. – Clarendon, Oxford, 1970. – 944 p.

[87] Lezova, I.E. Heat Capacity of Erbium-Doped Gallium-Gadolinium Garnet / I.E. Lezova, E.V. Shevchenko, E.V. Charnaya, E.N. Khazanov, A.V. Taranov // Physics of the Solid State. – 2018. – Vol.60. – №10. – P. 1948-1952.

[88] Gruber, J.B. Spectra and energy levels of $Er^{3+}(4f^{11})$ in $Gd_3Ga_5O_{12}$ / J.B. Gruber, D.K. Sardar, B. Zandi, J.A. Hutchinson, C.W. Trussell // Journal of Applied Physics. – 2003. – Vol.93. – №6. – P. 3137-3140.

[89] Tsui, Y.K. Study of the low temperature thermal properties of the geometrically frustrated magnet: Gadolinium gallium garnet / Y.K. Tsui, N. Kalechofsky, C.A. Burns, P. Schiffer // Journal of Applied Physics. – 1999. – Vol.85. –№8. – P. 4512-4514.

[90] Quilliam, J.A. Juxtaposition of spin freezing and long range order in a series of geometrically frustrated antiferromagnetic gadolinium garnets / J.A. Quilliam, S. Meng, H.A. Craig, L.R. Corruccini, G. Balakrishnan, O. A. Petrenko, A. Gomez, S. W. Kycia, M. J. P. Gingras, J. B. Kycia // Phys. Rev. B. – 2013. – Vol.87. – №17. – P. 174421.

[91] Gruber, J.B. Absorption spectra and energy levels of Gd^3+, Nd^3+, and Cr^3+ in the garnet $Gd_3Sc_2Ga_3O_{12}$ / J.B. Gruber, M.E. Hills, C.A. Morrison, G.A. Turner, M.R. Kokta // Physical Review. B, Condensed Matter. – 1988. – Vol.37. – №15. – P. 8564-8574.

[92] Gruber, J.B. Energy levels and correlation crystal-field effects in Er^{3+} - doped garnets / J.B. Gruber, J.R. Quagliano, M.F. Reid, F.S. Richardson, M.E. Hills, M. D. Seltzer, S. B. Stevens, C. A. Morrison, T. H. Allik // Phys. Rev. B. – 1993. – Vol.48. – №21. – P. 15561-15573.

[93] Gary, S.C. Analyses of 4f11 Energy Levels and Transition Intensities Between Stark Levels of Er^{3+} in $Y_3Al_5O_{12}$ / S.C. Gary, W. Burdick, J. B. Gruber, K. L. Nash, D.K. Sardar // Spectroscopy Letters. – 2010. – Vol.43. – №5. – P. 406-422.

[94] Langenberg, E. Analysis of the temperature dependence of the thermal conductivity of insulating single crystal oxides / E. Langenberg, E. Ferreiro-Vila, V. Leborán, A.O. Fumega, V. Pardo, F. Rivadulla // APL Materials. – 2016. – Vol.4. – №10. – P. 104815.

[95] Dai, W. Magnetothermal properties of sintered $Gd_3Ga_5O_{12}$ / W. Dai, E. Gmelin, R. Kremer // Journal of Physics D: Applied Physics. – 1988. – Vol.21. – №4. – P. 628-635.

[96] Barak, J. Electron paramagnetic resonance study of gadolinium–gallium–garnet / J. Barak, M.X. Huang, S.M. Bhagat // Journal of Applied Physics. – 1992. – Vol.71. – №2. – P. 849-853.

[97] Lezova, I.E. Calorimetry of $Dy_xY_{3-x}Al_5O_{12}$ garnet solid solutions in magnetic field / I.E. Lezova, E.V. Charnaya, E.V. Shevchenko, E.N. Khazanov, A.V. Taranov // Journal of Applied Physics. – 2020. – Vol.128. – №22. – P. 225101.

[98] Bridgman, P.W. Certain Physical Properties of Single Crystals of Tungsten, Antimony, Bismuth, Tellurium, Cadmium, Zinc, and Tin / P.W. Bridgman // Proceedings of the American Academy of Arts and Sciences. – 1925. – Vol.60. – №6. – P. 305-383.

[99] Keen, B.E. High-Resolution Specific-Heat Measurements on Dysprosium Aluminum Garnet / B.E. Keen, D.P. Landau, W.P. Wolf // Journal of Applied Physics. – 1967. – Vol.38. – №3. – P. 967-968.

[100] Ball, M. Thermal Properties of Dysprosium Aluminum Garnet near the Néel Temperature / M. Ball, M.J.M. Leask, W.P. Wolf, A.F.G. Wyatt // Journal of Applied Physics. – 1963. – Vol.34. – №4. – P. 1104-1105.

[101] Akhmetov, S.F Study of some rare-earth aluminium garnets / S.F. Akhmetov, G.L. Akhmetova, G.A. Gazizova, V.S. Kovalenko, T.F. Mirenkova // Zhurnal Neorganicheskoj Khimii. – 1977. – Vol.22. – №11. – P. 2966-2969.

[102] Lupei, A. Spectroscopic characteristics of Dy^{3+} doped $Y_3Al_5O_{12}$ transparent ceramics / A. Lupei, V. Lupei, C. Gheorghe, A. Ikesue, M. Enculescu // Journal of Applied Physics. – 2011. – Vol.110. – №8. – P. 083120.

[103] Grünberg, P. Crystal Field in Dysprosium Garnets / P. Grünberg, S. Hüfner, E. Orlich, J. Schmitt // Physical Review. – 1969. – Vol.184. – №2. – P. 285-293.

[104] Gehring, K.A. Magneto-optical effects and a Monte Carlo calculation for dysprosium aluminium garnet / K.A. Gehring, M.J.M. Leask, J.H.M. Thornley // Journal of Physics C: Solid State Physics. – 1969. – Vol.2. – №3. – P. 484-499.

[105] Landau, D.P. Magnetic and Thermal Properties of Dysprosium Aluminum Garnet. I. Experimental Results for the Two-Sublattice Phases / D.P. Landau, B.E. Keen, B. Schneider, W.P. Wolf // Physical Review B. – 1971. – Vol.3. – №7. – P. 2310-2343.

[106] Janssen, P. EPR in dysprosium aluminum garnet at far-infrared frequencies / P. Janssen, M. Mahy, W.P. Wolf // Physical Review B. – 1988. – Vol.37. – №10. – P. 4851-4863.

[107] Wolf, W.P. Magnetic and Thermal Properties of Dysprosium Aluminum Garnet. II. Characteristic Parameters of an Ising Antiferromagnet / W.P. Wolf, B. Schneider, D.P. Landau, B.E. Keen // Phys. Rev. B. – 1972. – Vol.5. – №11. – P. 4472-4496.

[108] Gschneidner, K.A. Recent developments in magnetocaloric materials / K.A. Gschneidner, V.K. Pecharsky, A.O. Tsokol // Reports on Progress in Physics. – 2005. – Vol.68. – №6. – P. 1479.

[109] Jang, D. T. Large magnetocaloric effect and adiabatic demagnetization refrigeration with $YbPt_2Sn$ / D. Jang, T. Gruner, A. Steppke, K. Mitsumoto, C. Geibel, M. Brando // Nature Communications. – 2015. – Vol.6. – P. 8680.

[110] Palacios, E. Magnetic structure and magnetocalorics of $GdPO_4$ / E. Palacios, J.A. Rodriguez-Velamazan, M. Evangelisti, G.J. McIntyre, G. Lorusso, D. Visser, L. J. de Jongh, L. A. Boatner // Physical Review B. – 2014. – Vol.90. – P. 214423.

[111] Lezova, I.E. Low-Temperature Heat Capacity and Phonon Kinetics in Some Rare-Earth Pentaphosphate Single Crystals and Glasses / I.E. Lezova, E.I. Salamatov, A.V. Taranov, E.N. Khazanov, E.V. Charnaya, E. V. Shevchenko // Journal of Experimental and Theoretical Physics. – 2019. – Vol.129. – №5. – P. 849-854.

[112] Gruber, J.B. Spectra and energy levels of $Nd^3 + (4f_3)$ in stoichiometric NdP_5O_{14}/ J.B. Gruber, D.K. Sardar, T.H. Allik, B. Zandi // Optical Materials. – 2004. – Vol.27. – №2. – P. 351-358.

[113] Hong, H.Y.-P. Crystal structures of neodymium metaphosphate (NdP_3O_9) and ultraphosphate (NdP_5O_{14}) / H.Y.-P. Hong // Acta Crystallographica Section B. – 1974. – Vol.30. – №2. – P. 468-474.

[114] Lezova, I.E. Heat capacity of erbium-doped gallium-gadolinium garnet / I.E. Lezova, E.V. Shevchenko, E.V. Charnaya, E.N. Khazanov, A.V. Taranov. – 2018. – T. 60. – No. 10. – P. 1906-1910.

[115] H.Y.-P. Hong, J.W. Pierce : Hong, H.Y.-P., J.W. Pierce. Crystal structure of Ytterbium ultraphosphate, YbP_5O_{14} / H.Y.-P. Hong, J.W. Pierce // Materials Research Bulletin. – 1974. – Vol.9. – №2. – P. 179-189.

[116] Mbarek, A. Synthesis and crystal structure determination of yttrium ultraphosphate YP_5O_{14} / A. Mbarek, M. Graia, G. Chadeyron, D. Zambon, J. Bouaziz, M. Fourati // Journal of Solid State Chemistry. – 2009. – Vol.182. – №3. – P. 509-516.

[117] Tranqui, D. Structure de l'ultraphosphate de samarium SmP_5O_{14} / D. Tranqui, M. Bagieu, A. Durif // Acta Crystallographica Section B. – 1974. – Vol.30. – №7. – P. 1751-1755.

[118] Lezova, I.E. Kinetic Characteristics of Phonons and the Structural Heterogeneities of the Monoaluminate $Y_{1-x}Er_xAlO_3$ Solid Solutions / I.E. Lezova, O.V. Karban', A.V. Taranov, E.N. Khazanov, E.V. Charnaya // Journal of Experimental and Theoretical Physics. – 2020. – Vol.130. – №1. – P. 76-81.

[119] Ramos-Gallardo, A. The Cation Arrays in the Garnet-Type $Al_5Ln_3O_{12}$ and Perovskite-Like AlLnO3Compounds / A. Ramos-Gallardo, A. Vegas // Journal of Solid State Chemistry. – 1997. – Vol.128. – №1. – 69-72 p.

[120] Bagdasarov, Kh.S. $YAlO_3$ with Tr^{3+} ion impurity as an active laser medium / Kh.S. Bagdasarov, A.A. Kaminskii. – 1969. – Vol.9. – №9. – P. 501-502.

[121] Vorotilova, L.S. Al NMR in mixed crystals $Y_xEr_{1-x}AlO_3$ / L.S. Vorotilova, S.N. Ivanov, V. Kasperovich S., E.V. Charnaya, E.N. Khazanov. – 1992. – T. 34. – No. 9. – P. 2911-2914.

[122] Chua, M. Energy transfer processes of Er^{3+} in $YAlO_3$ / M. Chua, S. Xia, P. A. Tanner // Journal of Physics: Condensed Matter. – 2003. – Vol.15. – №43. – P. 7423.

[123] Salamatov, E.I. Features of heat capacity and phonon transport in Er-containing aluminum-rare-earth garnets in the He-temperature region / E.I. Salamatov, A.V. Taranov, E.N. Khazanov, E.V. Charnaya, E.V. Shevchenko. – 2018. – T. 154. – No. 4. – P. 836-834.